Spring 1984

Block Transform Coding of Presample Filtered Data

Thomas A. Shull
Old Dominion University

BLOCK TRANSFORM CODING OF PRESAMPLE FILTERED DATA

by

Thomas A. Shull
B.S. June 1970, Virginia Polytechnic Institute
M.S. June 1972, Virginia Polytechnic Institute and
State University

A Dissertation Submitted to the Faculty of Old Dominion University
in Partial Fulfillment of the Requirements for the Degree of

DOCTOR OF PHILOSOPHY
in
ENGINEERING

OLD DOMINION UNIVERSITY
May, 1984

Approved by:

John W. Stoughton (Director)

ABSTRACT

BLOCK TRANSFORM CODING OF PRESAMPLE FILTERED DATA

Thomas A. Shull
Old Dominion University, 1984
Director: Dr. John W. Stoughton

This dissertation addresses the application of non-adaptive transform coding for bit rate reduction of presampled filtered data. Transform coding is examined as an alternative to conventional pulse code modulation (PCM) for multi-source, fixed rate data acquisition systems. Typical bandlimiting presample filters introduce redundancy into the sequence of data samples. Linear transformation of successive N-length blocks of the data sequence and subsequent binary coding of the resulting components is shown to lead to reduced average bit rate for the same less distortion as PCM.

Four Butterworth filters, two corresponding to eight bit PCM systems, and two corresponding to ten bit PCM systems, are considered. The orthonormal transforms (bases) examined are a filter derived Karhunen-Loueve, a discrete cosine, and a discrete Legendre transform. A reference for the previous use of the discrete Legendre basis for transform coding is not known.

Transformation is modeled as a bank of basis dependent FIR filters for analysis. Thus, transform coding is interpreted in terms of spectral energy capture. The magnitude squared transfer function of the presample filter is assumed to define the worst case spectral

envelope or power spectral density of the sampled filter output. This is incorporated into the model to establish an upper bound on the average component energy for the various bases. The bases are compared analytically using a bit rate reduction bound, adapted from Zelinski and Noll, and energy packing considerations. The analysis indicates that bit rate reduction is possible and that large block lengths are not required.

The transform coding strategy for $N = 16$ is implemented on simulated and real data. Bit rate reduction on the order of 25 percent establishes merit for the transform coding strategy. Additionally, transform coding is observed to result in less distortion than PCM for signals having intervals of reduced spectral activity.

DEDICATION

This is dedicated to my wife, Sue, and my son, Andy, for their love and support.

ACKNOWLEDGEMENTS

The author wishes to sincerely thank Dr. J. W. Stoughton for his direction and many discussions regarding the work presented in this dissertation. The assistance of Dr. Roland R. Mielke, Dr. Steven A. Zahorian, and Dr. Frank Allerio in reviewing this dissertation is also appreciated.

The author also wishes to thank Pamela R. Rinsland for help in system level programming and preparation of computer graphics software. The author is also grateful for the help and encouragement of other personnel of the Flight Instrumentation Branch, Langley Research Center.

The author wishes to thank Linda Budd and Mary Edwards for their outstanding talents in typing this dissertation.

The time and resources used in conducting this research and final preparation of this manuscript were provided by NASA Langley Research Center, Hampton, Virginia.

TABLE OF CONTENTS

LIST OF TABLES

LIST OF FIGURES

LIST OF SYMBOLS

a_m	basis coefficient
$\underline{a}$	coefficient vector
B_m	noninteger coefficient bit allocation
B_{PCM}	PCM bit rate
B_{TC}	transform coding bit rate
$C(e^{j\omega})$	defined in Chapter Three
$C'(e^{j\omega})$	defined in Chapter Three
$\bar{D}$	average quantization distortion energy
$\bar{D}_m$	average coefficient quantization distortion energy
$\bar{D}_{TC}, \bar{D}_{PCM}$	constants defined in Chapter Two
E^2	squared error defined in Chapter Two
$e_Q^*(p)$	reconstruction error sequence
$\underline{e}_Q$	reconstruction error vector
$\bar{e}_Q^2$	average reconstruction error energy
$e_x^*(p)$	approximation error sequence
$e_x(n)$	segment of approximation error sequence
$\underline{e}_x, \underline{e}_y, \underline{e}_z$	approximation error vector
$\bar{e}_x^2$	average approximation error energy
$F^*(e^{j\omega})$	discrete Fourier transform
$F_A(\Omega)$	analog filter transfer function
$h(t)$	analog filter impulse response
$h_m(n)$	impulse response defined in Chapter Two
I	identity matrix

j	$\sqrt{-1}$
k,m,n,p	integers
K,L,M,N,P	integers
Q	quantization step size
$\underline{\tilde{Q}}$	reconstruction error vector defined in Chapter Two
$\tilde{Q}^2$	reconstruction energy defined in Chapter Two
$R_{xx}, R_{\alpha\alpha}$	covariance matrices
$s(t)$	continuous time signal
$S_A(\Omega)$	Fourier transform
$S'(e^{j\omega})$	defined in Chapter Two
t	continuous time variable
T	sampling interval
$u_m(n)$	reference sequence
$\underline{u}_m$	basis vector
U	matrix of basis vectors
W	subspace defined in Chapter Two
W'	compliment subspace defined in Chapter Two
$x(t)$	continuous time input signal
$X_A(\Omega)$	Fourier transform
$X^*(e^{j\omega})$	discrete Fourier transform
$x^*(p), y^*(p), z^*(p)$	input sequence
$x(n), y(n), z(n)$	segment of input sequence
$\underline{x}, \underline{y}, \underline{z}$	input vectors
$\tilde{x}^*(p)$	approximation sequence
$\tilde{x}(n)$	segment of approximation sequence
$\underline{\tilde{x}}, \underline{\tilde{y}}, \underline{\tilde{z}}$	approximation vectors
$\underline{\hat{x}}$	reconstruction vector

$\bar{x}^2$	average input energy
$\bar{\tilde{x}}^2$	average approximation energy
ν	filter order used in Chapter Three
ρ_m	parameter defined in Chapter Two
σ^2	variance
$\underline{\phi}_m$	orthonormal basis vector
$\underline{\bar{\phi}}$	matrix of orthonormal basis vectors
$\underline{\psi}_m$	orthonormal vector defined in Chapter Four
ω	discrete radian frequency
Ω	analog radian frequency
Ω_c	cutoff frequency
Ω_s	sampling frequency
$\{*\}$	denotes set
$*^\dagger$	complex conjugate
$\lceil * \rceil$	integer greatest lower bound
$*^T$	transpose
$\|*\|$	norm of a vector
$*\perp *$	denotes orthogonal vectors
$\langle * \rangle$	vector inner product
α_m	orthonormal basis coefficient
$\alpha_m(k)$	coefficient sequence
$\alpha_m^*(p)$	sequence defined in Chapter Two
$\bar{\alpha}_m^2$	average coefficient energy
$\alpha_{Q,m}$	coefficient quantization error
$\bar{\alpha}_{Q,m}^2$	average coefficient quantization error energy
$\underline{\alpha}, \underline{\alpha}_x, \underline{\alpha}_y, \underline{\alpha}_z$	coefficient vectors
$\underline{\alpha}_Q$	coefficient quantization error vector

$\hat{\underline{\alpha}}$	quantized coefficient vector
δ_m	parameter defined in Chapter Two
δ_{km}	Kronecker delta
$\delta_{TC}, \delta_{PCM}$	constants defined in Chapter Two
ΔB	bit rate improvement
ΔB_{max}	constant defined in Chapter Two
η	constant defined in Chapter Three
θ	transformation matrix defined in Chapter Two
κ	scale factor defined in Chapter Two
λ_m	eigenvalues of R_{xx}

CHAPTER ONE

INTRODUCTION

This dissertation addresses the application of non-adaptive, real-time transform coding of data that has been bandlimited by presample filtering. This type of data is common to multi-source, fixed rate sampled data acquisition instrumentation systems. These systems historically use conventional pulse code modulation (PCM) for data representation. The presample filter is included to satisfy the sampling theorem [1]. The assertion is that the filter imposes redundancy on the sequence of data samples. Hence appropriate treatment of the redundancy is expected to lead to bit rate reduction compared to the independent sample coding of PCM. This research examines block transform coding as a viable strategy to effect bit rate reduction. The focus is on the comparative performance of a class of orthonormal bases (transforms) with respect to a representative family of filters. The bases considered are a Karhunen-Loueve basis derived from the filter characteristic, the discrete cosine basis, and a basis of discrete Legendre polynomials. The discrete Legendre basis has received little or no attention for transform coding. Bit rate reduction conditioned solely on presample filter imposed redundancy is a new application for transform coding. It is hoped that this work will lead to the incorporation of transform coding into future data acquisition systems.

There has been widespread use of sampled data acquisition systems over the past several decades. One area where it is quite common is

aerospace research where data are simultaneously gathered from many sources in real time for storage or transmission over a fixed rate channel. One of the most commonly used systems is the classical PCM system depicted in Figure 1.1 in which each analog source is sampled, quantized, then binary coded. The encoded samples from each source are then multiplexed with those of other sources for final disposition.

The figure also shows a presample low-pass filter, a system component that is almost always included in order to meet the bandlimited restriction imposed by the sampling theorem. These filters are non-ideal, i.e. have finite roll-off, and the sampling frequency is generally many times the filter cutoff (3 dB) frequency, typically twice the frequency at which the filter response falls below some predetermined relative distortion level. The rationale behind this is that any spectral component present beyond half the sampling frequency would be below the distortion level and indiscernable from quantizing noise.

As a result of presample filtering, the sampled source is known to have built-in redundancy in that the samples are not independent. That is, they are each related in some fashion to previous samples. This can be seen by recalling that the output of a real (causal) linear, time invariant filter can be written as

$$x(t) = \int_0^\infty h(\tau)\, s(t - \tau)\, d\tau \qquad (1.1)$$

the convolution of the input and the impulse response of the filter. The existence of redundancy suggests the possiblity of data compression over the independent sample encoding of PCM.

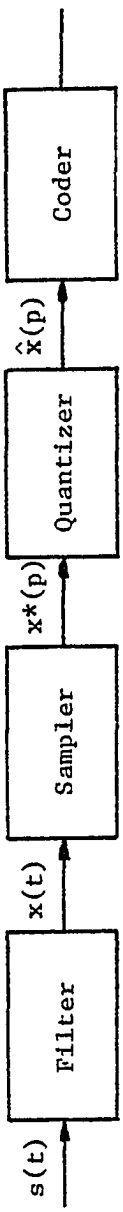

Figure 1.1. Conventional PCM System.

Frequently, in the data acquisition applications being considered, the transmission channel bit rate or available storage is limited. This leads, through system design trade-offs, to limitations on the sample rate (source bandwidth), and number of sources that can be accommodated by a system. If by preprocessing (transformation) of the samples from a filtered source the sample sequence could be represented by fewer bits, more sources could be accommodated within the same communication channel or alternately the filter cutoff frequency and sample rate of a given source could be increased.

Some techniques that are currently employed for source redundancy removal are linear predictive coding or differential PCM (DPCM), delta modulation, and transform coding. Netravali and Limb [2] give a review of these and several other techniques as applied to image data compression. Transform coding is addressed in this work. This technique involves treating successive blocks of the input sequence as vectors, and then performing a linear basis transformation to produce a new vector with less redundancy between components. The components of the new vector are then quantized and encoded more efficiently than the input samples. At the receiver the representation of the original sequence of source samples is reconstructed using the inverse transformation. This has been termed block quantization by Huang and Schultheiss [3] or basis restricted transform coding by Pearl [4]. This system is depicted in Figure 1.2.

Transform coding as applied to data compression has been considered by many authors over the past several decades. The work is traditionally related to the context of the signal. Huang and Schultheiss [3], Pearl [4], Davisson [5], Segall [6], and Yip and Rao [7] have considered

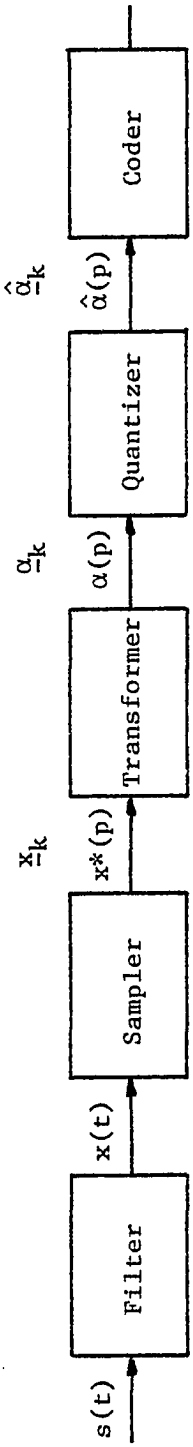

Figure 1.2. Transform Coding System.

the general problem of transform coding of stationary Gaussian vector sources. Campanella and Robinson [8], Guner and Granger [9], and many others have considered the application of transform coding to speech compression. Transform coding, both one-dimensional and two-dimensional, as applied to images has been reported by Netravali and Limb [2], Tasto and Wintz [10], Habibi and Wintz [11], and Kekre and Solanki [12], and many others. Application to video transmission has also been reported [13, 14]. However, little or no research on pre-sample filter created redundancy has been found.

As will be shown, the redundancy removal manifests itself in the redistribution of the source energy among the transformed components resulting in the use of a different number of binary bits (word length) for each component. If enough of the input energy is contained in a reduced number of components of the resulting vector then some components need not be retained or transmitted at all. Thus the energy redistribution may result in fewer total binary bits per block or fewer average binary bits per input sample to represent the sequence of transform components with the same mean square distortion as required of the original sequence representation (PCM).

In most practical telemetry data systems the quantizer is a single device, called an A-to-D converter (often shared by many sources), which has as output a natural binary representation of the uniformly spaced quantization level to be assigned to the analog input sample. Thus it is a combination of quantizer and binary coder. The transform coding system will require an input quantizer. The transformation is assumed to be a digital process with the output components quantized by appropriate truncation. Digital processing hardware and A-to-D converters

have improved to the point where real-time transformation prior to transmission or storage is realistic as a practical strategy for bit rate reduction.

The binary coded output of either system could be further encoded using, for example, a Huffman [15] code if the probability of occurrence of the quantizing levels are available or at the expense of additional buffering and processing. Haralick and Shanmugam [16] consider linear predictive coding of the transform components for speech applications and Tasto and Wintz [10] consider Huffman coding of image data. Binary representation of quantizer levels with no further encoding is to be considered in this dissertation work since this is common to telemetry systems.

Adaptive techniques which attempt to track changes in signal characteristics have been considered by Zelinski and Noll [17], Netravali and Limb [2], Tasto and Wintz [10], and Ekambaram and Kwatra [13] to name a few. These techniques involve variable bit assignment, variable basis selection or variable subspace (component) selection. These techniques require additional "side information" to be stored or provided to the receiver. Adaptive techniques are not considered in this work.

Many transforms or bases have been considered for data compression purposes. These include the Karhunen-Loueve [18] basis used by many authors, the discrete cosine [19, 20] and other trigonometric transforms [12], the Walsh-Hadamard transform [21, 22], the discrete Fourier transform [9], the slant and Haar transform [23], generalized discrete transforms [7, 24,], and a discrete linear basis having integer components [16]. These various bases have received attention due to some

special properties which are useful to a particular signal class or application.

The transform bases that are to be considered in this work are the Karhunen-Loueve bases derived from the presample filter transfer functions, the discrete cosine basis, and a basis of discrete Legendre polynomials. The Karhunen-Loueve basis is known to be optimum for stationary, zero mean sources. Thus it is the prime candidate for this application. The discrete cosine basis has been shown by many authors to match the Karhunen-Loueve performance for certain other applications and is thus also included. Transformation using the discrete Legendre basis is equivalent to least mean square curve fitting to polynomials of the form

$$P(t) = a_0 + a_1 t + a_2 t^2 + \ldots + a_m t^m \ . \qquad (1.2)$$

Polynomials receive widespread use for interpolation and curve fitting of sampled telemetry data. Thus this basis is also considered to be worthy of consideration in this study. A reference for its previous use in transform coding has not been found.

In this dissertation the application of transform coding to sampled data sequences which are the output of a low-pass filter with known transfer function is addressed. Only fixed a-priori basis selection and coefficient bit allocation are considered. The ability to achieve bit rate reduction over PCM while maintaining the same or less distortion is demonstrated. This is achieved without the burden of excessive computation load. Expressions for basis comparison and bit allocation using the presample filter characteristic are presented. Processing of signal plus noise is addressed for analysis of input digitizer effects. The

potential of transform coding to provide less distortion than PCM for signals with intervals of low activity, particularly for the DL basis, is also demonstrated.

In Chapter Two transform coding is modeled for the purpose of analysis, and bases mentioned above are defined and quantization and bit allocation are examined. In Chapter Three results of analysis are presented for comparison between the bases under consideration. In Chapter Four results of simulated transform coding on both simulated and real data are presented. Conclusion and a discussion of areas of future work are given in Chapter Five.

CHAPTER TWO

TRANSFORM CODING AND BASIS

2.0 Introduction

In this chapter the technique of transform coding of sequences is presented and modeled in a way that is suitable for the telemetry application analysis, and the three transforms (bases) under consideration are defined. In transform coding successive N-length segments of the input are treated as vectors in N-dimensional Euclidean signal space. Each vector is transformed or projected, onto a M-dimensional, $M < N$, subspace spanned by a set of orthonormal basis. The resulting set of components or basis coefficients is quantized and coded in place of the N original components or input samples. At the receiver the original sequence is reconstructed using the inverse transformation. Distortion is treated as the mean square error between the input sequence and the reconstructed sequence.

For $M < N$ the resulting vector represents the input with least mean square error. The least mean square criterion has practical significance since it can be interpreted in the terms of average energy in a finite sequence. This energy interpretation is used throughout this work.

Transformation results in redistribution of the input energy (dynamic range) among the components and can lead to data compression in two forms. First, it can lead to the use of fewer total binary digits for coding of the sequence of components than is required for the

original sequence of input samples. Secondly, if the resulting error of subspace ($M < N$) representation can be tolerated, the N samples can be replaced by M components, further reducing the average bit rate per input sample. The comparative performance between bases is then related to the energy redistribution.

In Section 2.1, transform coding is defined in terms of Hilbert signal space projection and the concept of energy capture is introduced. Some useful Hilbert space properties are given. The concept of component sequences and energy distribution or input energy capture for transformation of successive segments of the input sequence are introduced in Section 2.2. In Section 2.3 transformation is modeled by a bank of finite impulse response (FIR) filters for the purpose of coefficient energy prediction. This also provides a model for development of insight into the transform coding strategy. The presample filter is brought into the analysis in this section after making appropriate assumptions related to the application being addressed. The three bases under consideration are then defined. The well known Karhunen-Loueve transform basis, which is known to provide the theoretical optimum subspace energy capture and bit rate for stationary processes is presented in Section 2.4. The way in which an a-priori approximation is generated for this study is then presented. The discrete cosine basis, common to transform coding, and the discrete Legendre basis for which no reference pertaining to transform coding has been found are defined in Section 2.5. Finally, in Section 2.6 reconstruction error and known results on bit allocation are examined. This results in a measure for the analytical comparison of basis. Section 2.7 is a chapter summary.

2.1 Sequence Representation by Orthogonal Transformation

Let an ordered segment or block of N successive samples from a source sequence $x^*(p)$, $p \in [0, P-1]$ be denoted $x(n)$, $n \in [0, N-1]$. Now consider approximating $x(n)$ by a sequence denoted $\tilde{x}(n)$, $n \in [0, N-1]$ which is a linear combination of a subset of N linearly independent reference sequences $\{u_m(n), m \in [1,N], n \in [0, N-1]\}$. Then $\tilde{x}(n)$ can be written as

$$\tilde{x}(n) = \sum_{m=1}^{M} a_m u_m(n), \qquad n \in [0, N-1] . \tag{2.1.1}$$

The a_m are called the coefficients of the approximation. The criterion for the approximation is the minimization of the squared error defined by

$$E^2 = \sum_{n=1}^{N} e_x^2(n) = \sum_{n=1}^{N} [x(n) - \tilde{x}(n)]^2 . \tag{2.1.2}$$

Once the a_m are determined they can be used to represent the input in a least mean square sense relative to the set $\{u_m\}$. If $M = N$ the $\{a_m\}$ can be found such that the error is equal to zero. If $M < N$ and the resulting error can be tolerated, the set $\{a_m\}$ can be used in lieu of the input segment $x(n)$. The approximation $\tilde{x}(n)$ is obtained using equation (2.1.1).

Approximation using the minimum squared error criterion is mathematically tractable and has a practical significance since expressions of the form of equation (2.1.2) can be interpreted as the energy in a finite sequence. Thus the set of coefficients $\{a_m\}$ can be said to

represent $x(n)$ with the minimum error energy relative to the given set of reference sequences.

The above equations can be written in vector matrix form by equating the sequences to vectors in N-dimensional Euclidean signal space. Letting $*^T$ indicate the transpose of a vector, define

$$\underline{x} = [x(0),x(1),\ldots,x(N-1)]^T , \tag{2.1.3a}$$

$$\underline{\tilde{x}} = [\tilde{x}(0),\tilde{x}(1),\ldots,\tilde{x}(N-1)]^T , \tag{2.1.3b}$$

and

$$\underline{u}_m = [u_m(0), u_m(1),\ldots, u_m(N-1)]^T, \; m = 1,2,\ldots,N \tag{2.1.3c}$$

as the input, approximating, and reference vectors respectively. Since the $\underline{u}_m$ are linearly independent, they constitute a basis for the signal space of $\underline{x}$. Equation (2.1.1) can now be written as

$$\underline{\tilde{x}} = \sum_{m=1}^{M} a_m \underline{u}_m = U^T\underline{a} \tag{2.1.4}$$

where $U = [\underline{u}_1, \underline{u}_2,\ldots, \underline{u}_M]^T$ and is an $M \times N$ matrix $\underline{a} = (a_1, a_2, \ldots, a_M)^T$ is the coefficient vector. The vector $\underline{\tilde{x}}$ is contained in the M-dimensional subspace, denoted subspace W, spanned by $\{\underline{u}_m, m \in [1,M]\}$. Equation (2.1.2) can be rewritten in vector form as

$$E^2 = \langle \underline{e}_x, \underline{e}_x \rangle = \underline{e}_x^T \underline{e}_x \tag{2.1.5}$$

where $\underline{e}_x = \underline{x} - \underline{\tilde{x}}$ is the error vector and $\langle * \rangle$ denotes the vector inner product.

The coefficient vector which minimizes equation (2.1.5) is found by taking the vector derivative of E^2 with respect to $\underline{a}$, setting the result to zero and solving for $\underline{a}$ as

$$\frac{\partial E^2}{\partial \underline{a}} = \frac{\partial}{\partial \underline{a}}\left[(\underline{x} - \tilde{\underline{x}})^T(\underline{x} - \tilde{\underline{x}})\right] = \frac{\partial}{\partial \underline{a}}\left[(\underline{x} - U^T\underline{a})^T(\underline{x} - U^T\underline{a})\right]$$

$$= \frac{\partial}{\partial \underline{a}}\left[\underline{x}^T\underline{x} + 2(U\underline{x})^T\underline{a} + \underline{a}^T U\, U^T\underline{a}\right]$$

$$= 2U\underline{x} + 2UU^T\underline{a} = \underline{0} \ . \qquad (2.1.6)$$

This leads to the vector form of what is commonly called the "normal equations" given by

$$UU^T\underline{a} = U\underline{x} \ . \qquad (2.1.7)$$

Since $\{\underline{u}_m\}$ is a linearly independent set, UU^T is nonsingular and

$$\underline{a} = (UU^T)^{-1}U\underline{x} = \theta\underline{x} \ . \qquad (2.1.8)$$

The maxtix θ is said to perform a linear transformation from $\underline{x}$ to $\underline{a}$. If $M = N$ this same equation gives the $\underline{a}$ that results in zero approximation error, e.g. $\tilde{\underline{x}} = \underline{x}$.

Sequence representation can be interpreted in terms of Hilbert signal space [26, 27] by recalling that the inner product defines a norm denoted $\|\underline{x}\|$, as

$$\|\underline{x}\|^2 = \langle \underline{x}, \underline{x} \rangle = \sum_{n=0}^{N-1} x^2(n) \ . \qquad (2.1.9)$$

With this interpretation, all pertinent Hilbert space analysis can be utilized. The norm is an abstraction of the length of a vector. In the signal space interpretation, $\tilde{\underline{x}}$ is the vector contained in the

subspace, W, spanned by the basis set $\{\underline{u}_m\}$ for which the error vector has minimum norm (length). The coefficient vector can be found using the projection theorem which states that the norm of $\underline{e}_x$ is minimum if and only if $\underline{e}_x$ is orthogonal to $\underline{\tilde{x}}$, where two vectors are orthogonal if and only if

$$\langle \underline{e}, \underline{\tilde{x}} \rangle = 0 \ . \tag{2.1.10}$$

This is denoted symbolically as $\underline{e}_x \perp \underline{\tilde{x}}$. Use of this theorem leads to the same "normal equations" given above in equation (2.1.6). In Hilbert space terminology, $\underline{\tilde{x}}$ is the projection of $\underline{x}$ onto W.

As a property of orthogonal projection,

$$\|\underline{x}\|^2 = \|\underline{\tilde{x}}\|^2 + \|\underline{e}_x\|^2 \tag{2.1.11}$$

which is the N-dimensional equivalent to the Pythagorean theorem. With the vectors representing sequences, it is apparent from the definition of $\|x\|$ that this can be interpreted to mean that the energy in the approximating sequence $\tilde{x}(n)$ equals the energy of the input sequence $x(n)$ minus the energy of the error sequence $e_x(n)$. Thus as an alternate interpretation, $\tilde{x}(n)$ can be said to have captured the maximum amount of input energy for the given reference (basis) set $\{\underline{u}_m\}$.

Thus far the only restriction that has been placed on the reference set $\{\underline{u}_m\}$ has been linear independence, i.e. that they form a basis for the signal space of $\underline{x}$. It is well known that the solution to the normal equations is greatly simplified if the basis set is orthonormal; that is, if the basis has the property

$$\langle \underline{\phi}_k, \underline{\phi}_m \rangle = \delta_{km}, \ k, \ m = 1,2,\ldots,N \tag{2.1.12}$$

where $\underline{\phi}$ has been used to denote orthonormal basis and δ_{km} is the Kronecker delta. An orthogonal basis can always be generated from any given basis set by the Gram-Schmidt procedure [27]. For an orthonormal basis set, $\{\underline{\phi}_m,\ m \in [1, M]\}$ and corresponding M-dimensional subspace W, the approximation vector indicated by equation (2.1.4) is given by

$$\tilde{\underline{x}} = \Phi^T \underline{\alpha} \tag{2.1.13}$$

with $\Phi = [\underline{\phi}_1, \underline{\phi}_2, \ldots, \underline{\phi}_M]^T$ and $\underline{\alpha} = [\alpha_1, \alpha_2, \ldots, \alpha_M]^T$ the coefficient vector for the orthonormal basis. For an orthonormal basis $\Phi^T\Phi = I$, where I denotes identity matrix, and the normal equations (2.1.7) reduce to

$$\underline{\alpha} = \Phi\, \underline{x} \tag{2.1.14}$$

and no matrix inversion is required. Φ is said to perform an orthogonal transformation from $\underline{x}$ to $\underline{\alpha}$. Furthermore, the coefficients can be found separately from

$$\underline{\alpha}_m = \langle \underline{\phi}_m, \underline{x} \rangle \ . \tag{2.1.15}$$

An important consequence of $\{\underline{\phi}_m\}$ being an orthonormal basis is that

$$\|\tilde{\underline{x}}\|^2 = \sum_{m=1}^{M} (\alpha_m)^2 = \|\underline{\alpha}\|^2 \ . \tag{2.1.16}$$

When $M < N$, the set $\{\underline{\phi}_m,\ m = M + 1, \ldots, N\}$ is said to span the orthogonal compliment subspace W' and the error vector

$$\underline{e}_x = \sum_{m=M+1}^{N} \alpha_m \underline{\phi}_m \tag{2.1.17}$$

is the projection of $\underline{x}$ onto the subspace W'. Again for an orthonormal basis,

$$\|\underline{e}_x\|^2 = \sum_{m=M+1}^{N} (\alpha_m)^2 = \|\underline{\alpha}\|^2 . \tag{2.1.18}$$

Combining equations (2.1.9), (2.1.11), (2.1.16), and (2.1.18),

$$\sum_{n=1}^{N} \tilde{x}^2(n) = \|\underline{\tilde{x}}\|^2 = \sum_{m=1}^{M} (\alpha_m)^2 , \tag{2.1.19}$$

$$\sum_{n=1}^{N} e_x^2(n) = \|\underline{e}_x\|^2 = \sum_{m=M+1}^{N} (\alpha_m)^2 , \tag{2.1.20}$$

and

$$\sum_{n=1}^{N} x^2(n) = \|\underline{x}\|^2 = \sum_{m=1}^{N} (\alpha_m)^2 . \tag{2.1.21}$$

Or the sum of squares of the coefficients for an orthonormal basis is equal to the energy in the respective N-length sequences.

The above interpretation is equally valid for complex sequences and vectors where orthogonality is defined by

$$\langle \underline{x}, \underline{y}^\dagger \rangle = 0 \tag{2.1.22}$$

where $\underline{y}^\dagger$ denotes complex conjugate. In this case Φ is called a unitary transformation and $\Phi(\Phi^\dagger)^T = I$.

Finally, consider the input as the sum of two sequences

$$x^*(p) = y^*(p) + z^*(p) . \tag{2.1.23}$$

Letting $\underline{x} = x(n)$, $\underline{y} = y(n)$, and $\underline{z} = z(n)$ represent corresponding segments of $x^*(p)$, $y^*(p)$, and $z^*(p)$, respectively, leads to

$$\underline{x} = \underline{y} + \underline{z} \ . \tag{2.1.24}$$

Projection is a linear operator; thus the projection of $\underline{x}$ is the sum of the projections of $\underline{y}$ and $\underline{z}$. Or

$$\tilde{\underline{x}} = \tilde{\underline{y}} + \tilde{\underline{z}} \tag{2.1.25}$$

and

$$\underline{e}_x = \underline{e}_y + \underline{e}_z \ . \tag{2.1.26}$$

Note that the triangle inequality holds within a Hilbert subspace so that

$$\|\tilde{\underline{x}}\|^2 \leq \left(\|\tilde{\underline{y}}\| + \|\tilde{\underline{z}}\|\right)^2 \tag{2.1.27}$$

and

$$\|\underline{e}_x\|^2 \leq \left(\|\underline{e}_y\| + \|\underline{e}_z\|\right)^2 \ . \tag{2.1.28}$$

Equality holds if $\tilde{\underline{y}} \perp \tilde{\underline{z}}$ and $\underline{e}_y \perp \underline{e}_z$, respectively.

However note that every vector contained in W is orthogonal to every vector contained in W' and thus

$$\underline{e}_z \perp \tilde{\underline{y}} \quad \text{and} \quad \underline{e}_y \perp \tilde{\underline{z}} \ . \tag{2.1.29}$$

2.2 Energy Distribution and Energy Capture

So far only a single N-length segment of the input sample sequence $x^*(p)$ has been considered. For telemetry applications the coefficients are to be generated for successive N-length segments of an entire P-length input sequence. Let $x_k(n)$, $k \in [0, K-1]$, $K = P/N$ an integer, represent the k^{th} segment of $x^*(p)$, so that

$$x_k(N) = x^*(kN + n) \ . \tag{2.2.1}$$

For an input sequence of length P the average energy for the entire sequence, denoted $\bar{x}^2$, is

$$\bar{x}^2 = \frac{1}{P} \sum_{p=1}^{p-1} [x^*(p)]^2 = \frac{1}{P} \sum_{k=0}^{K-1} \sum_{n=0}^{N-1} [x_k(n)]^2 \ . \tag{2.2.2}$$

Now when the input is successively transformed using a fixed set of N orthonormal basis vectors it can be thought of as generating a set of N coefficient sequences $\alpha_m(k)$ where $\alpha_m(k)$ is the m^{th} coefficient for the k^{th} segment. Substituting equation (2.1.21) into equation (2.2.2) gives

$$\bar{x}^2 = \frac{1}{P} \sum_{k=0}^{K-1} \sum_{m=1}^{N} [\alpha_m(k)]^2 \tag{2.2.3}$$

or, rearranging the summations,

$$\bar{x}^2 = \sum_{m=1}^{N} \sum_{k=0}^{K-1} [\alpha_m(k)]^2 \ . \tag{2.2.4}$$

Distributing P between the summations, the average input energy can be written in terms of the average coefficient energy as

$$\bar{x}^2 = \frac{1}{N} \sum_{m=1}^{N} \frac{1}{K} \sum_{k=0}^{K-1} [\alpha_m(k)]^2 = \frac{1}{N} \sum_{m=1}^{N} \bar{\alpha}_m^2 \tag{2.2.5}$$

where $\bar{\alpha}_m^2$ denotes the average energy of the $\alpha_m(k)$ sequence. Thus the input energy has been redistributed among the coefficients or a portion of the input energy has been captured by each coefficient sequence.

For a subspace representation the input is approximated by $\tilde{x}^*(p)$ formed from the concatenation of the approximating N-length sequences $\tilde{x}_k(n)$ obtained from the $\alpha_m(k)$. The average energy for the sequence $x^*(p)$ represents the total portion of input energy captured by the successive approximations. For an orthonormal transformation this energy is given as in equation (2.2.4) by

$$\bar{\tilde{x}}^2 = \frac{1}{P} \sum_{p=0}^{P-1} [\tilde{x}^*(p)]^2 = \frac{1}{P} \sum_{m=1}^{M} \sum_{k=0}^{K-1} [\alpha_m(k)]^2 , \tag{2.2.6}$$

or in terms of average coefficient energy as

$$\bar{\tilde{x}}^2 = \frac{1}{N} \sum_{m=1}^{M} \bar{\alpha}_m^2 . \tag{2.2.7}$$

Likewise, the average error energy is

$$\bar{e}_x^2 = \frac{1}{P} \sum_{p=0}^{P-1} [e_x^*(p)]^2 = \frac{1}{N} \sum_{m=M+1}^{N} \bar{\alpha}_m^2 . \tag{2.2.8}$$

The ratio of the energy in the $\tilde{x}^*(p)$ sequence to the energy in the $x^*(p)$ sequence provides a measure of the total energy capture for the subspace representation. This ratio is called the energy packing efficiency (EPE) after Kitajima [22] and later Yip and Rao [7] who considered the ratio of coefficient variances for stationary processes. The EPE in terms of the orthonormal basis coefficients is given using equations (2.2.5) and (2.2.6) as

$$\text{EPE} = \frac{1/N \sum_{m=1}^{M} \bar{\alpha}_m^2}{1/N \sum_{m=1}^{N} \bar{\alpha}_m^2} . \tag{2.2.9}$$

A plot of $\bar{\alpha}_m^{-2}$ versus M for a source sequence can be viewed as a discrete energy distribution. The EPE as a function of M can be viewed as a discrete cumulative energy distribution. The $\bar{\alpha}_m^{-2}$ can be used as a measure of the energy of a coefficient sequence for bit allocation and subspace determination.

2.3 Finite Impulse Response (FIR) Filter Bank Model

In Section 2.2 the idea of energy capture was introduced and equations were developed involving the energy in the coefficient sequence resulting from orthonormal transformation or projection of successive segments of an input sequence. To be able to assess the merit of transform coding of presample filtered data and make an a-priori subspace selection and bit allocation, a means of estimating the coefficient energy is needed. This has been done for some applications, particularly speech data compression based on statistics and models derived from knowledge of the source generation mechanism. Some authors have used test cases of typical sources to generate estimates of the coefficient energy or variance. In all cases some knowledge, assumed or generated, of the signal source for specific applications is required. The knowledge that is available for the application considered here is that the source has been acted upon by a low-pass presample filter with known transfer function. In this section the presample filter transfer function is assumed to provide a worst case spectral envelope (power spectral density) for the signal to be sampled and transformed. Transformation using an orthonormal basis is modeled in the form of an FIR filter bank. Expressions to determine the maximum coefficient

energy that would result from transformation of segments of sampled filter output are then derived from the use of Parseval's theorem.

Recall the inner product equation (2.1.15) for the determination of a basis coefficient for the k^{th} input segment

$$\alpha_m(k) = \langle \underline{\phi}_m, \underline{x}_k \rangle \ , \tag{2.3.1}$$

or in terms of the sequence segment and reference sequence

$$\alpha_m(k) = \sum_{n=0}^{N-1} \phi_m(n) x_k(n) \ . \tag{2.3.2}$$

This equation has the form of a discrete finite convolution. Define a new sequence $h_m(n)$ as

$$h_m(n) = \phi_m(N - n), \quad n = 0,1,\ldots,N - 1; \tag{2.3.3}$$

that is, this new sequence is equal to the reverse order reference (basis) sequence. Recalling that $x_k(n)$ represents the n^{th} point in the k^{th} segment of input $x^*(p)$, or that

$$x_k(n) = x^*(kN + n) \ , \tag{2.3.4}$$

equation (2.3.2) can be rewritten as

$$\alpha_m(k) = \sum_{n=0}^{N-1} h_m(N - 1 - n)\, x^*(kN + n) \tag{2.3.5}$$

or

$$\alpha_m(k) = \sum_{n=0}^{N-1} h_m(n)\, x^*[(k + 1)N - 1 - n] \ . \tag{2.3.6}$$

Then $\alpha_m(k)$ can be considered as samples of an output sequence $\alpha_m^*(p)$, that results from an FIR filter with impulse response $h_m(n)$ acting upon the input sequence $x^*(p)$. The model is shown in Figure 2.1. This FIR filter bank model is equivalent to a running generalized spectral waveform analyzer [27, 30, 31].

The average transformation coefficient energy is equal to the average energy of the sampled sequence $\alpha_m(k)$. However, it is assumed that the average energy of the sequence $\alpha_m^*(p)$ is equal to that of the sampled sequence. If $\alpha^*(p)$ is assumed to be zero before and after the interval of consideration, that is, for $p \notin [0, P]$, the energy in the $\alpha_m^*(p)$ sequence is given by Parseval's theorem as

$$\sum_{p=0}^{p-1} [\alpha_m^*(p)]^2 = \frac{1}{2\pi} \int_{-\pi}^{\pi} |A_m(e^{j\omega})|^2 \, d\omega \qquad (2.3.7)$$

where $A_m(e^{j\omega})$ is the discrete Fourier transform (z-transform evaluated on the unit circle) of the sequence $\alpha_m^*(p)$. The error introduced by this assumption is small for intervals much larger than the impulse durations of the filters involved. It is known from discrete linear system theory that

$$A_m(e^{j\omega}) = H_m(e^{j\omega}) \, X^*(e^{j\omega}) \qquad (2.3.8)$$

where $H_m(e^{j\omega})$ is the Fourier transform of the impulse sequence $h_m(n)$ and $X^*(e^{j\omega})$ is the Fourier transform of the sampled low-pass presample filter output $x^*(p)$. So equation (2.3.7) can be written as

$$\sum_{p=0}^{p-1} [\alpha^*(p)]^2 = \frac{1}{2\pi} \int_{-\pi}^{\pi} |H_m(e^{j\omega})|^2 \, |X^*(e^{j\omega})|^2 \, d\omega \, . \qquad (2.3.9)$$

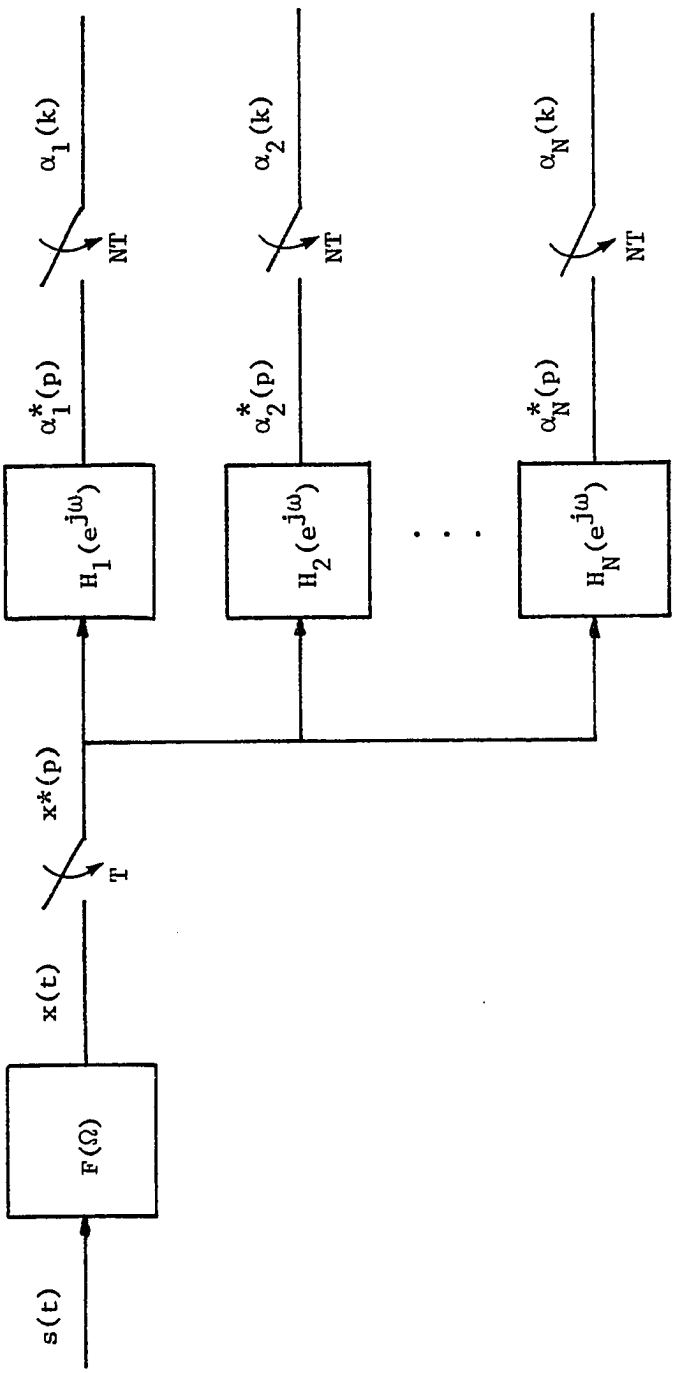

Figure 2.1. Filter Bank Model.

The magnitude squared α_m-filter transfer function $|H_m(e^{j\omega})|^2$ can be viewed as a spectral representation of the way in which the energy in the input sequence is captured by coefficient α_m. This same sort of energy capture or redistribution is encountered when using the discrete Fourier transform (basis) for spectral estimation. In that case it is generally undesirable and is called spectral energy leakage.

Assuming bandlimited sampling of the presample filter output, which is the function of the filter, the discrete Fourier transform of the sequence $x^*(p)$ derived from uniform sample $x(t)$ is

$$X^*(e^{j\omega}) = X_A\left(\frac{\omega}{T}\right) \tag{2.3.10}$$

where T is the sampling interval and $X_A(\Omega)$ is the Fourier transform of the analog signal $x(t)$. From linear system theory we know

$$X_A(\Omega) = F_A(\Omega)\, S_A(\Omega) \tag{2.3.11}$$

where $F_A(\Omega)$ is the presample filter transfer function and $S_A(\Omega)$ is the Fourier transform of the filter input $s(t)$. Thus the magnitude squared transform of the coefficient sequence can be written as

$$|A_m(e^{j\omega})|^2 = |H_m(e^{j\omega})|^2 |F^*(e^{j\omega})|^2 |S'(e^{j\omega})|^2 . \tag{2.3.12}$$

Here $S'(e^{j\omega})$ is not the Fourier transform of a sequence derived from sampling the filter input $s(t)$, but represents the effect of $S(\Omega)$ on the presample filter output [28].

It can be seen from equation (2.3.12) that the energy in the coefficient sequence $\alpha^*(p)$ is a function of the α_m-filter (basis sequence), the presample filter transform function, and the filter input $s(t)$. The input is in general not known, thus presenting a dilemma.

A practical PCM data system is expected to accommodate any real, finite signal that may be input to the presample filter as long as the filter input dynamic range is not exceeded. The specification of the presample filter is typically based on the assumption that the filter provides a (bandlimiting) spectral envelope for all signals. In keeping with this idea, it is assumed that the worst case (maximum energy) filter output is generated by a white noise input (wideband compared to the filter bandwidth). That is $|X^*(e^{j\omega})|^2 = \kappa|F(e^{j\omega})|^2$ where κ is a scale factor represents the worst case spectrum or poser spectral density of the filter output. Making this assumption, the cascade of the presample filter and the α_m-filter provide a spectral envelope for determining the maximum energy of a coefficient sequence. Then the expression

$$\bar{\alpha}_m^2 = \frac{\kappa}{2\pi\rho} \int_{-\pi}^{\pi} |F(e^{j\omega})|^2 |H_m(e^{j\omega})|^2 \, d\omega \qquad (2.3.13)$$

represents a bound on the maximum average energy for the α_m sequence. An expression of this same form results from assuming the input $x^*(p)$ is a stationary random process with $\frac{\kappa}{\rho}|F(e^{j\omega})|^2$ taken to be the power spectral density. Equation (2.3.13) then gives the variance of the FIR coefficient filter output process [1].

The FIR filter bank model and equations involving spectral interpretation provide insight into transform coding. Additional knowledge about the data source $s(t)$ is often in the form of spectral content or transfer function. Appropriate adjustment in equation (2.3.13) can be made to provide better estimates. Some judgment is still appropriate.

Since the α_m are being generated for an orthonormal basis, equation (2.2.r) leads to

$$\frac{1}{N}\sum \bar{\alpha}_m^2 = \frac{1}{N}\sum_{m=1}^{N}\frac{1}{2\pi}\int_{-\pi}^{\pi}|H_m(e^{j\omega})|^2|F(e^{j\omega})|^2\,d\omega$$

$$= \bar{x}^2 = \frac{1}{2\pi}\int_{-\pi}^{\pi}|F(e^{j\omega})|^2\,d\omega \qquad (2.3.14)$$

for any magnitude squared function $|F(e^{j\omega})|^2$. So, the expression

$$N\rho_m = \frac{\frac{1}{2\pi}\int_{-\pi}^{\pi}|H_m(e^{j\omega})|^2|F(e^{j\omega})|^2\,d\omega}{\frac{1}{2\pi}\int_{-\pi}^{\pi}|F(e^{j\omega})|^2\,d\omega} \qquad (2.3.15)$$

represents a normalized bound on the maximum average energy of coefficient α_m. This expression for $N\rho_m$ is assumed to be representative of the energy distribution for the basis. It can be seen by examination of equations (2.3.13) and (2.3.15) that the expected maximum energy in coefficient α_m would be

$$\bar{\alpha}^2 = N\rho_m\bar{x}^2 \qquad (2.3.16)$$

when $\bar{x}^2$, given by

$$\bar{x}^2 = \frac{1}{2\pi}\int_{-\pi}^{\pi}|F(e^{j\omega})|^2\,d\omega\,, \qquad (2.3.17)$$

represents the filter output signal energy. This is to be used to provide an a-priori method to estimate the maximum coefficient energy relative to the input energy for the purpose of bit allocation and basis comparison.

Note that for white, zero-mean noise with variance (energy) σ^2 as input to the α-filter bank, $|x(e^{j\omega})|^2 = \sigma^2$ a constant. Since

$$\sum_{n=0}^{N-1} h^2(n) = \frac{1}{2\pi} \int_{-\pi}^{\pi} |H_m(e^{j\omega})|^2 \, d\omega = 1 \qquad (2.3.18)$$

for orthonormal basis, equation (2.3.13) reduces to

$$\alpha_m^{-2} = \sigma^2$$

indicating white noise distributes equally among the coefficients.

2.4 Karhunen-Loueve (KL) Basis

It is well known that for a zero mean vector source $\underline{x}$ with $N \times N$ covariance matrix R_{xx}, the Karhunen-Loueve basis is optimum in the sense that when $M < N$ transform coefficients are used to represent the input vector, the expected value of the mean square error is minimum for all choices of M. It is also known that the KL provides the minimum bit rate as is to be shown in Section 2.6. The KL bases are the normalized eigenvectors of the covariance matrix R_{xx}. That is, they are solutions to the equation

$$R_{xx} \, \underline{\phi}_m = \lambda_m \, \underline{\phi}_m, \; m \in [1,N] \qquad (2.4.1)$$

where $\underline{\phi}_m$ represents the eigenvector associated with the eigenvalue λ_m. When a matrix Φ is used to perform a linear transformation from the source vector $\underline{x}$ into the coefficient vector $\underline{\alpha}$, the covariance matrix of $\underline{\alpha}$ is given by [27]

$$R_{\alpha\alpha} = \Phi \, R_{xx} \, \Phi^T . \qquad (2.4.2)$$

If Φ represents the $N \times N$ matrix of KL basis vectors

$$\Phi = [\underline{\phi}_1, \underline{\phi}_2, \cdots, \underline{\phi}_N] , \tag{2.4.3}$$

then

$$R_{\alpha\alpha} = \text{diag}[\lambda_m] \tag{2.4.4}$$

so that Φ diagonalizes the covariance matrix $R_{\alpha\alpha}$. Thus the KL basis is said to completely decorrelate the coefficients. Note that the variance (average energy) of the coefficient is equal to the eigenvalue. If the eigenvectors are arranged in order of decreasing eigenvalues, $\lambda_m > \lambda_{m+1}$, the choice for optimum $M < N$ representation are the eigenvectors associated with the first M eigenvalues. In statistics, representation of a vector source by the eigenvectors of the covariance is called expansion by principal components [13].

If the presample filter output were a zero-mean stationary source, the segments could be treated as a vector source and the covariance matrix could be formed using the autocorrelation sequence. The KL basis generated from this matrix would then be the optimum basis for sequence representation. The EPE would be given by

$$\text{EPE} = \frac{\sum_{m=1}^{M} \lambda_m}{\sum_{m=1}^{N} \lambda_m} . \tag{2.4.5}$$

In practice the KL basis is commonly generated from an estimate of the covariance matrix. Typically the entries are obtained from estimates of the source autocovariance sequence. If this is done for each sequence to be transformed (adaptively), it requires considerable computation prior to actual transformation and coding. If it is done a-priori, thus generating a fixed basis, the actual performance of the

KL basis becomes a function of the estimation process and changes as the actual source statistics change.

In this dissertation a covariance matrix is generated from the autocorrelation sequence that results from taking the inverse FFT of the magnitude squared presample filter transfer function $|F^*(e^{j\omega})|^2$. The eigenvectors of this matrix are used as the KL basis for the sampled, filtered source. If the presample filtered source is the result of a zero mean, white filter input, this KL transform is optimum and is sufficient to demonstrate that data compression is achievable for filter induced redundancy. This fixed, filter dependent KL basis is then used for comparison with two fixed, nonfilter dependent polynomial bases.

The length 16 KL basis resulting from a six-pole Butterworth magnitude squared spectrum to be presented in Chapter Three is shown in Figure 2.2. Note that the generated basis vectors have a smooth shape and can easily be ordered by sequencing or zero crossing. Note also that they are symmetric. The associated eigenvalues (expected coefficient energy) are given in Table 2.1. Note that they decrease monotonically with the sequency of the basis. Figure 2.2 also shows the spectral transfer functions for the FIR α-filters of this basis. These curves were obtained by performing a 256-point FFT on the basis generated $h_m(n)$ impulse response (with zero fill). It is not surprising that the main lobe of the transfer function increases with the number of zero crossings. It can been seen from these figures that the optimum basis and associated $|H_m(e^{j\omega})|^2$ generated by $|F^*(e^{j\omega})|^2$ are

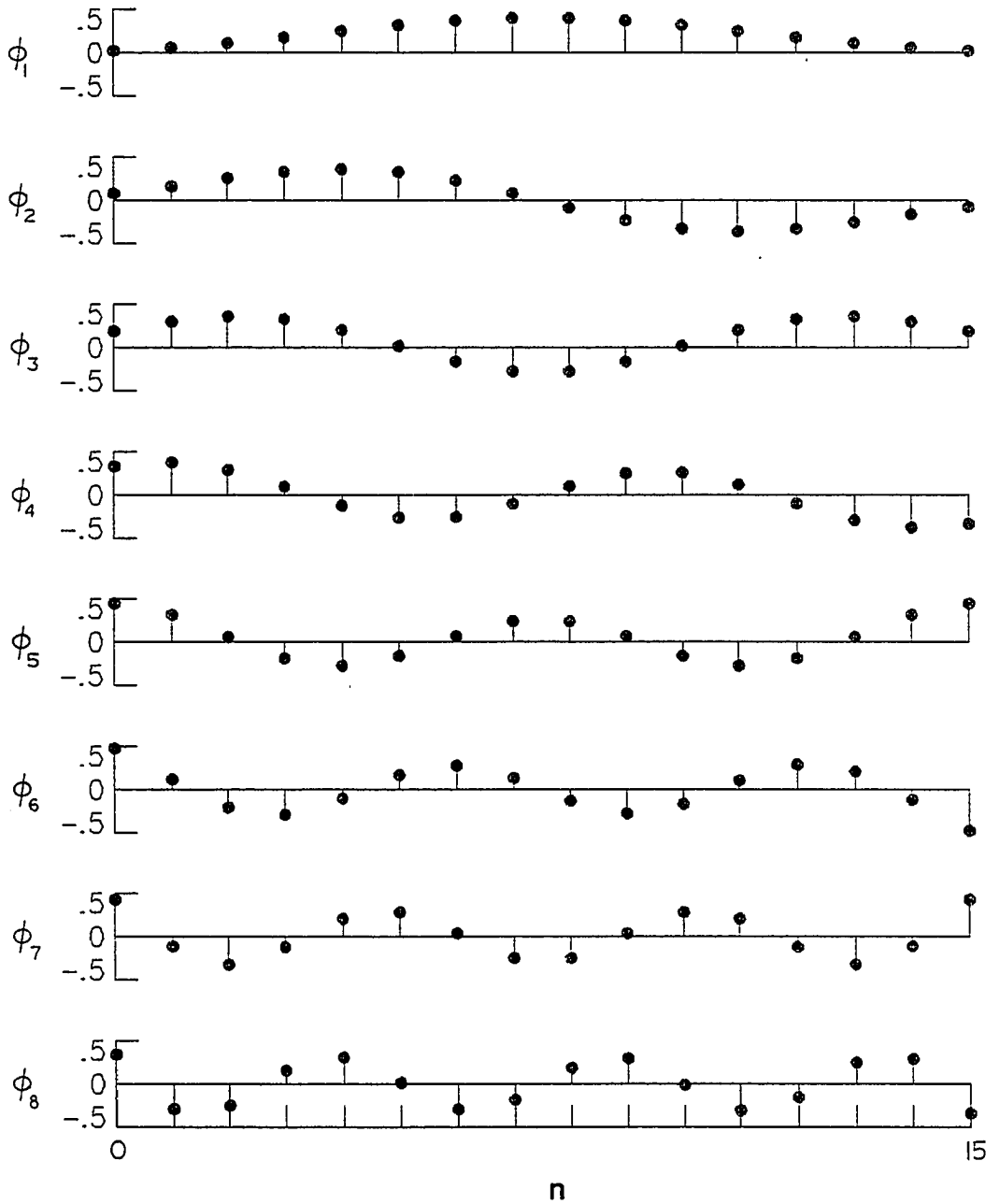

Figure 2.2(a). KL_4 Basis, $\phi_m(n)$, m = 1,...,8.

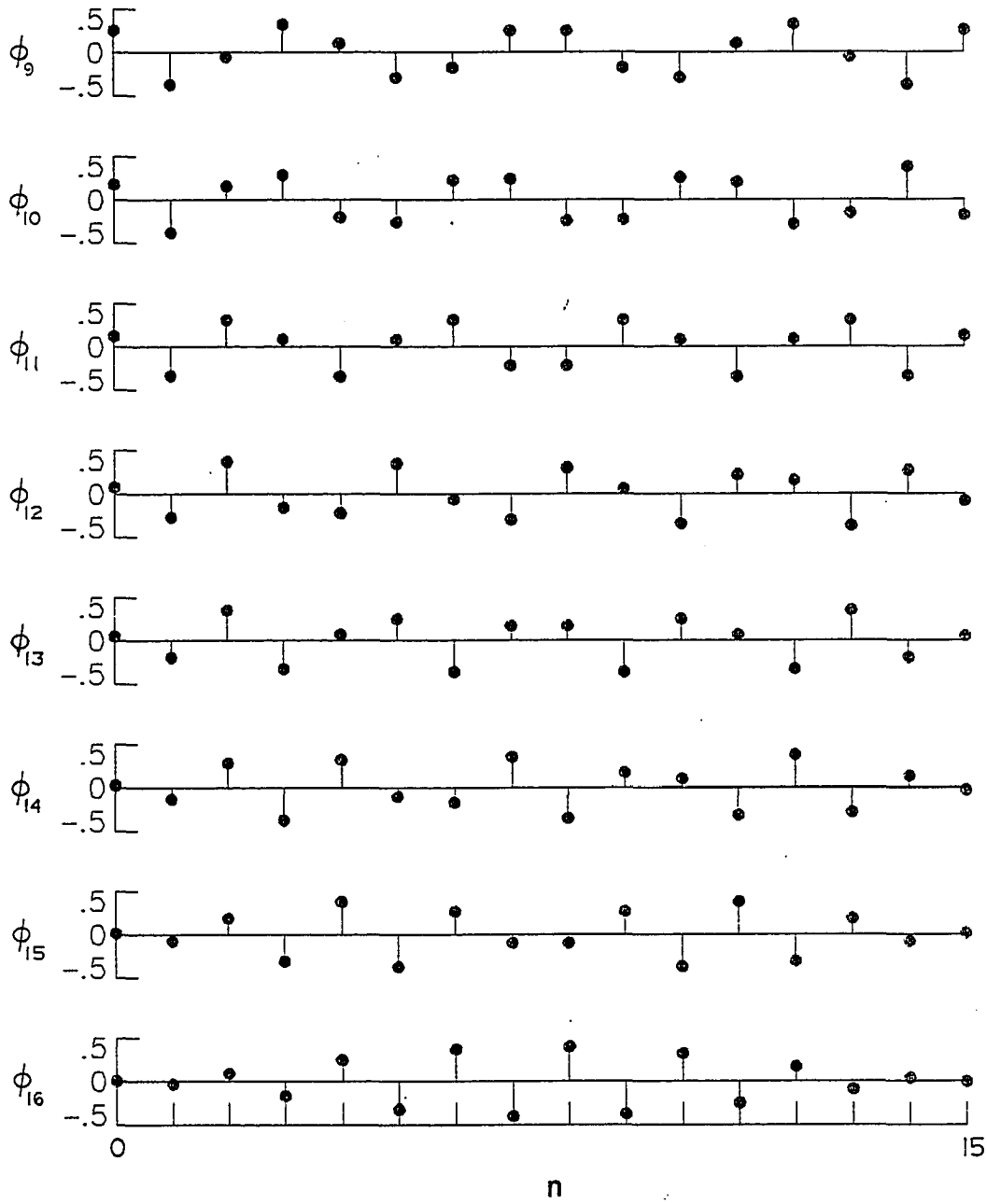

Figure 2.2(b). KL_4 Basis, $\phi_m(n)$, m = 9,...,16.

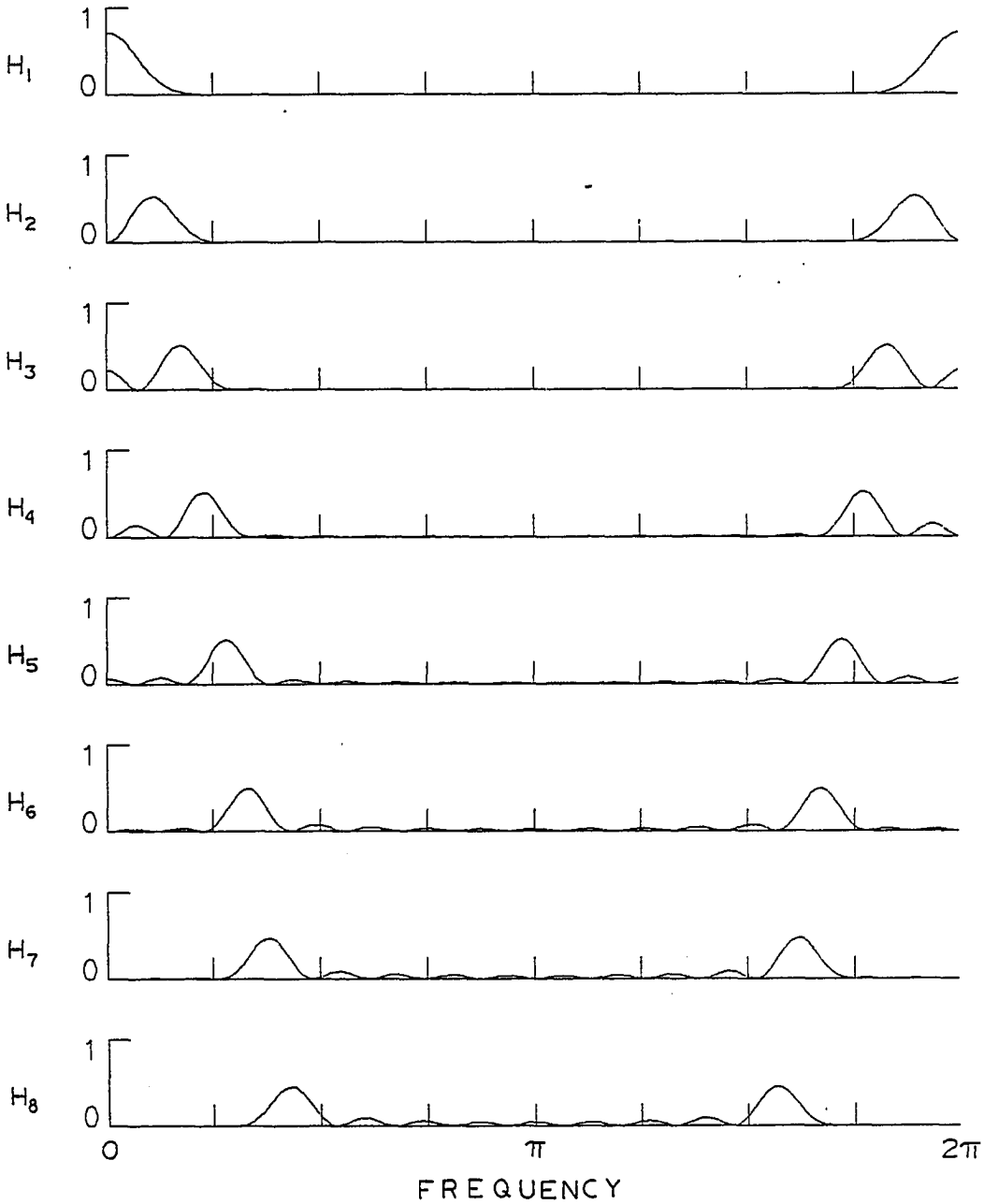

Figure 2.2(c). KL_4 Basis, $|H_m(e^{j\omega})|^2$, m = 1,...,8.

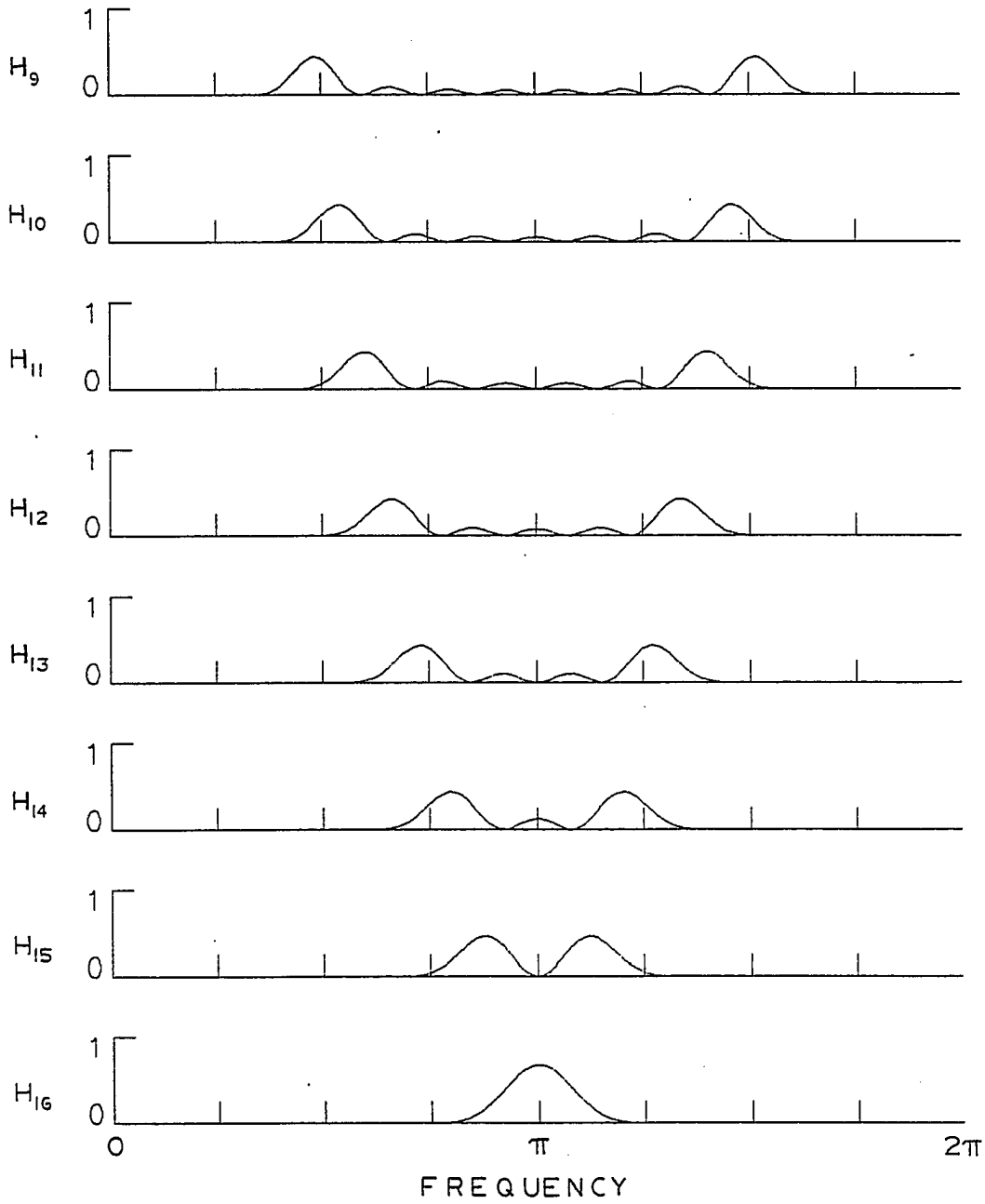

Figure 2.2(d). KL_4 Basis, $|H_m(e^{j\omega})|^2$, m = 9,...,16.

TABLE 2.1 EIGENVALUES OF KL_4, N = 16

m	VALUE
1	.9998
2	.9962
3	.9641
4	.8161
5	.4948
6	.1911
7	.527E-1
8	.127E-1
9	.304E-2
10	.764E-3
11	.204E-3
12	.581E-4
13	.173E-4
14	.532E-5
15	.161E-5
16	.460E-6

spectrally selective. Considering the equation for the expected coefficient variance of eigenvalue given by

$$\lambda_m = \frac{\kappa}{2\pi} \int_{-\pi}^{\pi} |F^*(e^{j\omega})|^2 |H_m(e^{j\omega})|^2 \, d\omega \quad , \tag{2.4.6}$$

this property is understandable and is anticipated to be characteristic of monotonically decreasing filter (power spectral density) functions. Note that the KL does not have a constant basis. Thus, if the process (sequence) under consideration has a mean or average value, it contributes (projects onto) more than one coefficient, predominately the first and third according to the $|H_m(e^{j\omega})|^2$ curves. This should be kept in mind if using the KL basis for nonzero mean sources.

2.5 Deterministic Polynomial Bases

2.5.1. Discrete Cosine (DC) Basis

The discrete cosine basis reported by Ahmed, Natarajan, and Rao [19] is suboptimal in that it is a fixed basis, and a function of N only. The DC basis has been shown to approach the performance of the KL basis for low order Markov processes [19, 20] and to experimentally approach the KL basis performance for speech [17, 20] and imagery [2, 29] applications. It is defined as

$$\begin{aligned} \phi_o(n) &= \frac{1}{\sqrt{N}} \; ; \; n = 0,\ldots,N-1 \\ \phi_m(n) &= \sqrt{\frac{2}{N}} \cos \frac{(2n+1)\, m\pi}{2N} \; ; \; n = 0,\ldots,N-1 \\ m &\neq 0 \end{aligned} \tag{2.5.1}$$

Ahmed and Rao show that the coefficients can be computed using a 2N-point FFT. This makes the DC transform computationally efficient, particularly for large values of N. They also show that the DC basis vectors are a form of discrete Chebychev polynomial. Figure 2.3 shows the N = 16 cosine basis and associated FIR α-filter functions ordered by sequency in the same manner as the KL basis. Note that they also have a smooth shape with spectrally selective $|H_m(e^{j\omega})|^2$ similar to the KL. Thus it is anticipated that it will have comparable performance. The DC basis is used frequently in practice as an alternative to the KL basis. It is included in this work for evaluation in the application to presample filtered data.

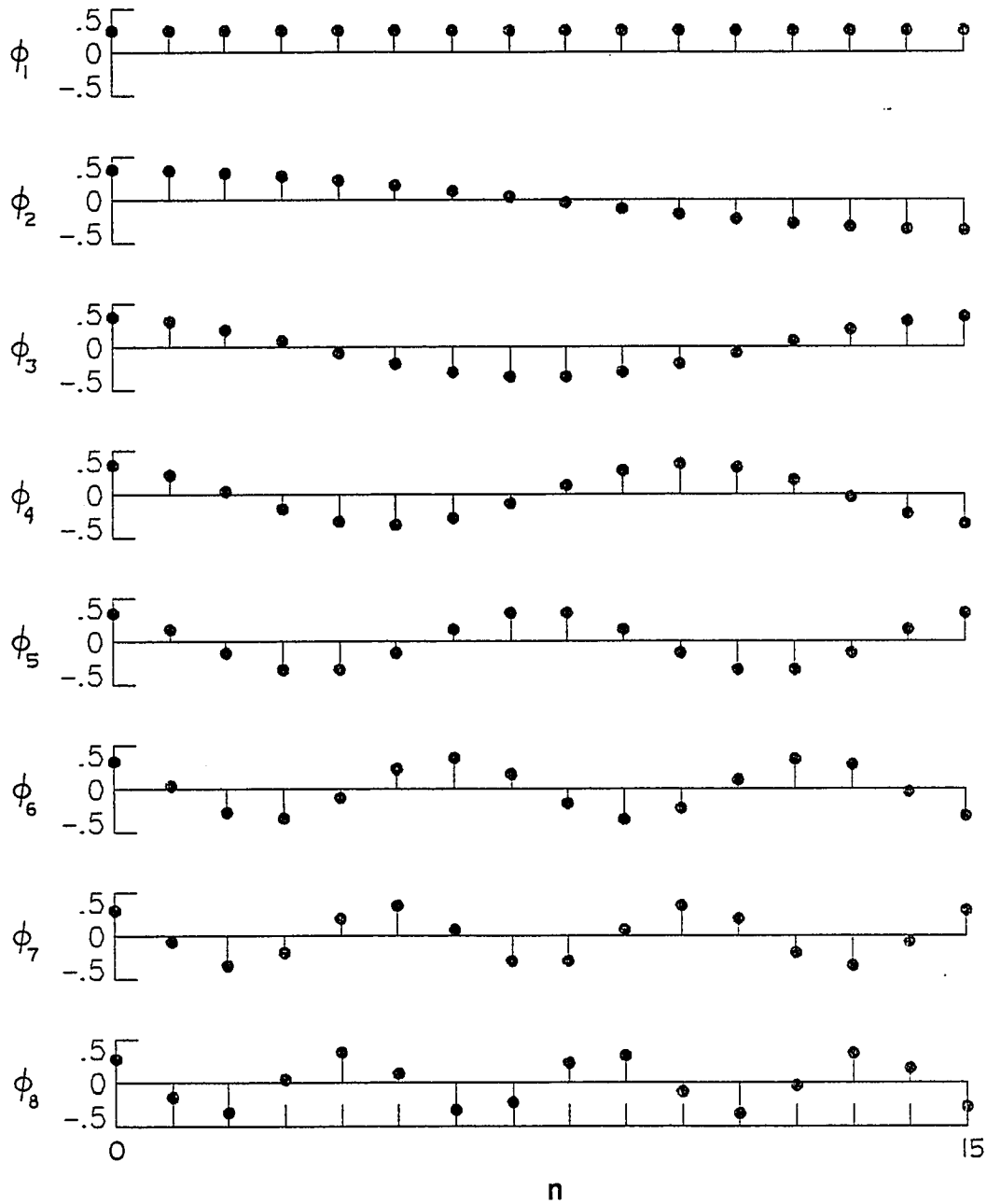

Figure 2.3(a). DC Basis, $\phi_m(n)$, m = 1,...,8.

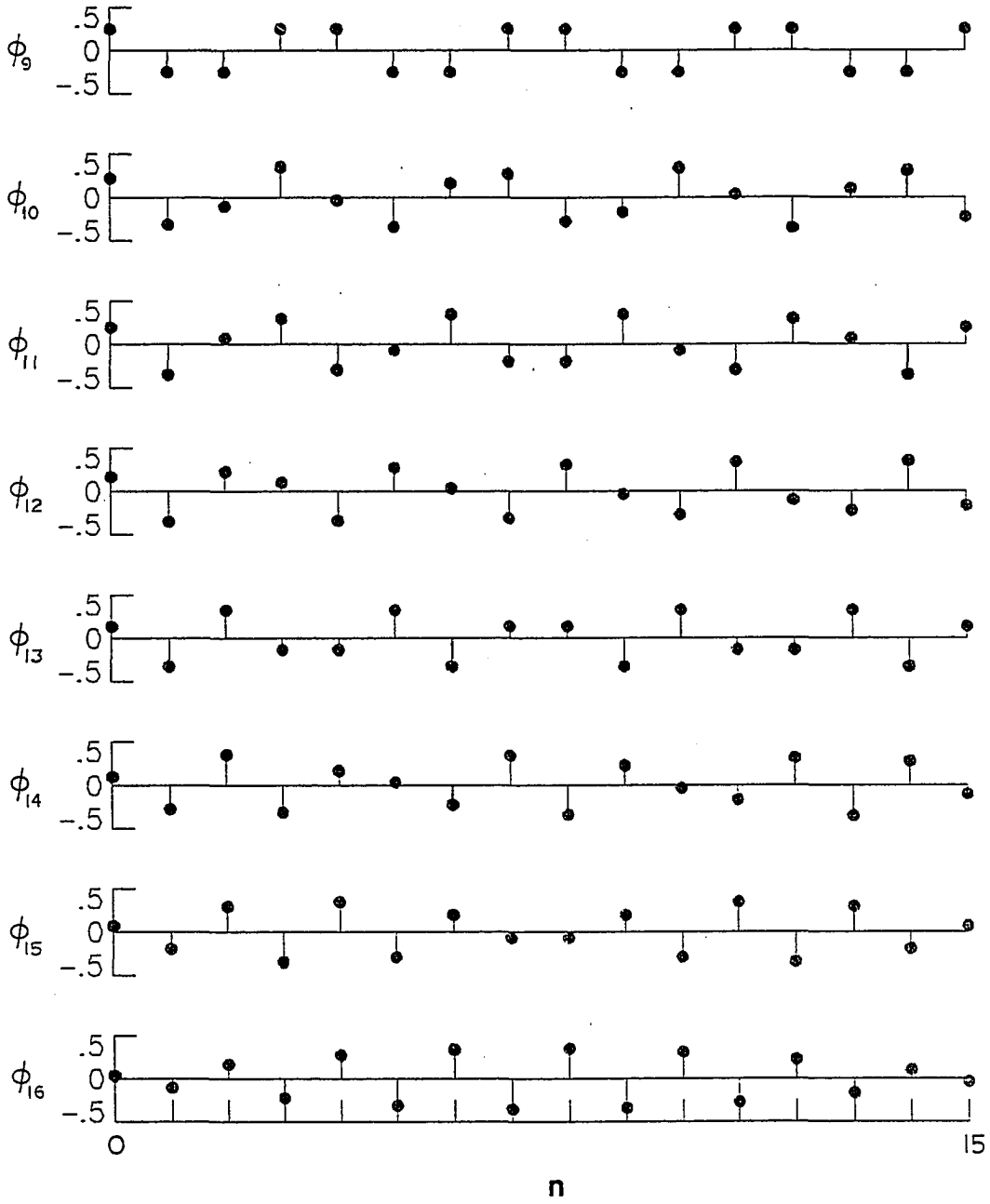

Figure 2.3(b). DC Basis, $\phi_m(n)$, m = 9,...,16.

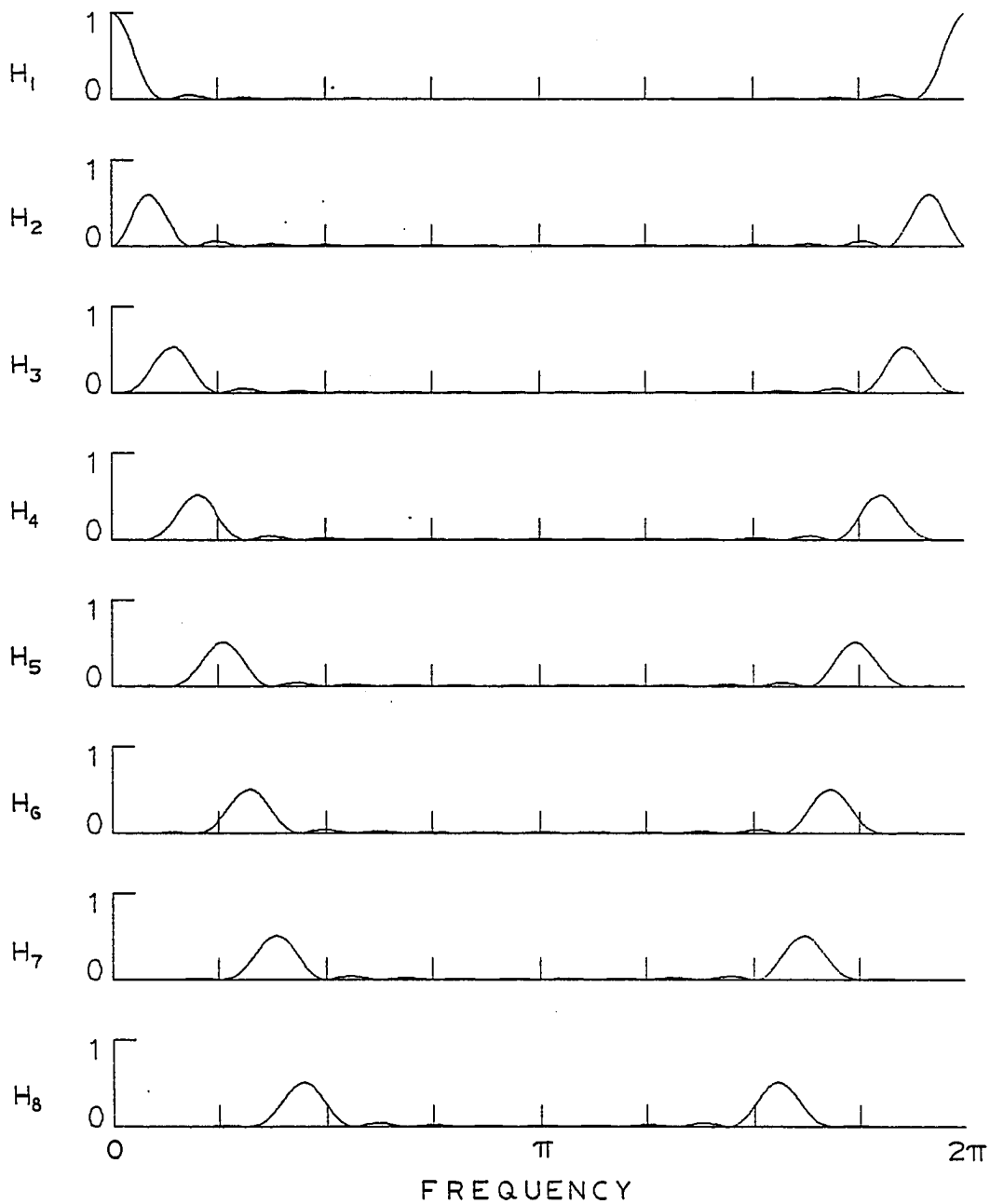

Figure 2.3(c). DC Basis, $|H_m(e^{j\omega})|^2$, m = 1,...,8.

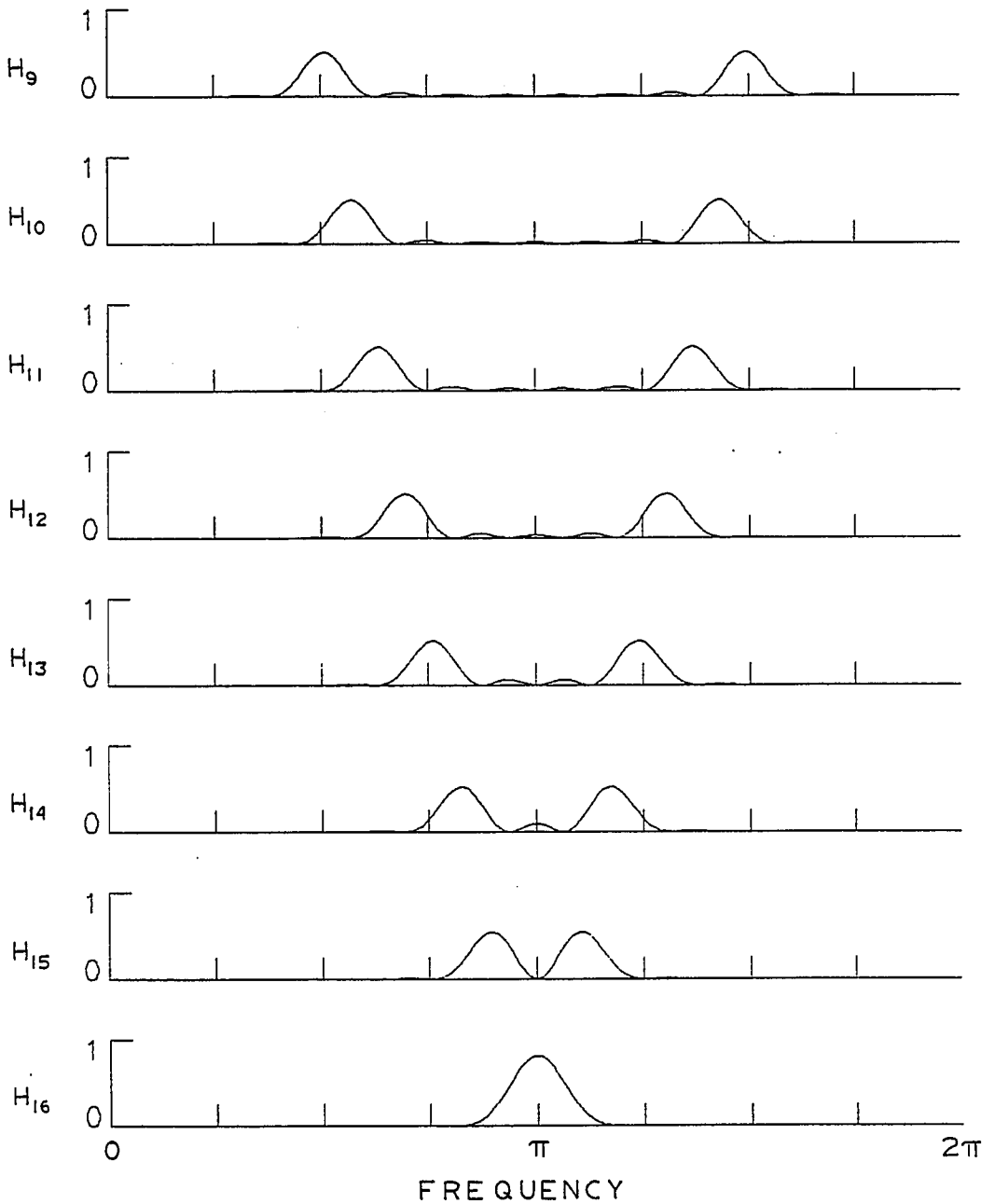

Figure 2.3(d). DC Basis, $|H_m(e^{j\omega})|^2$, m = 9,...,16.

2.5.2 Discrete Legendre (DL) Basis

The alternate deterministic basis that is of interest for this work is the discrete Legendre basis. It is formed from the orthonormalization of the basis of discrete ordinary polynomials $u_m(n) = n^m$ over the interval $n \in [0, N-1]$. This basis is considered because of the use of ordinary polynomials for the fitting and interpolation of real (telemetry) data with "low-pass" characteristic. As reported by Peterson [25], a set of discrete orthogonal polynomials $P_m(x_n)$ can be recursively generated from

$$P_1(x_n) = 1 \ ,$$
$$P_2(x_n) = x_n - \sum_{n=0}^{N-1} x_n / N \ , \tag{2.5.2a}$$

and

$$P_{m+1}(x_n) = (x_n - A_m) P_m(x_n) - B_m P_{m-1}(x_n) \tag{2.5.2b}$$

where

$$A_m = \sum_{n=0}^{N-1} x_n P_m^2(x_n)/W_m \ , \tag{2.5.2c}$$

$$B_m = W_m/W_{m-1} \ , \tag{2.5.2d}$$

and

$$W_m = \sum_{n=0}^{N-1} P_m^2(x_n) = \|P_m\|^2 \ . \tag{2.5.2e}$$

By letting $x_n = n$, $n = 0,\ldots, N - 1$ and scaling each polynomial so generated to produce unit norm, the orthonormal basis

$$\{\underline{\phi}_m = [\phi_m(0),\ldots, \phi_m(N - 1)]^T\} \tag{2.5.3}$$

where

$$\phi_m(n) = P_m(n)/W_m \tag{2.5.4}$$

is generated. This same basis can be generated by the Gram-Schmidt procedure [26] on the ordered polynomial basis

$$u_m(n) = n^m, \quad n = 0,\ldots, N - 1 . \tag{2.5.5}$$

Hence the name discrete Legendre basis [27].

Figure 2.4 shows the DL basis for $N = 16$ and associated $|H_m(e^{j\omega})|^2$ ordered according to sequency. Again note the similarity to the KL basis.

Since both the DC and DL bases resemble the KL, it is anticipated that representation of a filtered white sequence by either the DC or DL would have reasonable performance compared to that of the optimal KL. Note however, that the DC and DL have a constant (dc) basis which would capture any offset in the filter output.

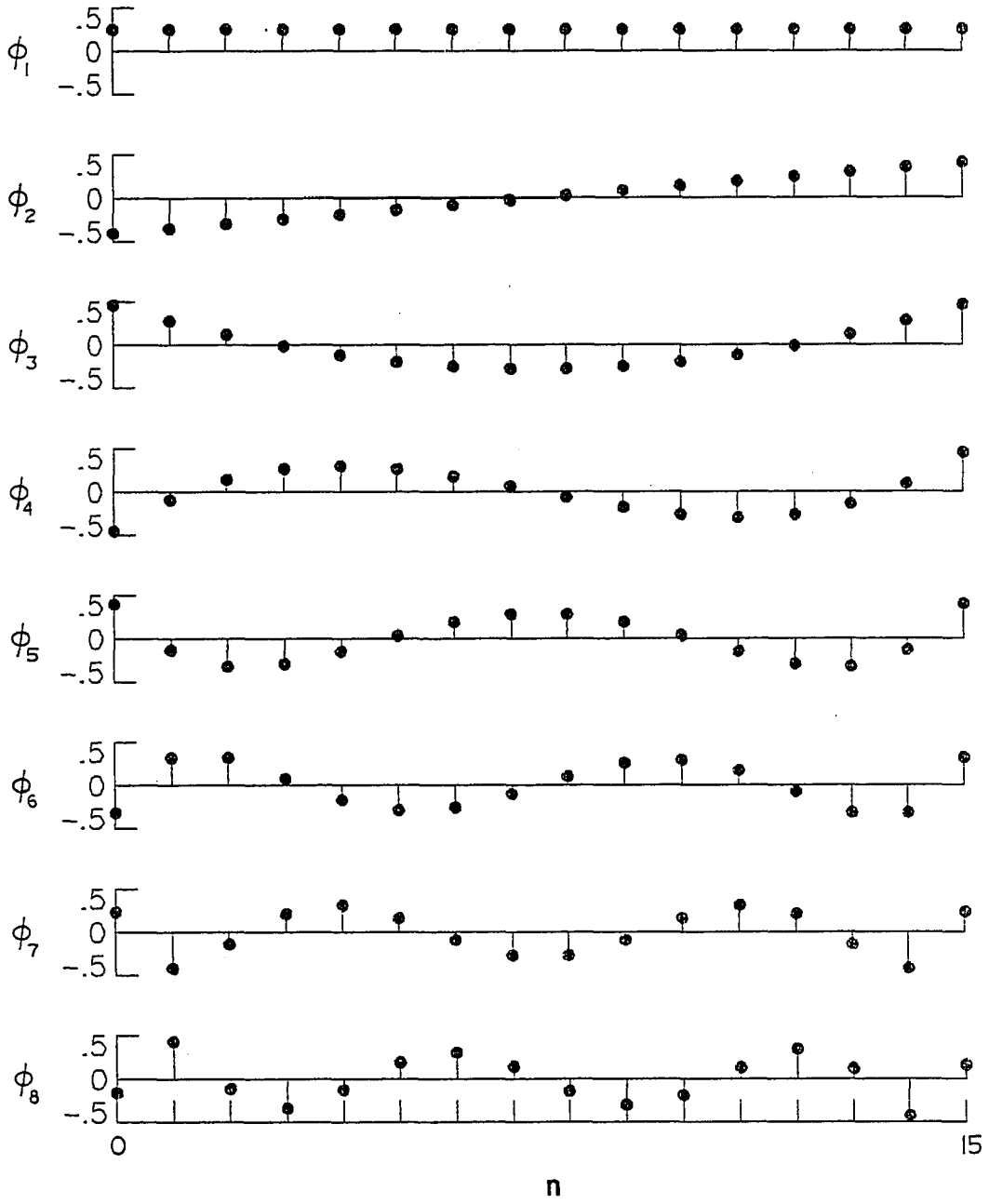

Figure 2.4(a). DL Basis, $\phi_m(n)$, m = 1,...,8.

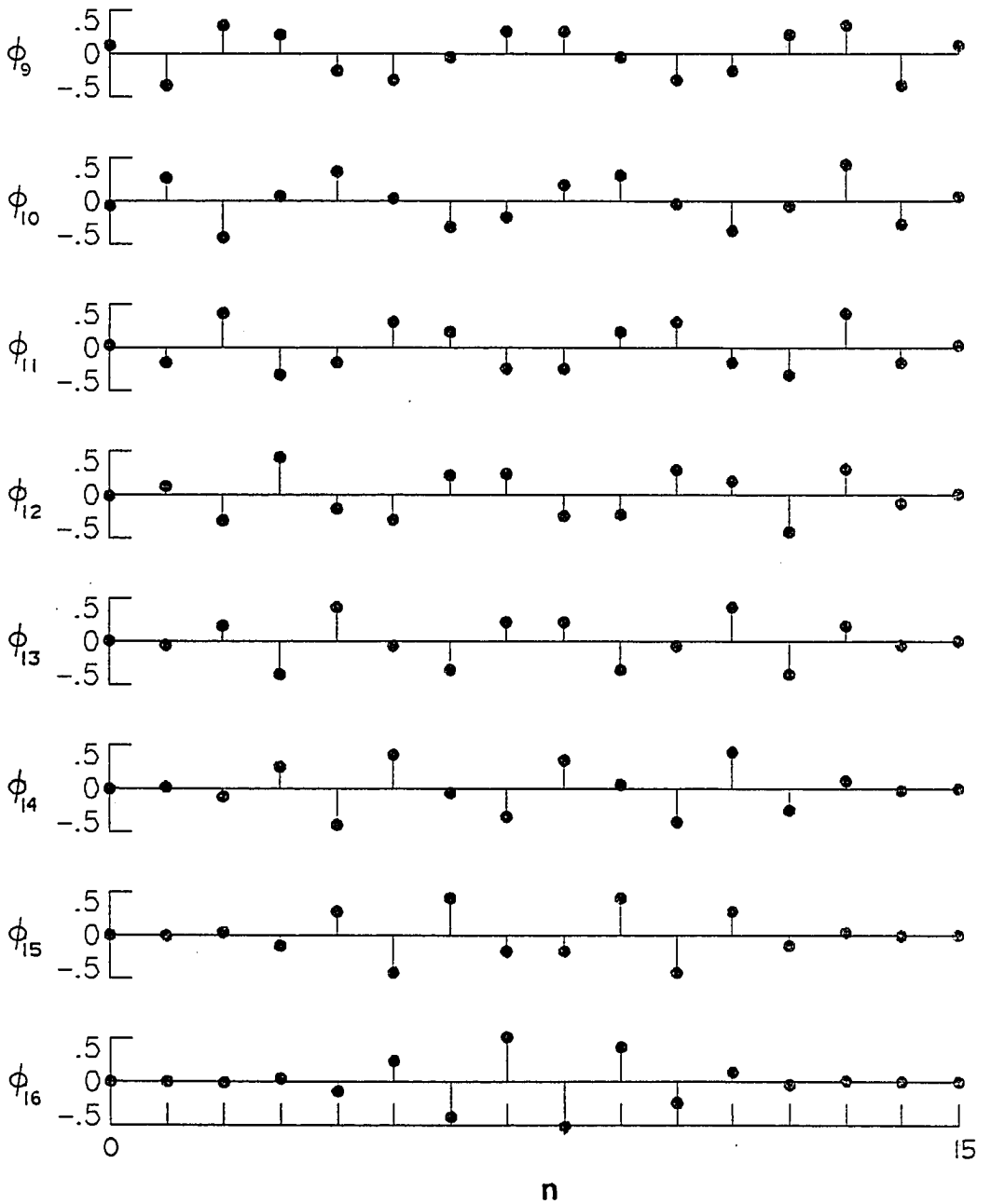

Figure 2.4(b). DL Basis, $\phi_m(n)$, m = 9,...,16.

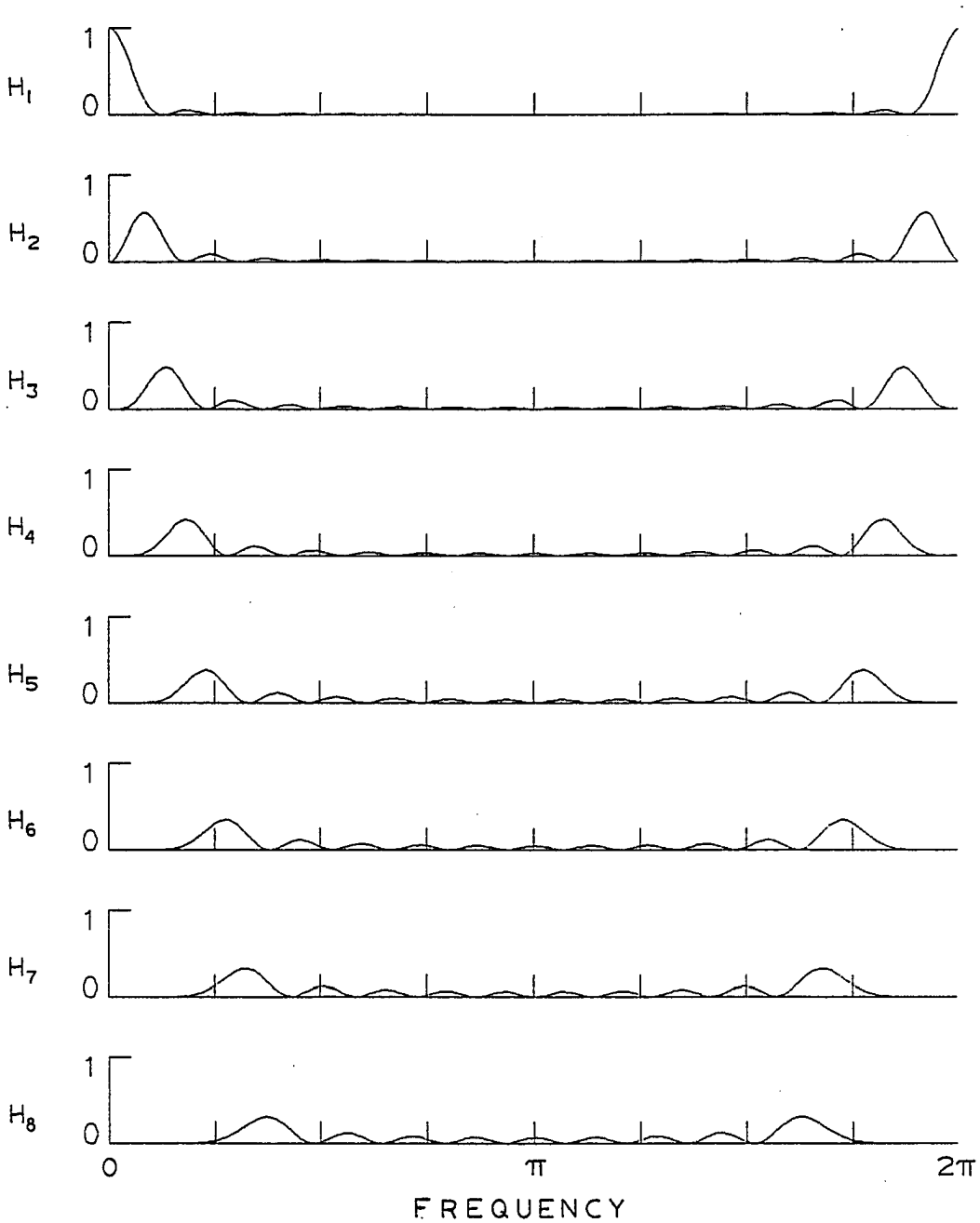

Figure 2.4(c). DL Basis, $|H_m(e^{j\omega})|^2$, m = 1,...,8.

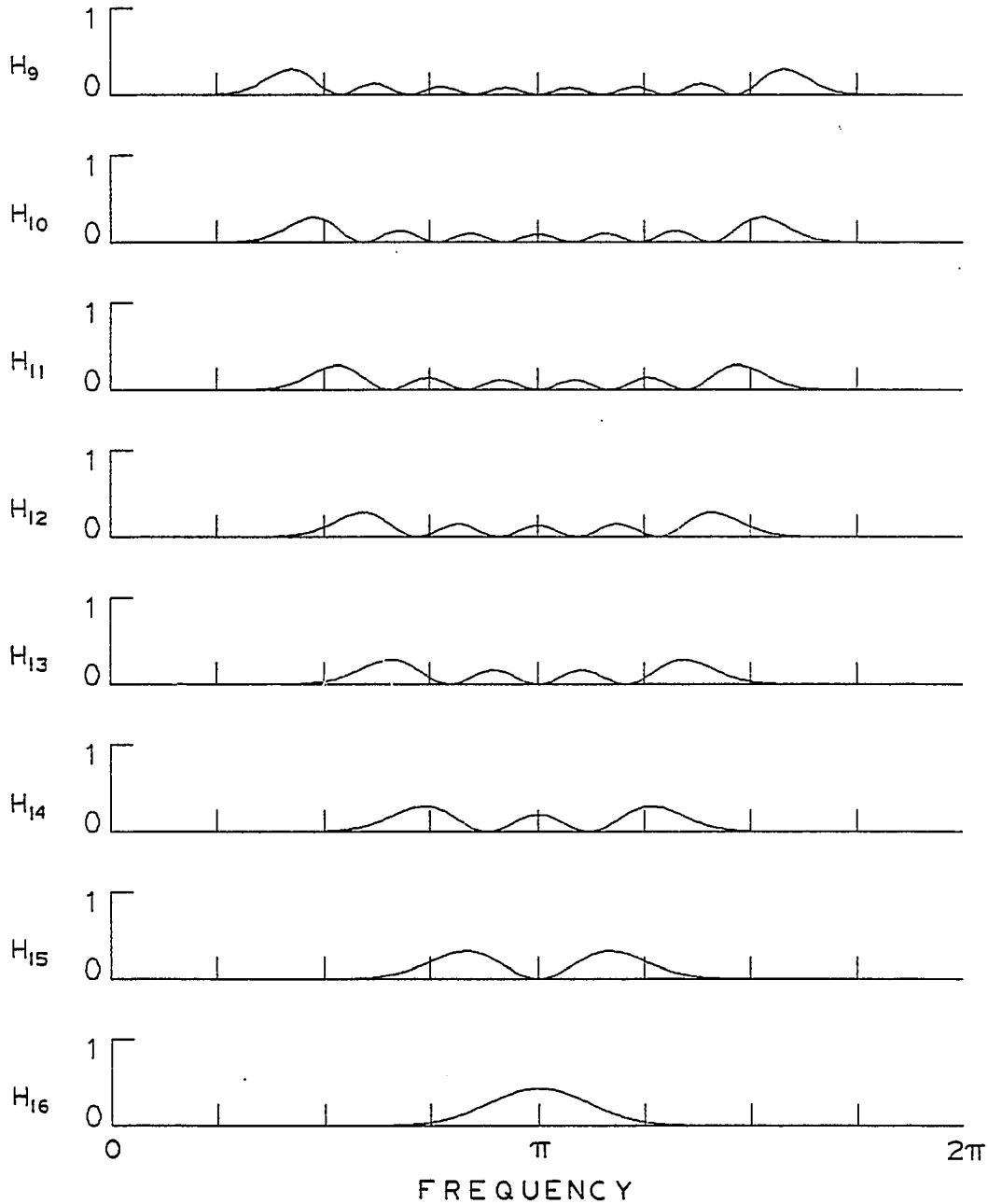

Figure 2.4(d). DL Basis, $|H_m(e^{j\omega})|^2$, m = 9,...,16.

2.6 Coefficient Quantizing and Bit Allocation

The selection of basis relative to the energy capture for subspace representation (sample reduction) is only one data compression aspect of transform coding. For telemetry applications where data is to be transmitted over a fixed rate channel, the coefficient used to represent the input must be quantized and encoded before transmission as do the samples in PCM. The strategy considered here is to quantize and encode the coefficients individually. This is called basis restricted transform coding after Pearl [4], or block quantization after Huang and Schultheiss [3] who were among the first to consider the use of block transformation for bit rate reduction. It is called simply transform coding in this dissertation. Even if all the coefficients are generated for transmission, energy redistribution resulting from transformation prior to quantization and coding can lead to a reduction in the total number of bits required to transmit the source sequence with the same specified mean square distortion as PCM. Since the focus of the application addressed here is to use transform coding in lieu of conventional PCM telemetry, the work presented in this dissertation is limited to the consideration of uniform quantizers common to practical telemetry systems. The coefficients, once quantized, are to be natural binary coded using a fixed number of bits (word length) per coefficient, but varying lengths over the set of coefficients. The purpose of the analysis to follow is to generate guidelines for the a-priori selection of quantization or distortion levels to be used for each coefficient, and determination of coefficient bit allocation.

Consider the generation and quantization of all N coefficients (full space representation) for each segment. The segment index k used in Sections 2.2 and 2.3 is implied but will not be used in the remainder of this dissertation unless needed for clarification. Quantizing a coefficient vector $\underline{\alpha}$ of the transformation input vector $\underline{x}$ produces a new coefficient vector

$$\hat{\underline{\alpha}} = \underline{\alpha} + \underline{\alpha}_Q \cdot \tag{2.6.1}$$

This introduces error in the reconstructed input at the receiver in the form of an additive error vector $\underline{e}_Q$. The reconstructed vector is

$$\hat{\underline{x}} = \Phi^T \underline{\alpha} + \Phi^T \underline{\alpha}_Q = \underline{x} + \underline{e}_Q \cdot \tag{2.6.2}$$

The squared error (distortion) in $\hat{\underline{x}}$ due to quantizing is then given by

$$\|\underline{x} - \hat{\underline{x}}\|^2 = \|\underline{e}_Q\|^2 \cdot \tag{2.6.3}$$

For an orthonormal basis, the quantizing error energy can be written as

$$\|\underline{e}_Q\|^2 = \sum_{m=1}^{N} \alpha_{Q,m}^2 = \sum_{m=1}^{N} D_m \tag{2.6.4}$$

where $\alpha_{Q,m}$ represents the components of $\underline{\alpha}_Q$ and $D_m = \alpha_{Q,m}^2$ is used to simplify the notation. As in Section 2.2 when the entire input sequence $x^*(\rho)$ is considered, the average error, denoted $\bar{e}_Q^2$, due to quantizing is

$$\bar{e}_Q^2 = \frac{1}{N} \sum_{m=1}^{N} \bar{\alpha}_{Q,m}^2 = \frac{1}{N} \sum_{m=1}^{N} \bar{D}_m \tag{2.6.5}$$

where $\bar{D}_m$ represents the average distortion energy of component α_m.

It has been shown in Section 2.2 that transformation leads to the distribution of input energy among the coefficient sequences. In general, the average energies $\bar{\alpha}_m^2$ of the coefficients are not the same. Thus the optimum quantization may involve different quantization levels (distortion $\bar{D}_m$) and a different number of levels for each coefficient. In order to examine this, let the number of levels used for coefficient α_m be expressed as 2^{B_m}. Then B_m represents the (noninteger) number of bits required to represent the coefficient. As suggested by Zelinski and Noll [17], B_m can be written as a function of the average coefficient energy $\bar{\alpha}_m^2$ and the average coefficient quantization distortion $\bar{D}_m$ as

$$B_m = \delta_m + \frac{1}{2} \log_2(\bar{\alpha}_m^2/\bar{D}_m) \tag{2.6.6}$$

where δ_m reflects the performance of practical quantizers and, in general, is a function of the distribution or crest factor of the coefficient sequence. Note that $\delta_m = 0$ gives the Shannon rate distortion limit, in terms of information bits, for a discrete Gaussian source with Gaussian distortion. It also gives the expression used for selecting the number of bits for uniform quantizing of uniform sources [27]. Following the logic of Zelinski and Noll, the coefficient distributions or crest factors are assumed to be equal for each coefficient so that δ_m is replaced by a constant, denoted δ_{TC}, for each coefficient quantizer and the fact that B_m should be an integer for binary coding is overlooked. The distortion contributed by coefficient α_m is then given, using equation (2.6.6), by

$$\bar{D}_m = 2^{\delta_{TC}} 2^{-2B_m} \bar{\alpha}_m^2 . \tag{2.6.7}$$

The problem then is to select B_m so as to minimize the average distortion subject to the constraint of fixed total bit allocation. The method of Lagrange multipliers can be used to minimize the total average distortion $\bar{D} = \frac{1}{N} \sum_{m=1}^{N} \bar{D}_m$, subject to $\sum_{m=1}^{N} B_m = NB_{TC}$ a constant, by setting

$$\frac{\partial}{\partial B_m} \left[\frac{1}{N} \sum_{m=1}^{N} D_m + \beta \left(\sum_{m=1}^{N} B_m - NB_{TC} \right) \right]$$

$$= -\frac{1}{N} 2^{\delta_{TC}} \sigma_m^{-2} 2^{-2B_m} 2 \ln 2 + \beta = 0 \qquad (2.6.8)$$

for $m = 1,\ldots,N$. It follows that

$$2^{2\delta_{TC}} 2^{-2B_m} \sigma_m^{-2} = N\beta/2 \ln 2 \qquad (2.6.9)$$

a constant for each m. So the optimum quantizing level and corresponding bit assignment are those for which $\bar{D}_m = \bar{D}_{TC}$, a constant for all m. This result was first derived by Huang and Schultheiss [3] for Gaussian sources and has been used by many authors since. Note that this result also holds for any subset of M coefficients as long as the constraint and averages are imposed on the subset. When this condition is imposed it leads to an expression for B_m in terms of the geometric mean of the coefficient energies,

$$B_m = B_{TC} + \frac{1}{2} \log_2 \left[\sigma_m^{-2} \Big/ \left(\prod_{m=1}^{N} \sigma_m^{-2} \right)^{1/N} \right] , \qquad (2.6.10)$$

where $B_{TC} = \frac{1}{N} \sum_{m=1}^{N} B_m$ is the average bit rate per coefficient. It is interesting to note that Zelinski and Noll show that the geometric mean, and hence the bit rate for stationary sources, is minimized by the KL

transform. This was also derived by Huang and Schultheiss. Thus near-optimal bit rate can be expected when employing a basis similiar to the KL.

For PCM, which can be considered the identity transform, the average distortion can be obtained from equation (2.6.6), with $\bar{\alpha}_m$ replaced by $\bar{x}^2$, as

$$\bar{D}_{PCM} = 2^{\delta_{PCM}} 2^{-2B_{PCM}} \bar{x}^2 \qquad (2.6.11)$$

where B_{PCM} is the PCM bit rate per sample. Again following Zelinski and Noll, the same quantization mechanism is assumed for both the coefficients sequence and the input sequence (PCM), that is, it is assumed that the crest factor is not appreciably altered by transformation. Then $\delta_{PCM} = \delta_{TC}$, and the expression for the average transform coding bit rate to give the same distortion as PCM is obtained by setting equation (2.6.7) equal to equation (2.6.11) and solving for B_{TC}. This gives

$$B_{TC} = B_{PCM}\left[-\frac{1}{2} \log_2 \bar{x}^2 \Big/ \left(\prod_{m=1}^{N} \bar{\alpha}_m^2 \right)^{1/N} \right] = B_{PCM} + \Delta B. \qquad (2.6.12)$$

With appropriate redefinition of terms the equations here can be seen to be the same as those of Campanella and Robinson [8]. Since the equations above are derived without requiring integer values for B_m, further coding, such as Huffman coding, would have to be employed to attain the reduction of (2.6.12). Actual integer bit allocation involves some trial and error and consideration of the assumption $\delta_m = \delta_{TC} = \delta_{PCM}$.

Equation (2.6.12) provides a useful analytical measure in the form of a rate improvement bound given by

$$\Delta B = -\frac{1}{2}\log_2\left[\bar{x}^2 \Big/ \left(\prod_{m=1}^{N}\bar{\alpha}_m^2\right)^{1/N}\right] \qquad (2.6.13)$$

for the comparison of bases. This is equivalent to the ratio of total information (minimum bit rate) in N independent identically distributed sources given by $\sum_{n=1}^{N}\frac{1}{2}\log_2\bar{\alpha}_m^2$ where PCM is treated as N sources with average energy $\bar{x}^2$. Equation (2.3.16) can be used to write this in terms of the normalized estimate of average coefficient energy $N\rho_m$ as

$$\Delta B = -\frac{1}{2}\log_2\left[N\left(\prod_{m=1}^{N}\rho_m\right)^{1/N}\right] . \qquad (2.6.14)$$

This equation is used in Chapter Three for basis comparison.

As a guide in actual bit assignment, the value of B_{TC} from equation (2.6.12) can be substituted into equation (2.6.10) to give

$$B_m = B_{PCM} - \frac{1}{2}\log_2\left(\bar{x}^2/\bar{\alpha}_m^2\right) . \qquad (2.6.15)$$

Equation (2.6.15) can also be written in terms of ρ_m as

$$B_m = B_{PCM} + \frac{1}{2}\log_2(N\rho_m) . \qquad (2.6.16)$$

Note that this equation simply provides the appropriate adjustment in bit allocation for two sources of different energies in order to maintain equal quantization distortion. This is essentially a dynamic range adjustment to accommodate the same quantization level. This equation is used in Chapter Four for generation of actual integer bit allocation.

Bit allocation itself can lead to the discarding of coefficients. Equation (2.6.16) can produce negative B_m indicating zero bits should be used, or the coefficient α_m should be discarded. When coefficients are a-priori discarded for any reason, the average quantizing distortion present in the reconstructed input is

$$\bar{D}'_{TC} = \frac{1}{N} \sum_{m=1}^{M} \bar{D}_{TC} + \frac{1}{N} \sum_{m=M+1}^{N} \bar{\alpha}_m^2 \qquad (2.6.17)$$

where α_m, $m \in [M + 1, N]$, represents the set of discarded coefficients. This is less than $\bar{D}_{TC}$ if the energy of a coefficient is less than the desired distortion, i.e. $\bar{\alpha}_m^2 < \bar{D}_{TC}$.

This effect can be written in vector notation by writing the reconstructed vector as

$$\hat{\underline{x}} = \tilde{\underline{x}} + \tilde{\underline{Q}} + \underline{e}_x \qquad (2.6.18)$$

where

$$\tilde{\underline{Q}} = \Phi^T \underline{\alpha}_Q, \quad \alpha_{Q,m} = 0, \quad \alpha_m \text{ discarded} \qquad (2.6.19)$$

$$\underline{e}_x = \Phi^T \underline{\alpha}, \quad \alpha_m = 0, \quad \alpha_m \text{ retained} \qquad (2.6.20)$$

and

$$\tilde{\underline{x}} = \Phi^T \underline{\alpha}, \quad \alpha_m = 0, \quad \alpha_m \text{ discarded.} \qquad (2.6.21)$$

The tilde is used to indicate that $\tilde{\underline{Q}}$ and $\tilde{\underline{x}}$ are contained in the same subspace W spanned by the basis corresponding to the retained coefficients. The error vector $\underline{e}_x$ is equivalent to the approximation error presented in Section 2.1 with respect to discarded components.

The error $\tilde{\underline{Q}}$ due to quantization of the retained (for whatever reason) coefficients is in addition to the error due to subspace representation. The combined error is

$$\hat{\underline{x}} - \underline{x} = \underline{e}_Q = \tilde{\underline{Q}} + \underline{e}_x \ . \tag{2.6.22}$$

Since $\tilde{\underline{Q}} \perp \underline{e}_x$,

$$\|\underline{e}_Q\|^2 = \|\tilde{\underline{Q}}\|^2 + \|\underline{e}_x\|^2 \tag{2.6.23}$$

which leads to an expression for the average reconstruction error energy as

$$\bar{e}_Q^2 = \bar{\tilde{Q}}^2 + \bar{e}_x^2 \tag{2.6.24}$$

where $\bar{\tilde{Q}}^2$ represents the average error due to quantizing the retained coefficients and $\bar{e}_x^2$ represents the average error due to discarded coefficients. Equation (2.6.24) can be seen to be equivalent to equation (2.6.17) and can be used to make error tradeoffs regarding the combined effects of subspace representation and quantizing.

2.7 Summary

The technique of transform coding is described and the way in which the method can produce bit rate reduction is presented. Transform coding is defined in terms of orthogonal transformation or projection in a Hilbert signal space. Useful properties of orthogonal transformation are presented for later use. The concept of energy distribution or energy capture by a transform coefficient sequence resulting from successive block transformation is introduced. Energy packing efficiency is defined. In order to provide insight into transform

coding, it is modeled in terms of a bank of finite impulse response filters equivalent to a generalized running waveform analyzer. The concept of spectral energy capture is thus introduced. The presample filter is incorporated into the analysis by assuming it defines the worst case spectral envelope (power spectral density) of the filter output and thus coding of a white filter input is taken to be the task of the transform coder. Parseval's relation is used to provide an expression for the estimate of the worst case coefficient energy. The three bases for consideration are presented. They are a filter derived Karhunen-Loueve (KL) basis, which is assumed to be optimum for the filtered source, the discrete cosine basis and the discrete Legendre basis. Both the discrete cosine and Legendre bases are seen to have properties similar to the KL and are anticipated to have comparable performance. Optimum coefficient quantizing and bit allocation are examined following the logic of Zelinski and Noll [17] with the result that each coefficient is to be quantized using the same quantization level that would be used for PCM. The bit allocation then becomes an adjustment of dynamic range. A theoretical bound for bit rate improvement is presented. This is only attainable by the use of something other than natural binary coding. Reconstruction error is shown to be the sum of coefficient quantizing error and error due to subspace representation.

CHAPTER THREE

ANALYTICAL COMPARISON

3.0 Introduction

In this chapter the analytical comparison of the three bases defined in Chapter Two is examined for the application to presample filtered random data. The rationale commonly used for filter specification for sampled data systems is discussed and the four filter magnitude squared transfer functions (MSF) used in the analysis are given in Section 3.1. The MSF's are used in the equations developed in Chapter Two and the resulting expected coefficient energy distribution and analytical bit rate improvement are presented in Sections 3.2 and 3.3, respectively. Section 3.4 introduces another view of the spectral energy capture of transform coding with a comparison for the bases under consideration in this dissertation. The chapter is summarized in Section 3.5.

3.1 Presample Filter

For sampled data (PCM) applications, analog filters are often used to bandlimit continuous signals prior to sampling. The filter output is then sampled uniformly at a rate of $1/T$ samples per second where T is the sample interval. Filters whose magnitude squared frequency response $|F(\Omega)|^2$, denoted MSF, is monotonically decreasing beyond the cutoff frequency and remains below some specified relative attenuation

level η, beyond $\Omega_s/2 = \pi/T$, the Nyquist or folding frequency, are consistant with practice. The level commonly used is $\eta = 2^{-2(B-1)}$ where B is the number of bits to be used for the natural binary (PCM) sample representation. The rationale for doing this is that spectral components of the filter output beyond the folding frequency resulting from full-scale filter inputs would be below the quantizing level and indiscernable from quantizing noise. This in effect normalizes the filter to the quantizing level and gives the highest cutoff to sample rate ratio possible for the filter order. This is often what is meant in practical systems by "bandlimited" signal. Note that if the filter MSF as described here is the sampled signal PSD and if η is the quantizing level for a uniform quantizer, then $\eta^2/12$ is the quantizing distortion and the transform coefficient expected energy (variance) is always greater than the quantization distortion. This can be seen from

$$\bar{\alpha}_m^2 = \frac{1}{2\pi} \int_{-\pi}^{\pi} |F(e^{j\omega})|^2 |H_m(e^{j\omega})|^2 \, d\omega$$

$$> \frac{1}{2\pi} \eta^2 \int_{-\pi}^{\pi} |H(e^{j\omega})|^2 \, d\omega = \eta^2 > \eta^2/12 \, . \qquad (3.1.1)$$

Thus no coefficient should be discarded as having less expected energy than the quantization distortion, and full space representation is needed for direct PCM replacement.

There are several well-known classes of analog filters that are used for telemetry applications. The commonly used Butterworth filter has been selected for use in this study. This filter class has maximally flat amplitude response in the pass band and monotonically

decreasing response beyond the cutoff frequency. The MSF as a function of radian frequency $\Omega = 2\pi f$ is given by

$$|F(\Omega)|^2 = \frac{1}{1 + (\Omega/\Omega_c)^{2\nu}} \tag{3.1.2}$$

where ν is the number of poles or filter order and Ω_c represents the radian cutoff frequency. The filter design trade-offs for sampled data applications involve the filter complexity, represented by the number of poles, the cutoff frequency (sometimes considered the highest frequency of interest), the sample rate, and the distortion level η. These quantities can be related by

$$|F(\Omega_s/2)|^2 \approx \left(\frac{\Omega_s}{2\Omega_c}\right)^{-2\nu} = \eta \tag{3.1.3}$$

which is used to specify the filters for this study. Plots of log (MSF) for the four filters used, designated filters F1 through F4, are shown in Figure 3.1 normalized to the sampling frequency. Filters F1 and F2 are based on actual filters used in two different aerospace telemetry systems. The other two are related to these through equation (3.1.3) by changing the number of poles and requiring the same value of η (same PCM word length). Since the coding is being done on the samples of the filter output, the transfer functions shown are actually plots of $|F^*(e^{j\omega})|^2$ where

$$|F^*(e^{j\omega})|^2 = \left|\sum_{r=-\infty}^{\infty} F\left(\frac{\omega}{T} j + \frac{2\pi r}{T} j\right)\right|^2 \tag{3.1.4}$$

is the MSF of a sequence derived from sampling a continuous waveform with Fourier transform $F(\Omega)$ [1].

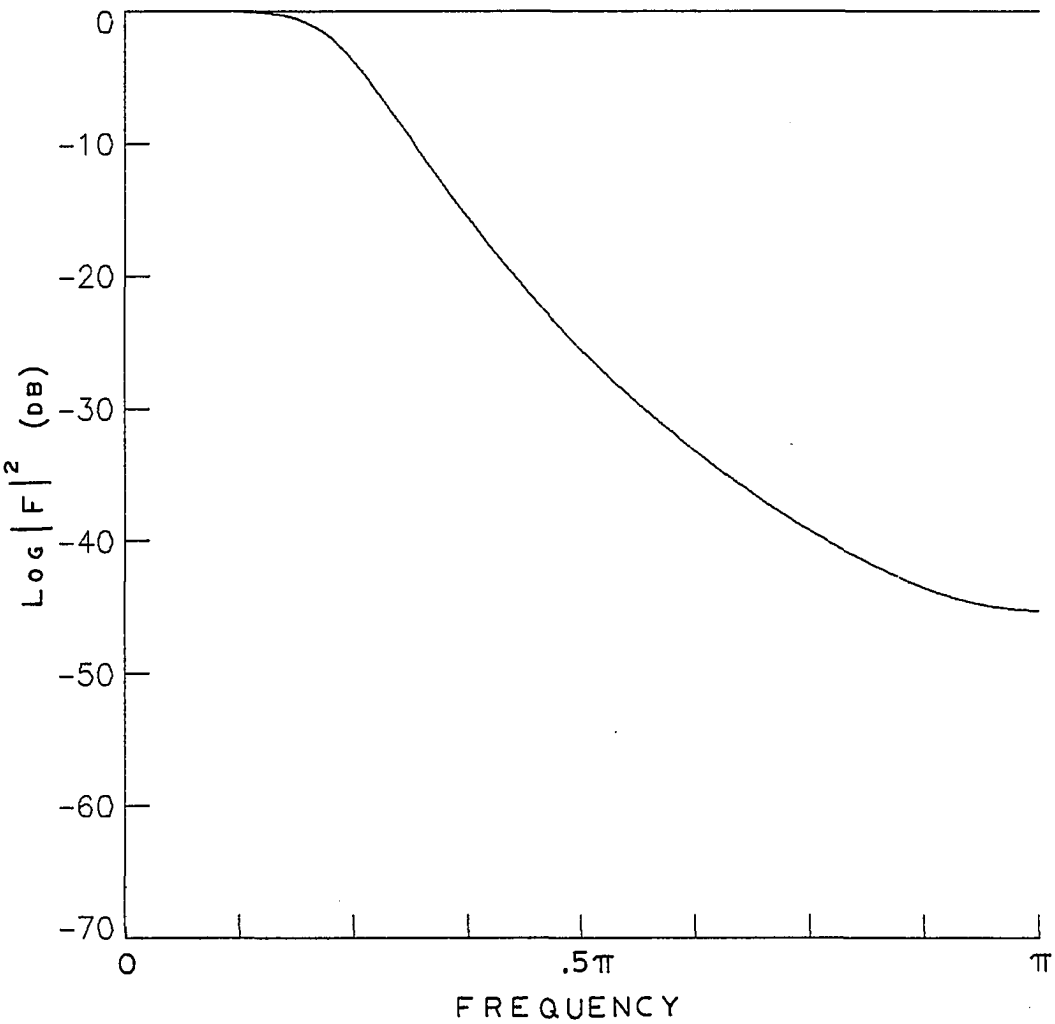

Figure 3.1(a). Log MSF of Filter F1.

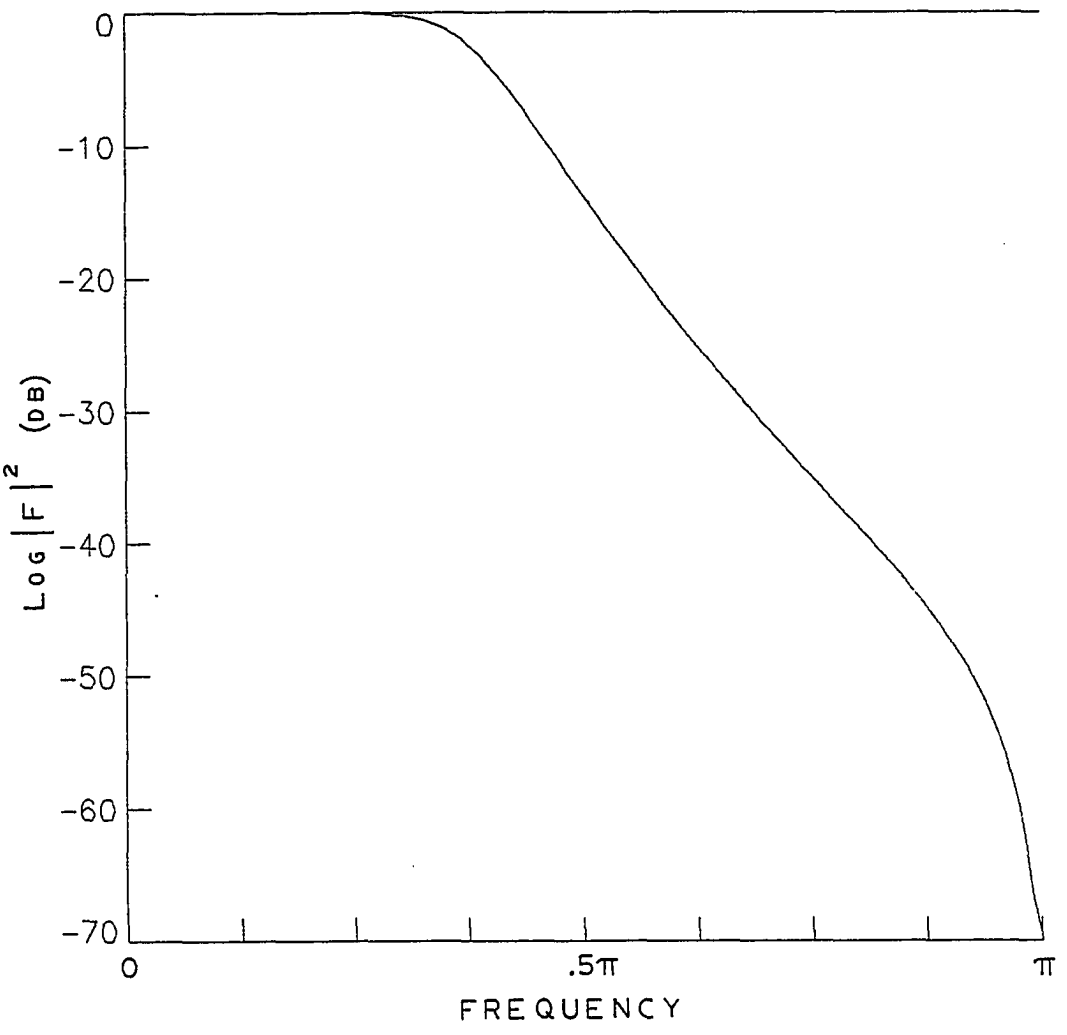

Figure 3.1(b). Log MSF of Filter F2.

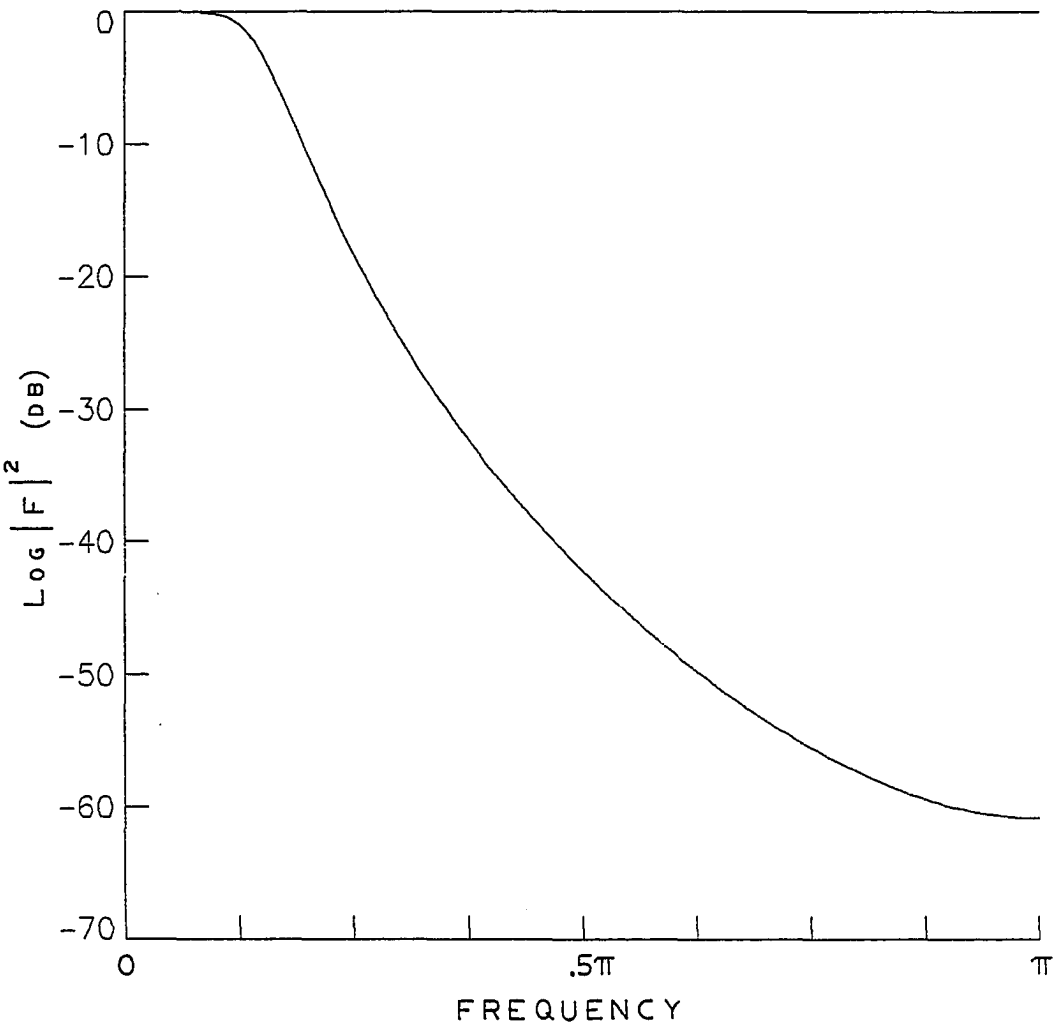

Figure 3.1(c). Log MSF of Filter F3.

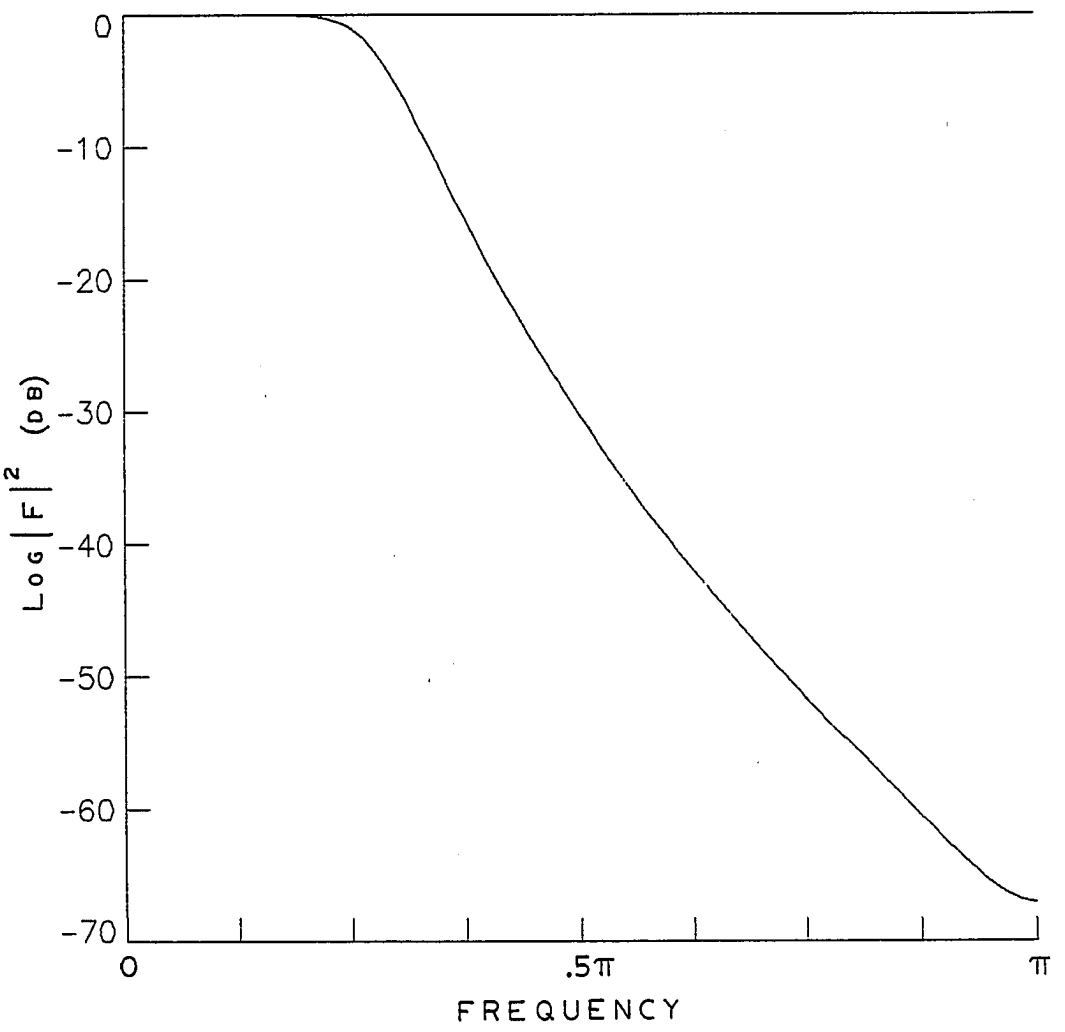

Figure 3.1(d). Log MSF of Filter F4.

3.2 Energy Distribution and Energy Capture

One primary aspect of this research is the investigation of the way in which the presample filter MSF effects the energy distribution or subspace energy capture performance of the DL and DC bases compared to the KL basis for the filter. The spectral selectivity properties of the basis under consideration have already been illustrated in Chapter Two. The way in which these properties combine with the filter MSF to result in energy redistribution can be examined by consideration of the normalized estimate of the maximum coefficient energy defined in Section 2.3 as $N\rho_m\bar{x}^2$. Recall from the definition that this represents the expected coefficient energy or variance when the presample filter is assumed to have a zero mean, white (wideband) input. The values $N\rho_m\bar{x}^2$ have been calculated using equations (2.3.15) and (2.3.17) with $\kappa = 1$. $\text{Log}(N\rho_m\bar{x}^2)$ is plotted against M for each filter and two different values of N in Figures 3.2 and 3.3. Also included on the plots are the relative input (PCM sample) energy $\bar{x}^2$. This is to illustrate the redistribution of energy. Note that $N\rho_m\bar{x}^2$ is monotonically decreasing in all cases. As stated in Chapter Two, this is anticipated because of the monotonic nature of the filter MSF and the spectral selectivity of $|H_m(e^{j\omega})|^2$. In fact, it has been reported [5, 8] that for a stationary process the KL and DC basis coefficient energies approach the power spectral density as N goes to infinity. This does not appear to be the case for the DL basis as the values of $N\rho_m\bar{x}^2$ appear to be diverging from the KL basis as N increases for both low- and high-order coefficients. The DC and KL bases track closely for low-order, high-energy coefficients. However, the DC tends to diverge from the KL as m approaches N, particularly for the two filters, F3 and F4, that have

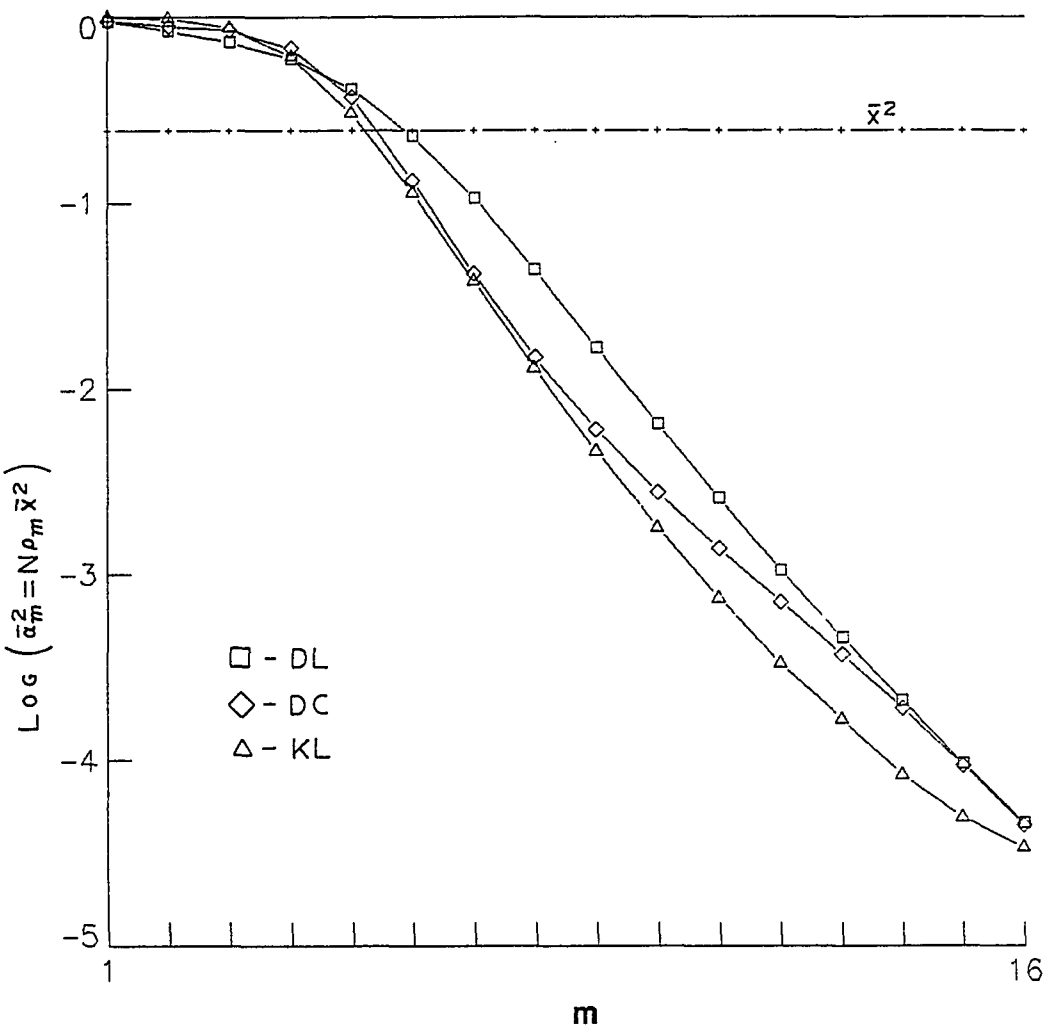

Figure 3.2(a). Normalized Coefficient Energy Distribution, N = 16, Filter F1.

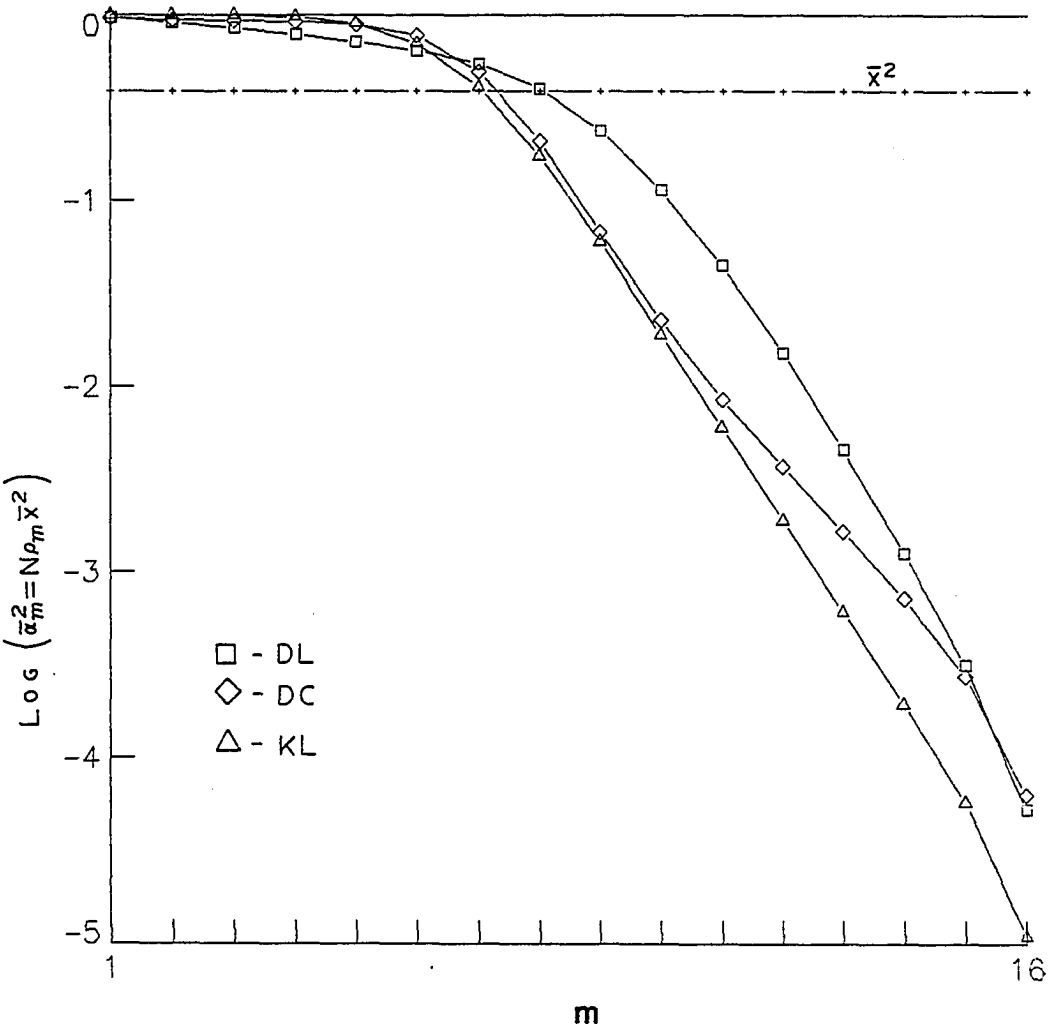

Figure 3.2(b). Normalized Coefficient Energy Distribution, N = 16, Filter F2.

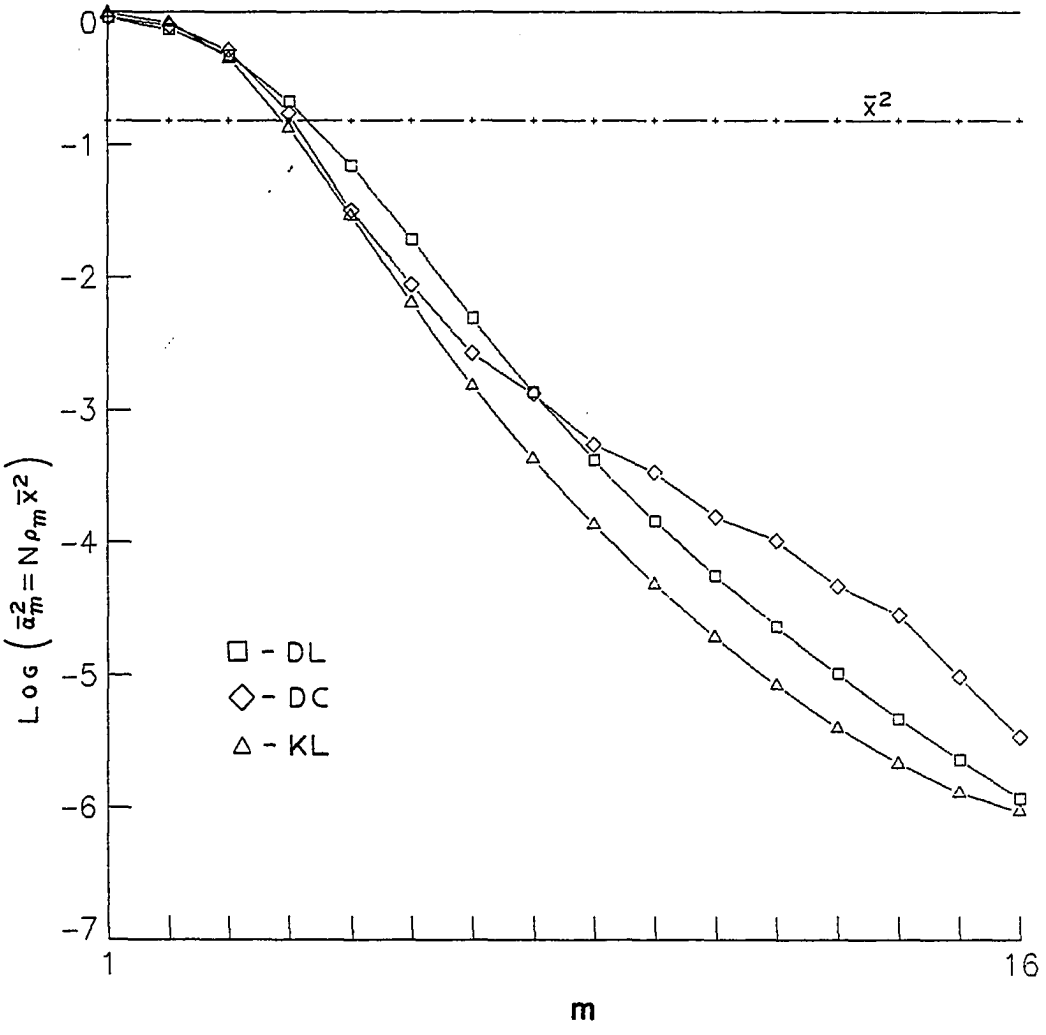

Figure 3.2(c). Normalized Coefficient Energy Distribution, N = 16, Filter F3.

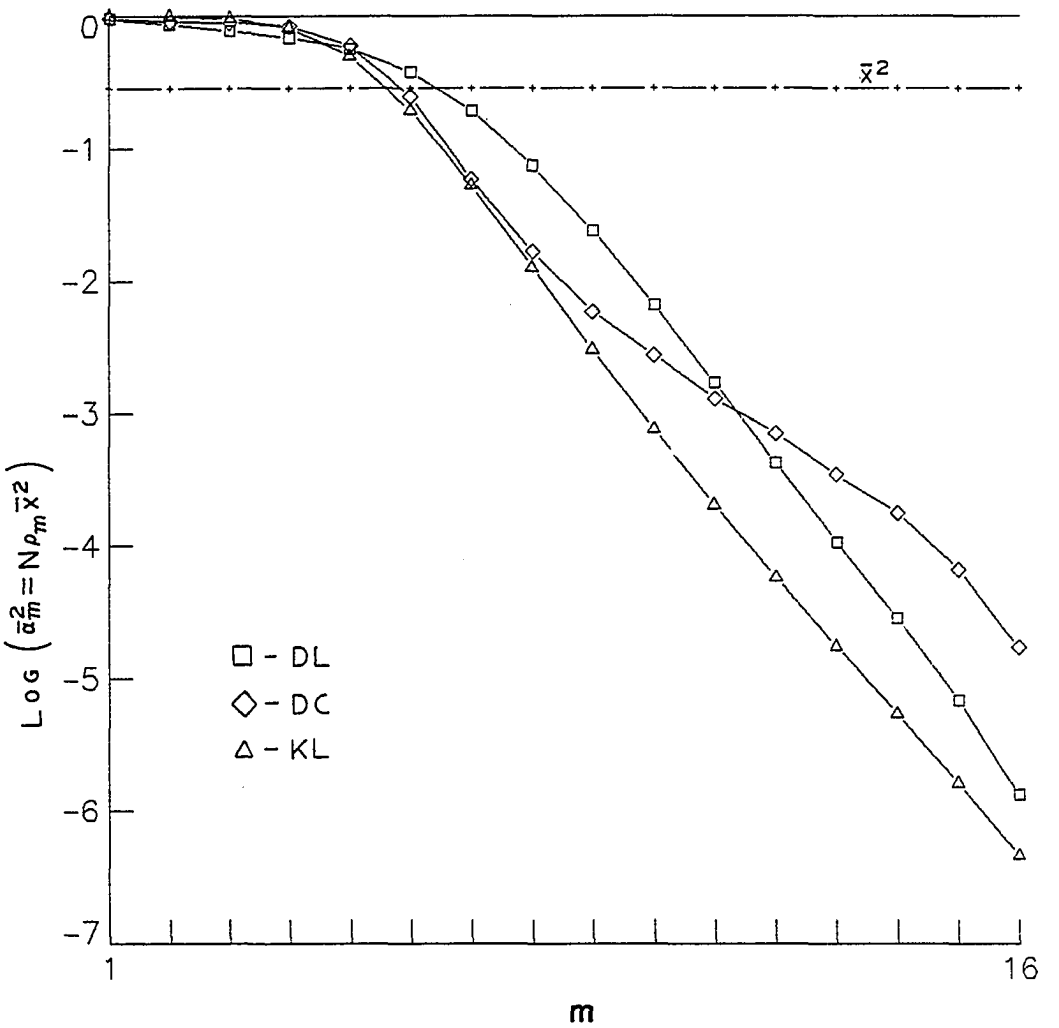

Figure 3.2(d). Normalized Coefficient Energy Distribution, N = 16, Filter F4.

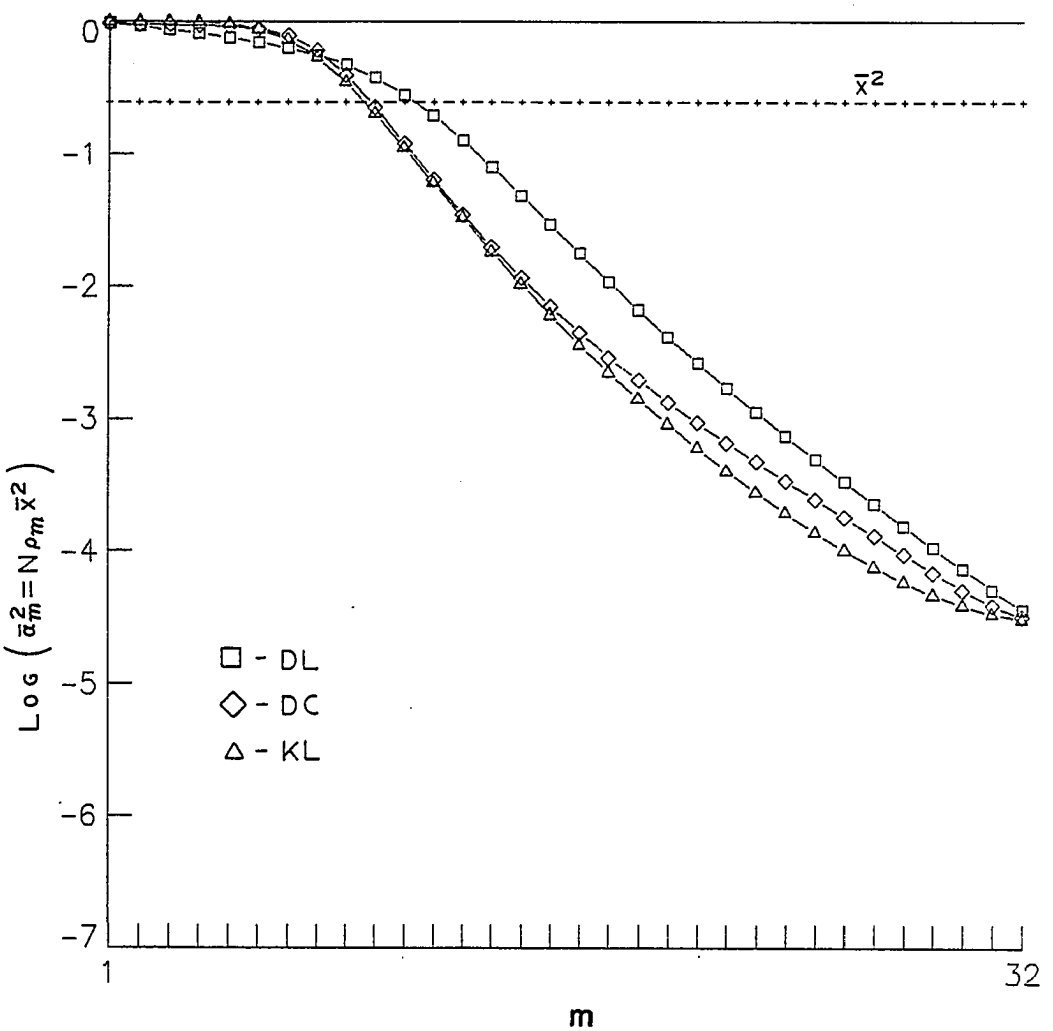

Figure 3.3(a). Normalized Coefficient Energy Distribution, N = 32, Filter F1.

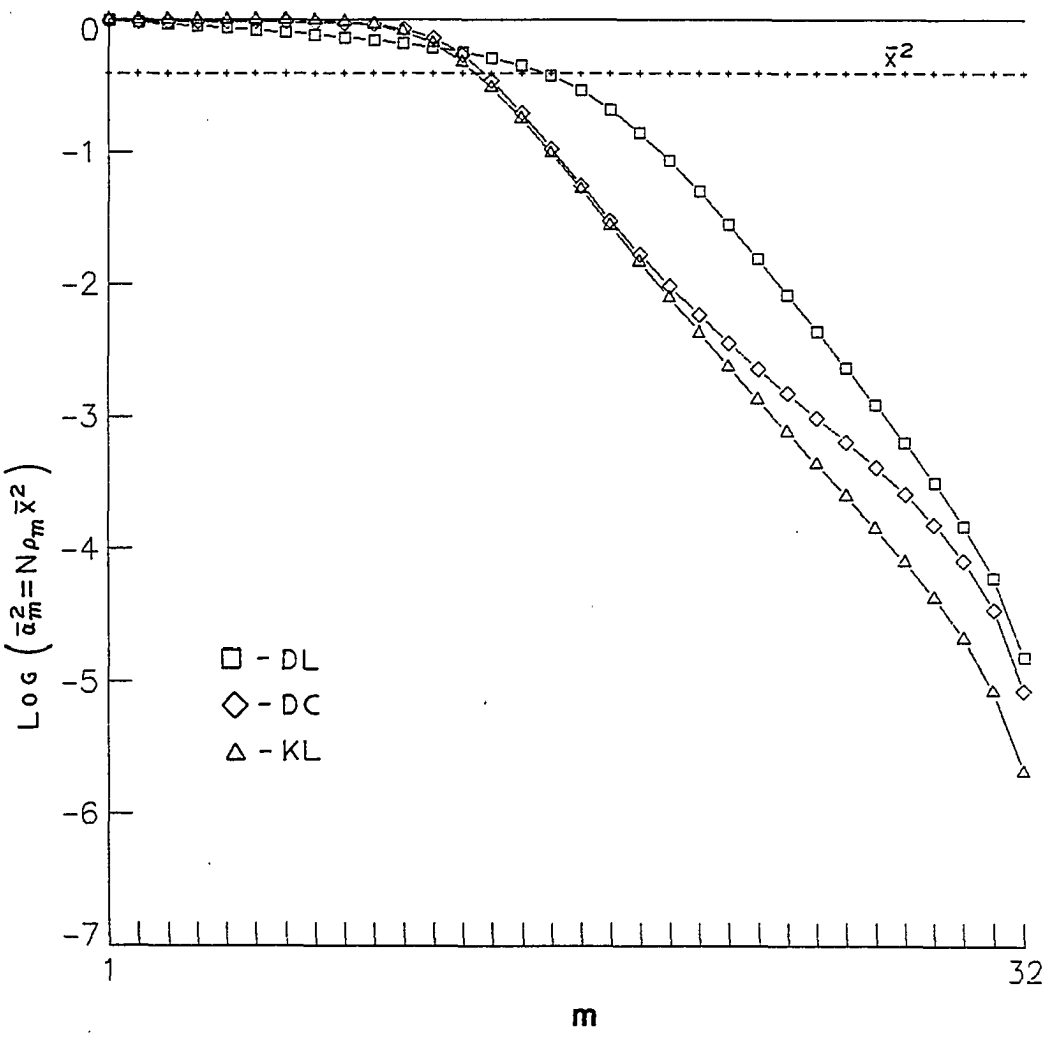

Figure 3.3(b). Normalized Coefficient Energy Distribution, N = 32, Filter F2.

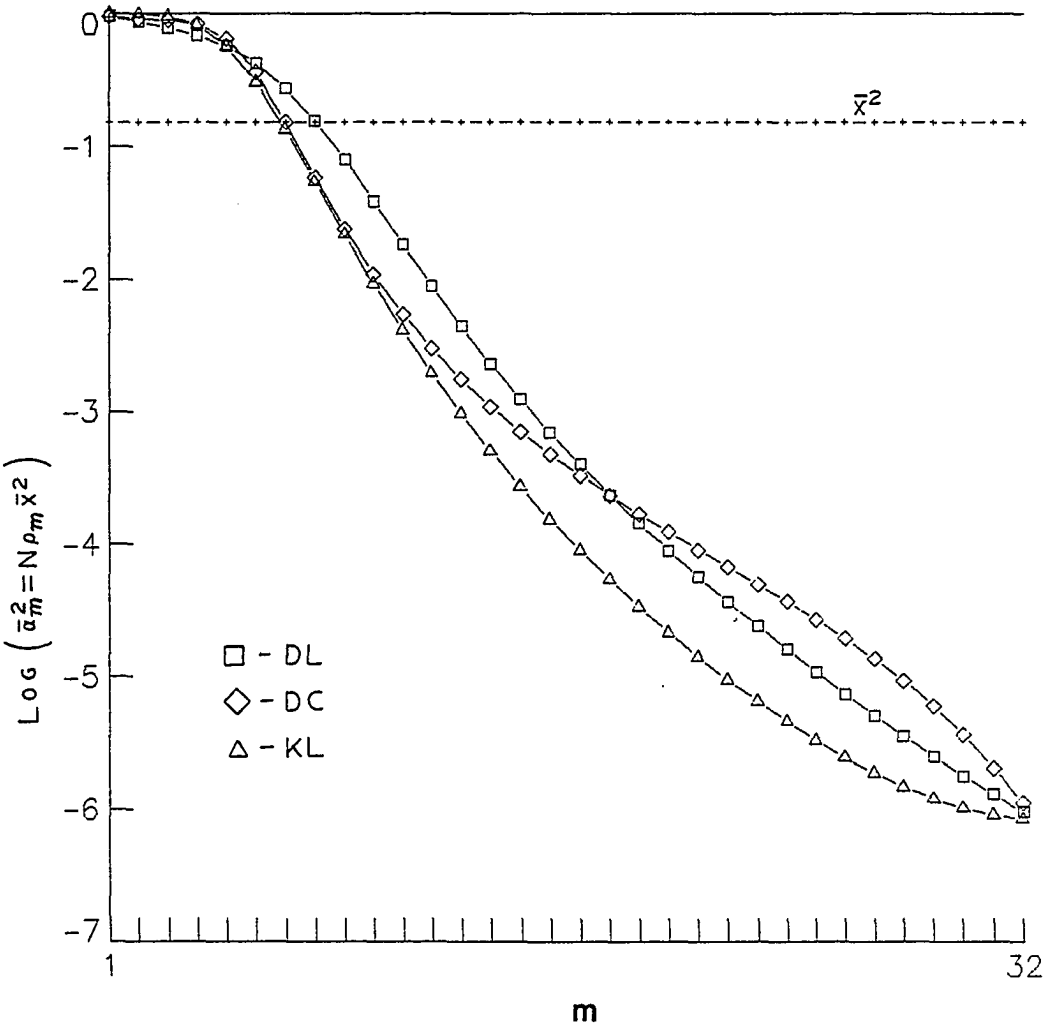

Figure 3.3(c). Normalized Coefficient Energy Distribution, N = 32, Filter F3.

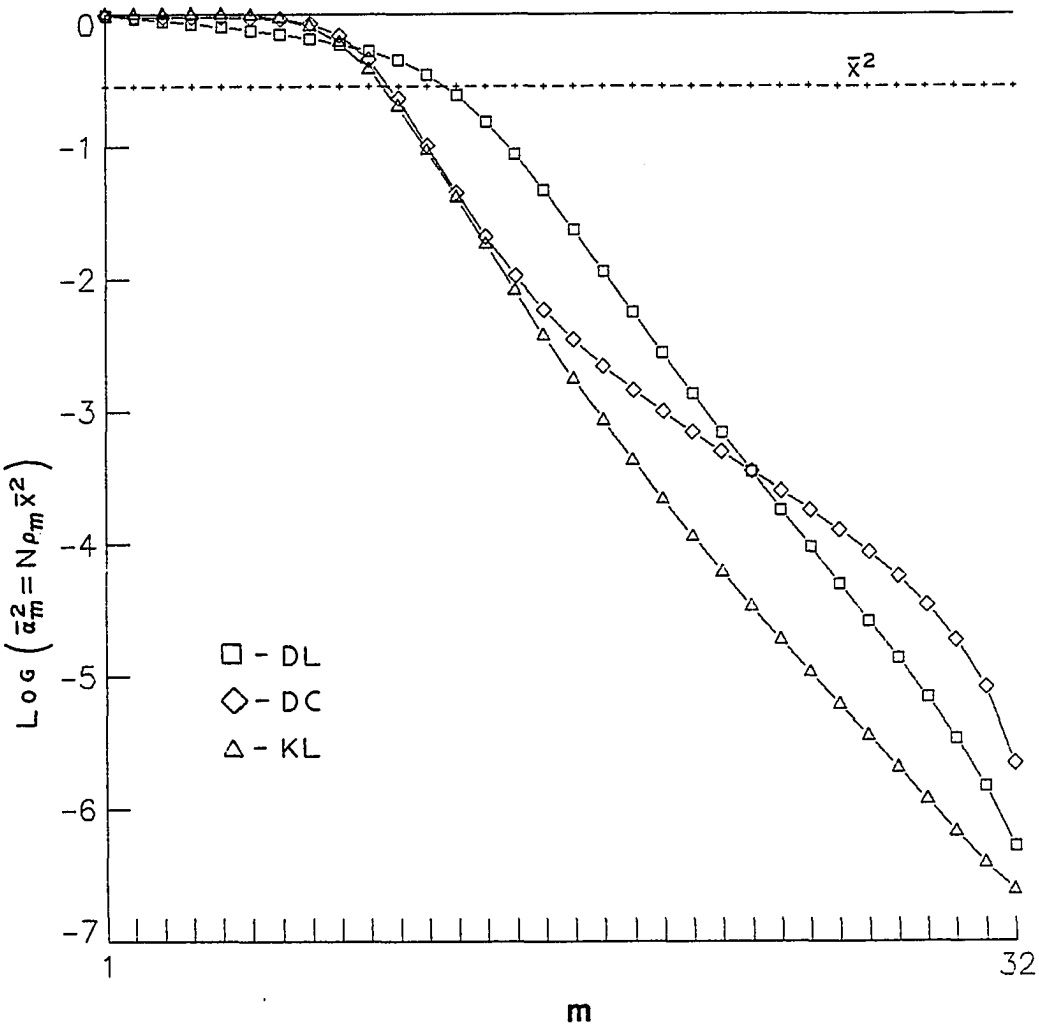

Figure 3.3(d). Normalized Coefficient Energy Distribution, N = 32, Filter F4.

the greater attenuation. The DC high-order coefficient energies exceed even those of the DL for these filters. This means that for these filters, discarding of coefficients for m close to N eliminates more energy for the DC than the DL basis. Note that the energies in these coefficients for either basis are several orders of magnitude below the first few coefficients so the choice of basis and subspace dimension depend on the relative energy capture that is acceptable, that is, on whether the goal is say 90 percent capture or 99.9 percent capture. This is a subjective criterion and will only be addressed for comparison. Figure 3.4, included for illustration, is the $N\rho_m x^{-2}$ distribution of the four $N = 32$ KL bases applied to F3. This illustrates that what is best for one filter may not be the best for another.

Total subspace energy capture is reflected in the EPE defined in Section 2.2. It can be seen by examination of the definition of EPE by equation (2.2.9) and of ρ_m in equation (2.3.16) that

$$\text{EPE} = \sum_{m=1}^{M} \rho_m \, . \tag{3.2.1}$$

Tables 3.1 and 3.2 give the EPE and 1-EPE values versus m corresponding to the $N\rho_m x^{-2}$ curves already given. These tables illustrate the comparative energy packing performance for the bases. They particularly accent the low-order, high-energy coefficients. Note that the KL packing efficiency is the best, as expected. However, note that the other bases generally exhibit the same packing performance.

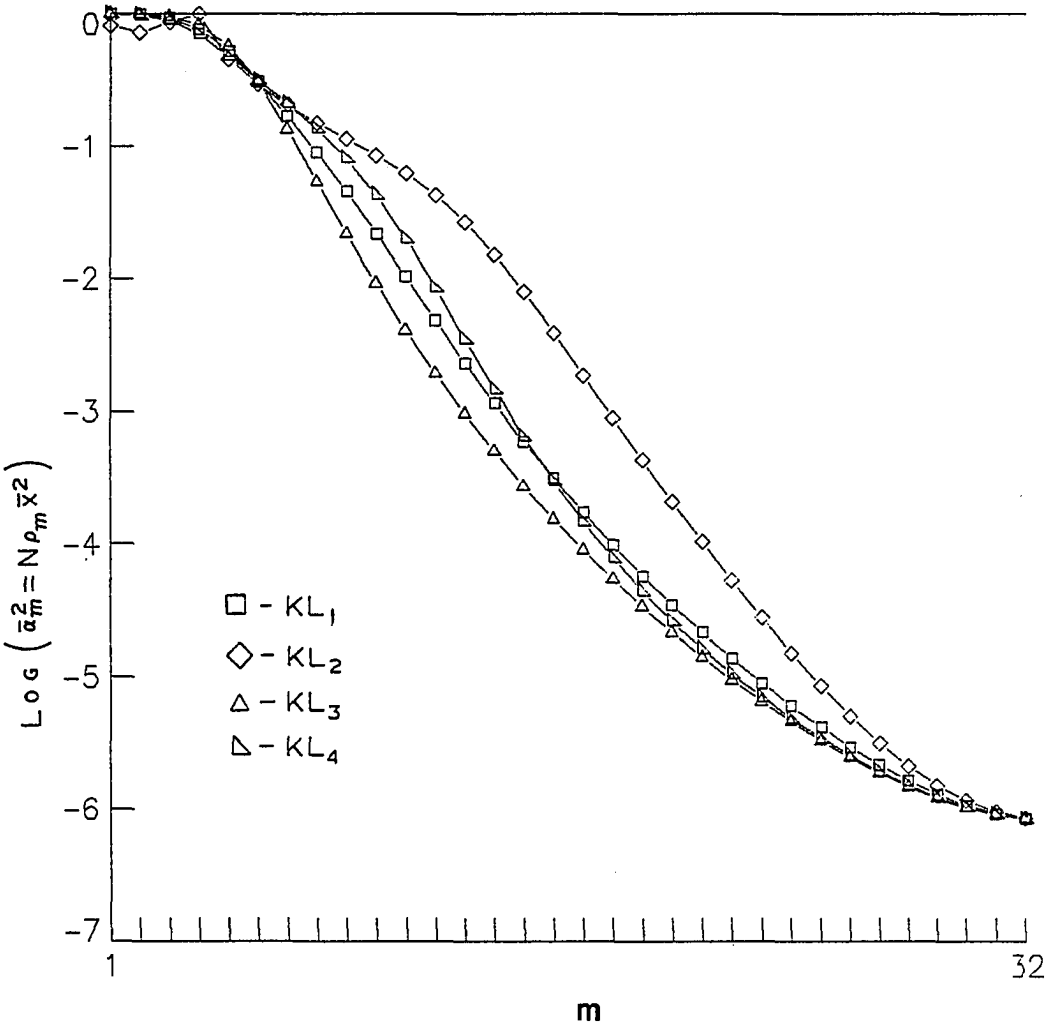

Figure 3.4. Normalized Coefficient Energy Distribution, N = 32, Filter F3, KL_1 - KL_4 Bases.

TABLE 3.1(a) EPE and 1-EPE, N = 16, FILTER F1

	DL		DC		KL	
m	EPE	1-EPE	EPE	1-EPE	EPE	1-EPE
1	.2410	.7590	.2410	.7590	.2536	.7464
2	.4546	.5454	.4666	.5334	.5021	.4979
3	.6406	.3594	.6828	.3172	.7241	.2760
4	.7923	.2077	.8554	.1446	.8796	.1204
5	.8968	.1032	.9492	.508E-1	.9564	.436E-1
6	.9550	.450E-1	.9827	.173E-1	.9852	.148E-1
7	.9820	.180E-1	.9933	.673E-2	.9948	.523E-2
8	.9930	.700E-2	.9970	.295E-2	.9980	.198E-2
9	.9972	.275E-2	.9986	.141E-2	.9992	.808E-3
10	.9989	.112E-2	.9993	.707E-3	.9996	.356E-3
11	.9995	.473E-3	.9996	.359E-3	.9998	.168E-3
12	.9998	.205E-3	.9998	.178E-3	.9999	.831E-4
13	.9999	.883E-4	.9999	.837E-4	1.000	.424E-4
14	1.000	.359E-4	1.000	.351E-4	1.000	.211E-4
15	1.000	.116E-4	1.000	.113E-4	1.000	.862E-5
16	1.000	0	1.000	0	1.000	0

TABLE 3.1(b) EPE and 1-EPE, N = 16, FILTER F2

	DL		DC		KL	
m	EPE	1-EPE	EPE	1-EPE	EPE	1-EPE
1	.1553	.8447	.1553	.8447	.1600	.8400
2	.3013	.6987	.3058	.6942	.3199	.6801
3	.4376	.5624	.4555	.5445	.4794	.5206
4	.5638	.4362	.6033	.3968	.6360	.3640
5	.6783	.3217	.7461	.2539	.7805	.2195
6	.7811	.2188	.8701	.1300	.8929	.1071
7	.8688	.1312	.9497	.503E-1	.9582	.418E-1
8	.9330	.670E-1	.9832	.168E-1	.9960	.140E-1
9	.9712	.288E-1	.9940	.602E-2	.9956	.444E-2
10	.9894	.106E-1	.9976	.239E-2	.9986	.140E-2
11	.9966	.342E-2	.9990	.102E-2	.9996	.445E-3
12	.9990	.996E-3	.9996	.434E-3	.9999	.141E-3
13	.9997	.262E-3	.9999	.171E-3	1.000	.423E-4
14	.9999	.585E-4	1.000	.538E-4	1.000	.109E-4
15	1.000	.848E-5	1.000	.101E-4	1.000	.175E-5
16	1.000	0	1.000	0	1.000	0

TABLE 3.1(c) EPE AND 1-EPE, N = 16, FILTER F3

	DL		DC		KL	
m	EPE	1-EPE	EPE	1-EPE	EPE	1-EPE
1	.3753	.6247	.3753	.6247	.4043	.5957
2	.6806	.3194	.7000	.3000	.7464	.2536
3	.8752	.1248	.9106	.894E-1	.9298	.702E-1
4	.9612	.388E-1	.9812	.188E-1	.9846	.154E-1
5	.9894	.106E-1	.9942	.575E-2	.9966	.345E-2
6	.9971	.286E-2	.9978	.216E-2	.9991	.886E-3
7	.9992	.831E-3	.9989	.105E-2	.9997	.264E-3
8	.9997	.272E-3	.9995	.507E-3	.9999	.900E-4
9	.9999	.997E-4	.9997	.282E-3	1.000	.346E-4
10	1.000	.399E-4	.9999	.145E-3	1.000	.147E-4
11	1.000	.170E-4	.9999	.785E-4	1.000	.685E-5
12	1.000	.750E-5	1.000	.360E-4	1.000	.342E-5
13	1.000	.334E-5	1.000	.170E-4	1.000	.178E-5
14	1.000	.142E-5	1.000	.547E-5	1.000	.907E-6
15	1.000	.482E-6	1.000	.141E-5	1.000	.379E-6
16	1.000	0	1.000	0	1.000	0

TABLE 3.1(d) EPE AND 1-EPE, N = 16, FILTER F4

	DL		DC		KL	
m	EPE	1-EPE	EPE	1-EPE	EPE	1-EPE
1	.2111	.7889	.2111	.7889	.2206	.7794
2	.4036	.5964	.4123	.5877	.4405	.5595
3	.5746	.4254	.6098	.3902	.6532	.3468
4	.7259	.2741	.7951	.2049	.8333	.1667
5	.8510	.1490	.9266	.733E-1	.9425	.575E-1
6	.9342	.657E-1	.9807	.193E-1	.9847	.153E-1
7	.9763	.237E-1	.9938	.617E-2	.9963	.370E-2
8	.9928	.719E-2	.9975	.247E-2	.9991	.903E-3
9	.9980	.195E-2	.9988	.118E-2	.9999	.232E-3
10	.9995	.496E-3	.9994	.573E-3	.9999	.634E-4
11	.9999	.125E-3	.9997	.290E-3	1.000	.183E-4
12	.9999	.319E-4	.9999	.133E-3	1.000	.546E-5
13	1.000	.797E-5	.9999	.575E-4	1.000	.163E-5
14	1.000	.180E-5	1.000	.184E-4	1.000	.457E-6
15	1.000	.291E-6	1.000	.372E-5	1.000	.101E-6
16	1.000	0	1.000	0	1.000	0

TABLE 3.2(a) EPE AND 1-EPE, N = 32, FILTER F1

	DL		DC		KL	
m	EPE	1-EPE	EPE	1-EPE	EPE	1-EPE
2	.2408	.7562	.2440	.7559	.2539	.7461
4	.4547	.5452	.4831	.5169	.5059	.4941
6	.6396	.3604	.7119	.2881	.7382	.2618
8	.7906	.2094	.8872	.1128	.8991	.1009
10	.8983	.1017	.9658	.342E-1	.9686	.314E-1
12	.9583	.417E-1	.9890	.110E-1	.9902	.979E-2
14	.9843	.157E-1	.9960	.411E-2	.9967	.335E-2
16	.9941	.592E-2	.9982	.176E-2	.9987	.128E-2
18	.9977	.234E-2	.9992	.825E-3	.9995	.544E-3
20	.9990	.973E-3	.9996	.410E-3	.9998	.251E-3
22	.9996	.422E-3	.9998	.209E-3	.9999	.125E-3
24	.9998	.187E-3	.9999	.107E-3	.9999	.661E-4
26	.9999	.820E-4	1.000	.526E-4	1.000	.358E-4
28	1.000	.338E-4	1.000	.241E-4	1.000	.189E-4
30	1.000	.110E-4	1.000	.897E-5	1.000	.812E-5
32	1.000	0	1.000	0	1.000	0

TABLE 3.2(b) EPE AND 1-EPE, N = 32, FILTER F2

	DL		DC		KL	
m	EPE	1-EPE	EPE	1-EPE	EPE	1-EPE
2	.1553	.8447	.1565	.8435	.1600	.8400
4	.3013	.6987	.3116	.6884	.3199	.6801
6	.4375	.5625	.4663	.5337	.4798	.5202
8	.5635	.4365	.6197	.3803	.6385	.3615
10	.6783	.3217	.7684	.2316	.7887	.2112
12	.7804	.2196	.8946	.1054	.9066	.934E-1
14	.8671	.1329	.9658	.342E-1	.9691	.309E-1
16	.9332	.668E-1	.9898	.102E-1	.9911	.893E-2
18	.9732	.268E-1	.9966	.338E-2	.9974	.258E-2
20	.9911	.889E-2	.9987	.127E-2	.9992	.783E-3
22	.9974	.263E-2	.9995	.512E-3	.9997	.248E-3
24	.9993	.737E-3	.9998	.207E-3	.9999	.790E-4
26	.9998	.194E-3	.9999	.766E-4	1.000	.238E-4
28	1.000	.437E-4	1.000	.223E-4	1.000	.595E-5
30	1.000	.610E-5	1.000	.347E-5	1.000	.843E-6
32	1.000	0	1.000	0	1.000	0

TABLE 3.2(c) EPE AND 1-EPE, N = 32, FILTER F3

	DL		DC		KL	
m	EPE	1-EPE	EPE	1-EPE	EPE	1-EPE
2	.3756	.6245	.3838	.6162	.4096	.5904
4	.6758	.3242	.7391	.2609	.7743	.2257
6	.8801	.1199	.9469	.531E-1	.9536	.463E-1
8	.9683	.317E-1	.9901	.991E-2	.9920	.802E-2
10	.9925	.754E-2	.9972	.279E-2	.9983	.167E-2
12	.9980	.198E-2	.9989	.106E-2	.9996	.437E-3
14	.9994	.607E-3	.9995	.484E-3	.9999	.138E-3
16	.9998	.213E-3	.9998	.242E-3	1.000	.506E-4
18	.9999	.825E-4	.9999	.127E-3	1.000	.211E-4
20	1.000	.344E-4	.9999	.672E-4	1.000	.979E-5
22	1.000	.151E-4	1.000	.347E-4	1.000	.496E-5
24	1.000	.687E-5	1.000	.168E-4	1.000	.269E-5
26	1.000	.312E-5	1.000	.733E-5	1.000	.151E-5
28	1.000	.135E-5	1.000	.263E-5	1.000	.817E-6
30	1.000	.464E-6	1.000	.651E-6	1.000	.359E-6
32	1.000	0	1.000	0	1.000	0

TABLE 3.2(d) EPE AND 1-EPE, N = 32, FILTER F4

	DL		DC		KL	
m	EPE	1-EPE	EPE	1-EPE	EPE	1-EPE
2	.2112	.7888	.2135	.7865	.2207	.7793
4	.4032	.5968	.4241	.5760	.4412	.5588
6	.5750	.4250	.6322	.3678	.6590	.3410
8	.7246	.2754	.8272	.1728	.8507	.1493
10	.8482	.1518	.9534	.466E-1	.9596	.404E-1
12	.9362	.638E-1	.9898	.102E-1	.9918	.823E-2
14	.9801	.199E-1	.9970	.296E-2	.9983	.169E-2
16	.9949	.508E-2	.9988	.115E-2	.9996	.384E-3
18	.9988	.123E-2	.9995	.524E-3	.9999	.983E-4
20	.9997	.307E-3	.9997	.255E-3	1.000	.278E-4
22	.9999	.809E-4	.9999	.124E-3	1.000	.850E-5
24	1.000	.219E-4	.9999	.570E-4	1.000	.273E-5
26	1.000	.578E-5	1.000	.230E-4	1.000	.885E-6
28	1.000	.136E-5	1.000	.709E-5	1.000	.272E-6
30	1.000	.222E-6	1.000	.116E-5	1.000	.673E-7
32	1.000	0	1.000	0	1.000	0

Recall that this capture is relative to input energy level and is not a fixed distortion as is quantization. Thus, for low-energy inputs (or intervals of input), the distortion due to subspace representation is going to be reduced relative to, and possibly less than, that due to quantization. Also recall that the energy distribution and capture reflected in the plots and tables are indicative of the expected maximum for wideband (white) filter inputs. If the actual signal is not wideband the distribution of coefficient energies is altered according to the spectral content. Thus, actual subspace capture as a percent of total energy is greatly effected by the true spectral content of the signal source.

3.3 Full Space Rate Reduction

The goal of transform coding for telemetry applications is bit rate reduction. As shown in Section 2.6, bit rate reduction is possible even when all the coefficients are retained. The theoretical bound as a measure of the bit rate improvement, denoted ΔB, has been presented in Section 2.6. Curves of ΔB versus N for the bases and filters under consideration are shown in Figure 3.5 for comparison. Note the improvement with increasing N, a manifestation of the spread in $\bar{\alpha}_m$. This improvement is not linear and asymptotically approaches a limit. The equation for the value ΔB_{max}, also included in the figure, to which the KL and DC approach in the limit is taken from Davisson [5]. The equation is based on the knowledge that the KL and DC energy distribution approach the power spectral density as $N \to \infty$. It also assumes that the coding distortion is less than the signal energy. This is consistent with the assumption used in the presample filter specification.

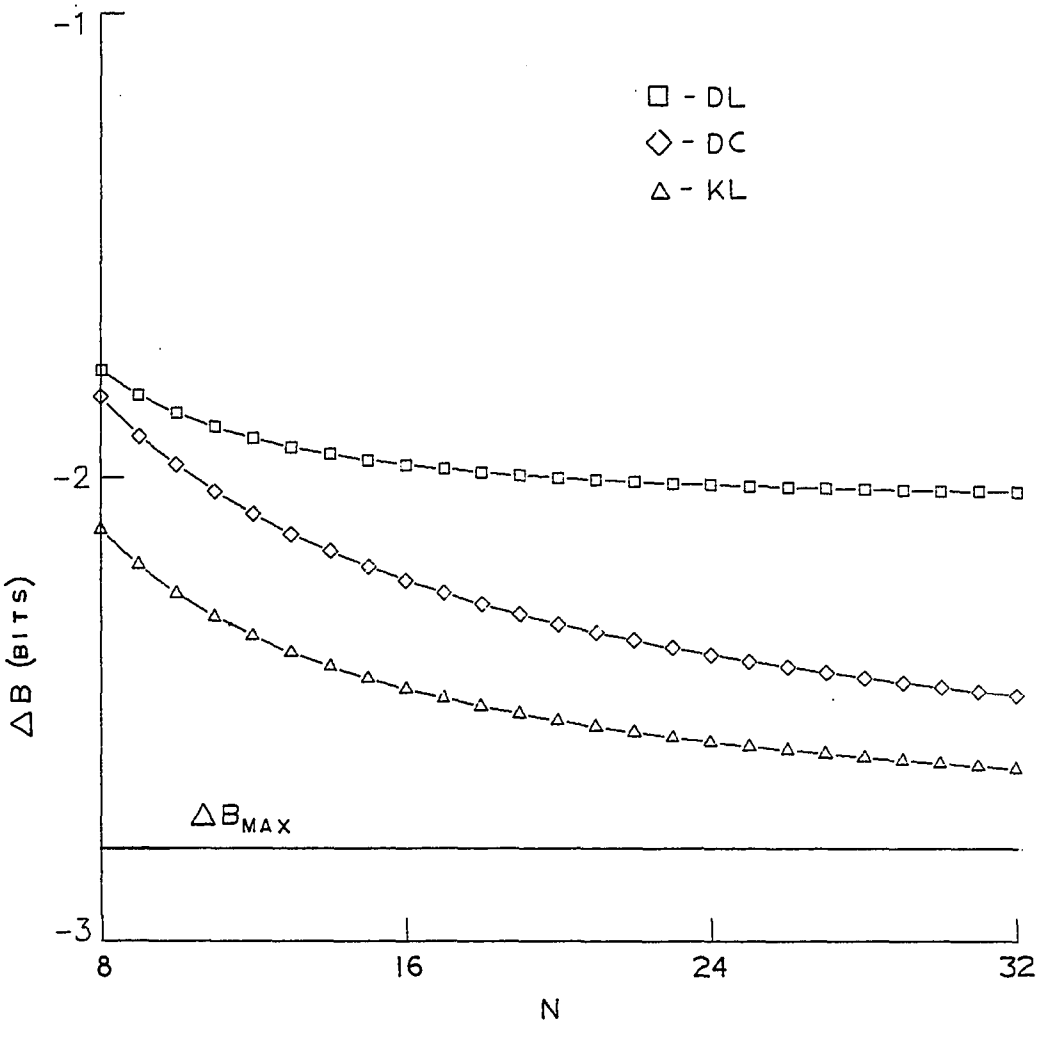

Figure 3.5(a). Bit Rate Improvement, ΔB, Filter F1.

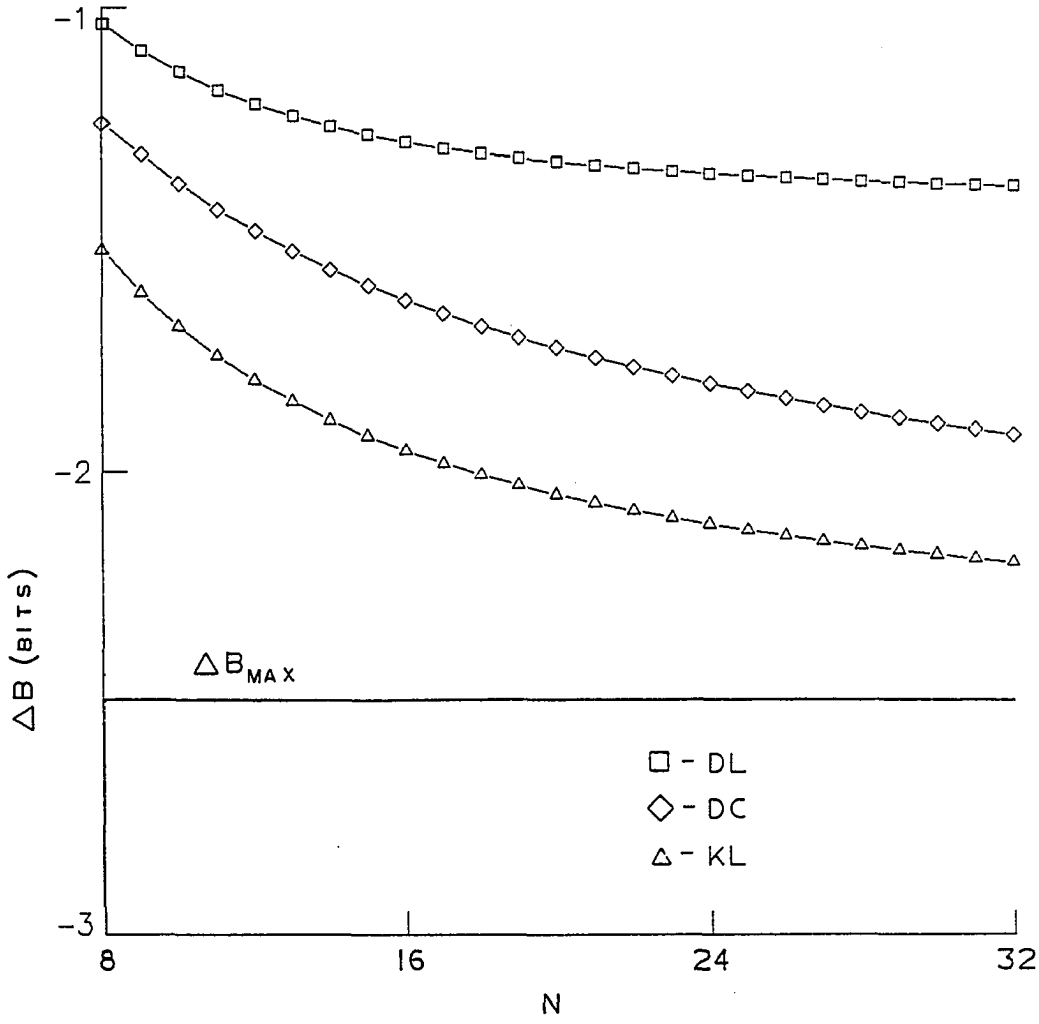

Figure 3.5(b). Bit Rate Improvement, ΔB, Filter F2.

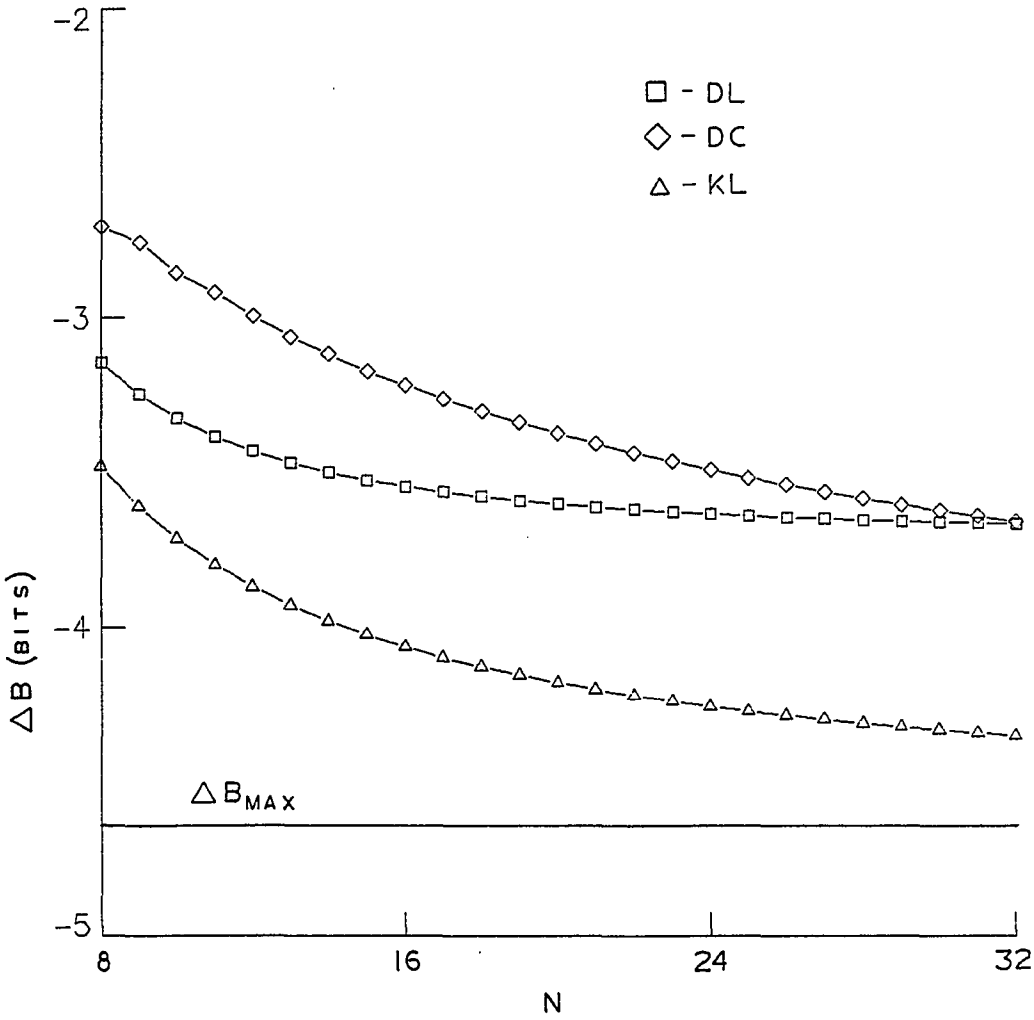

Figure 3.5(c). Bit Rate Improvement, ΔB, Filter F3.

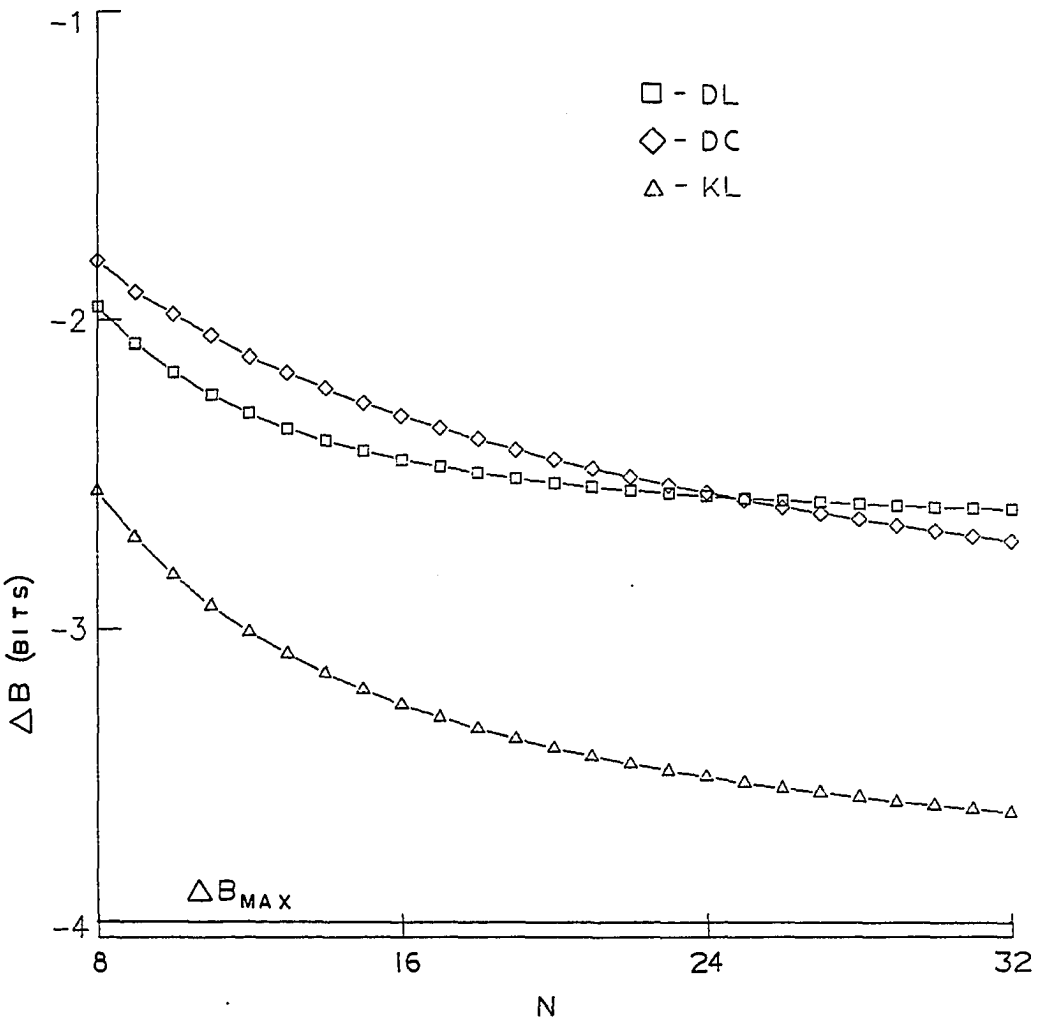

Figure 3.5(d). Bit Rate Improvement, ΔB, Filter F4.

The equation for ΔB_{max} is

$$\Delta B_{max} = \frac{1}{2\pi} \int_{-\pi}^{\pi} \frac{1}{2} \log_2 \left|F^*(e^{j\omega})\right|^2 d\omega$$

$$- \frac{1}{2} \log \int_{-\pi}^{\pi} \left|F^*(e^{j\omega})\right|^2 d\omega \, . \qquad (3.3.1)$$

The first term represents the rate limit for infinite length block coding ($N \to \infty$) or the limit for totally utilizing the redundancy as described by the power spectral density. The second term is the rate limit for single sample encoding (PCM). Equal distortion for both techniques is implied. Note that the limit relates to the spectral shape, that is, the amount of redundancy in the signal.

It appears that the DL does not approach this limit. This is consistent with the observation in Section 3.3 that the DL does not approach the power spectral density. For filters F3 and F4 and low values of N, the DL more closely represents the KL. In all cases the DL flattens out and the DC continues to improve. Thus, values of N greater than about 32 would not be expected to produce any improvement for the DL. For the DC and KL the increase in improvement must be traded off against increased computational load.

3.4 Composite Spectral Energy Capture

As shown in Section 2.3, the magnitude squared FIR transfer function $|H_m(e^{j\omega})|^2$ represents the way in which spectral energy is captured by a transform coefficient. When M coefficients are to be used to represent an input sequence x*(p), equation (2.2.7) represents the total energy capture for the subspace representation and can be rewritten using equation (2.3.14) to give

$$\frac{1}{P}\sum_{p=0}^{P-1}(\tilde{x}^*(p))^2 = \frac{1}{N}\sum_{m=1}^{M}\bar{\alpha}_m^2$$

$$= \frac{1}{N}\sum_{m=1}^{M}\frac{1}{2\pi}\int_{-\pi}^{\pi}|H_m(e^{j\omega})|^2|X^*(e^{j\omega})|^2 d\omega$$

$$= \frac{1}{2\pi}\int_{-\pi}^{\pi}\frac{1}{N}\sum_{m=1}^{M}|H_m(e^{j\omega})|^2|X^*(e^{j\omega})|^2 d\omega \ . \qquad (3.4.1)$$

The composite magnitude squared function given by

$$C(e^{j\omega}) = \sum_{m=M+1}^{N}|H_m(e^{j\omega})|^2 \qquad (3.4.2)$$

is then used to indicate the way in which spectral energy is captured by the subspace representation. Likewise, the complimentary composite magnitude squared function

$$C'(e^{j\omega}) = \sum_{m=M+1}^{N}|H_m(e^{j\omega})|^2 \qquad (3.4.3)$$

represents the extent to which input spectral energy contributes to the error for a subspace representation. Note that for orthonormal basis

$$C'(e^{j\omega}) = 1 - C(e^{j\omega}) \ , \qquad (3.4.4)$$

Plots of $C(e^{j\omega})$ and Log $C'(e^{j\omega})$ for $N = 16$ and several values of M are given in Figures 3.5 and 3.6, respectively for the DC, DL and two KL bases. The KL basis designated KL_1 is derived from the 4-pole Butterworth filter F1 spectrum and KL_4 is the same as that of Section 2.4 derived from the 6-pole Butterworth filter F4 spectrum. The selection of the basis, and the subspace dimensions M for a particular application depends on the way in which the composite spectrum combines with the input (presample filter) spectrum as indicated in equation (3.1.1). If the KL spectrum is taken to be optimum, then the polynomial basis, whose composite spectrum more closely resembles that of the KL for the presample filter, would be expected to provide the better total energy capture of the two. It may be more informative to examine the complimentary composite spectrum $C'(e^{j\omega})$. Recall that this is indicative of the energy that is discarded by subspace reduction. Note the tails of $C'(e^{j\omega})$. Those of the DL basis are smaller than those of the DC basis and are more like those of the KL basis. This suggests that for monotonically decreasing input spectra, elimination of coefficients of high sequency basis vectors tends to remove less "pass band" energy for the KL and DL basis. Thus the spectral composition of the energy, as well as the total energy loss, provides useful insight in comparing the energy capture properties of candidate transforms. With this in mind the user of the data may be willing to accept the total energy loss to achieve further bit rate reduction knowing that energy in the "pass band" is being captured.

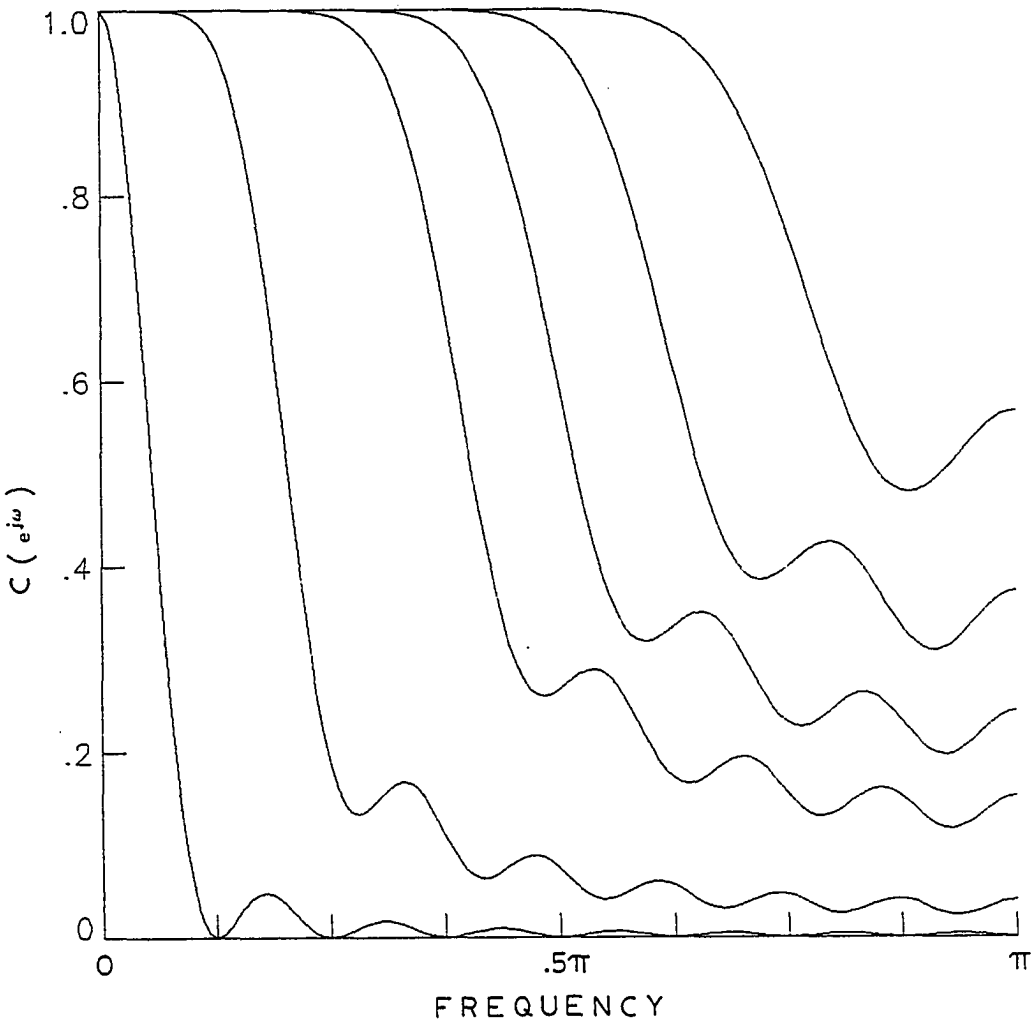

Figure 3.6(a). Composite Magnitude Squared Function, N = 16, M = 1, 4, 8, 10, 12, 14, DL Basis.

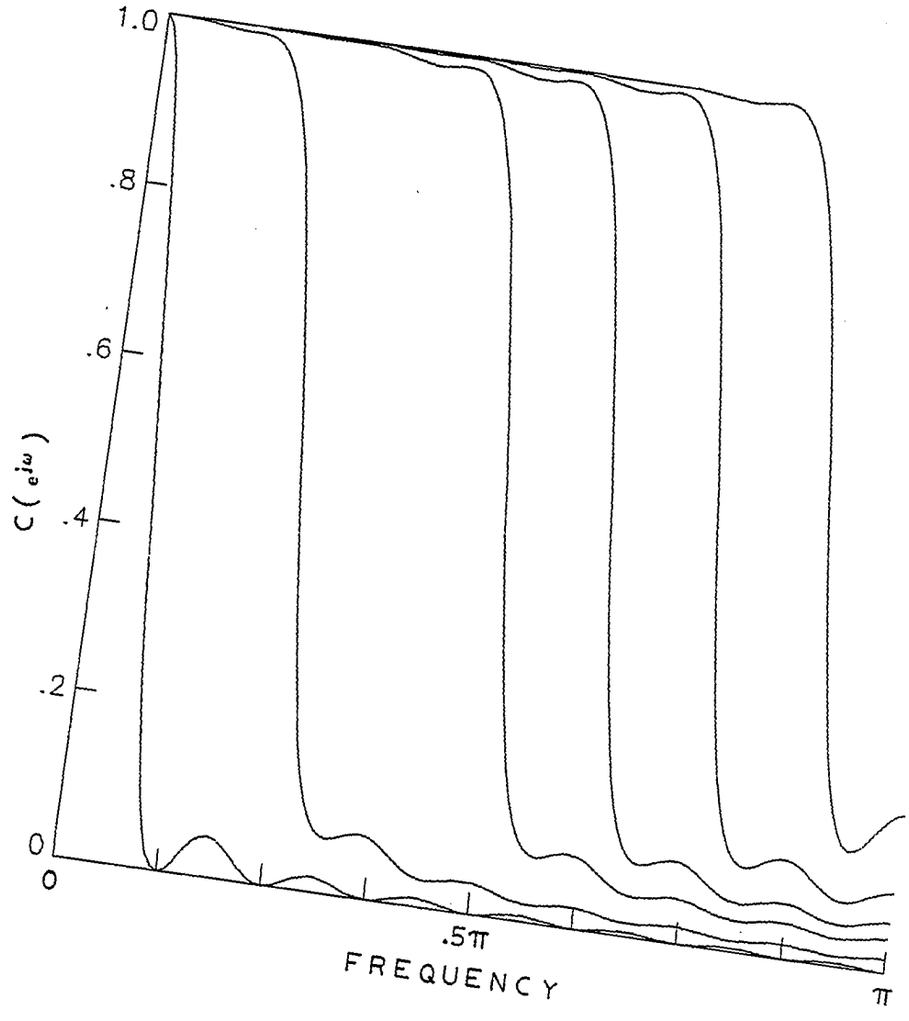

Figure 3.6(b). Composite Magnitude Squared Function, N = 16, M = 1, 4, 8, 10, 12, 14, DC Basis.

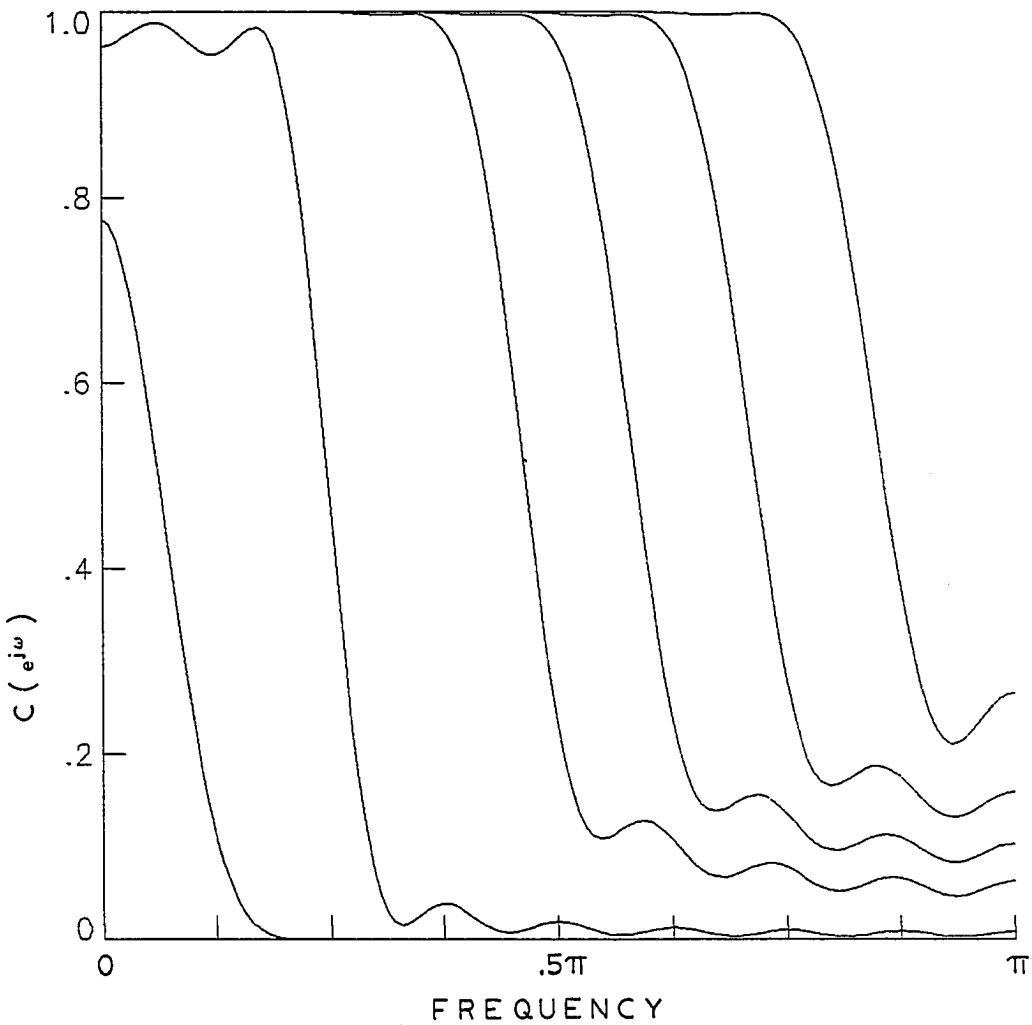

Figure 3.6(c). Composite Magnitude Squared Function, N = 16, M = 1, 4, 8, 10, 12, 14, KL_1 Basis.

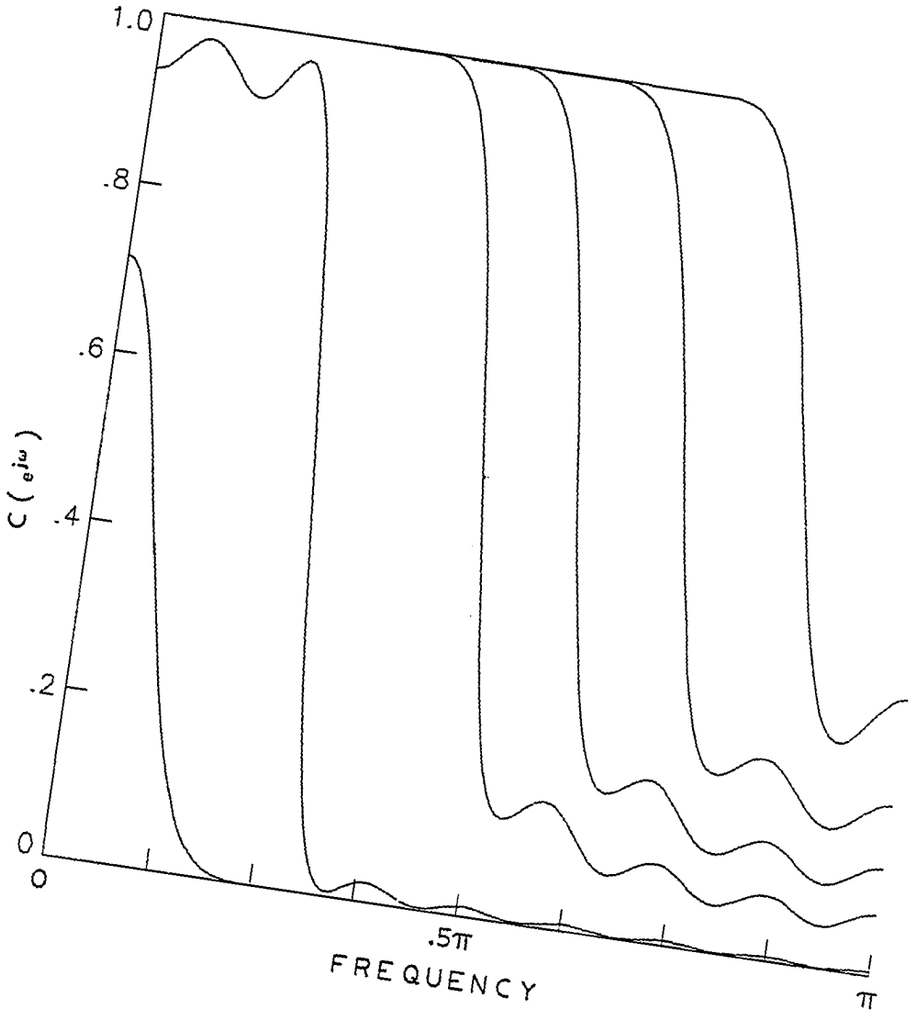

Figure 3.6(d). Composite Magnitude Squared Function, N = 16, M = 1, 4, 8, 10, 12, 14, KL_4 Basis.

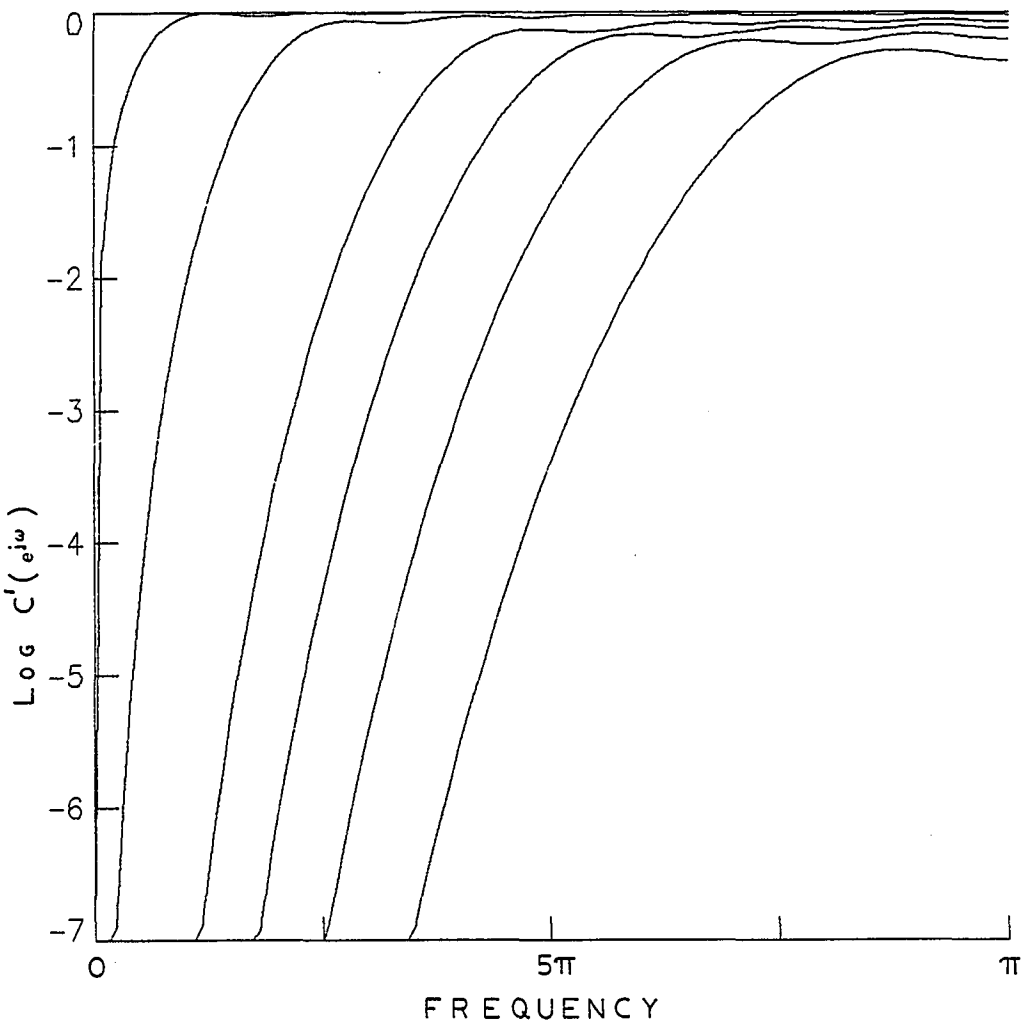

Figure 3.7(a). Log Complimentary Magnitude Squared Function, N = 16, M = 1, 4, 8, 10, 12, 14, DL Basis.

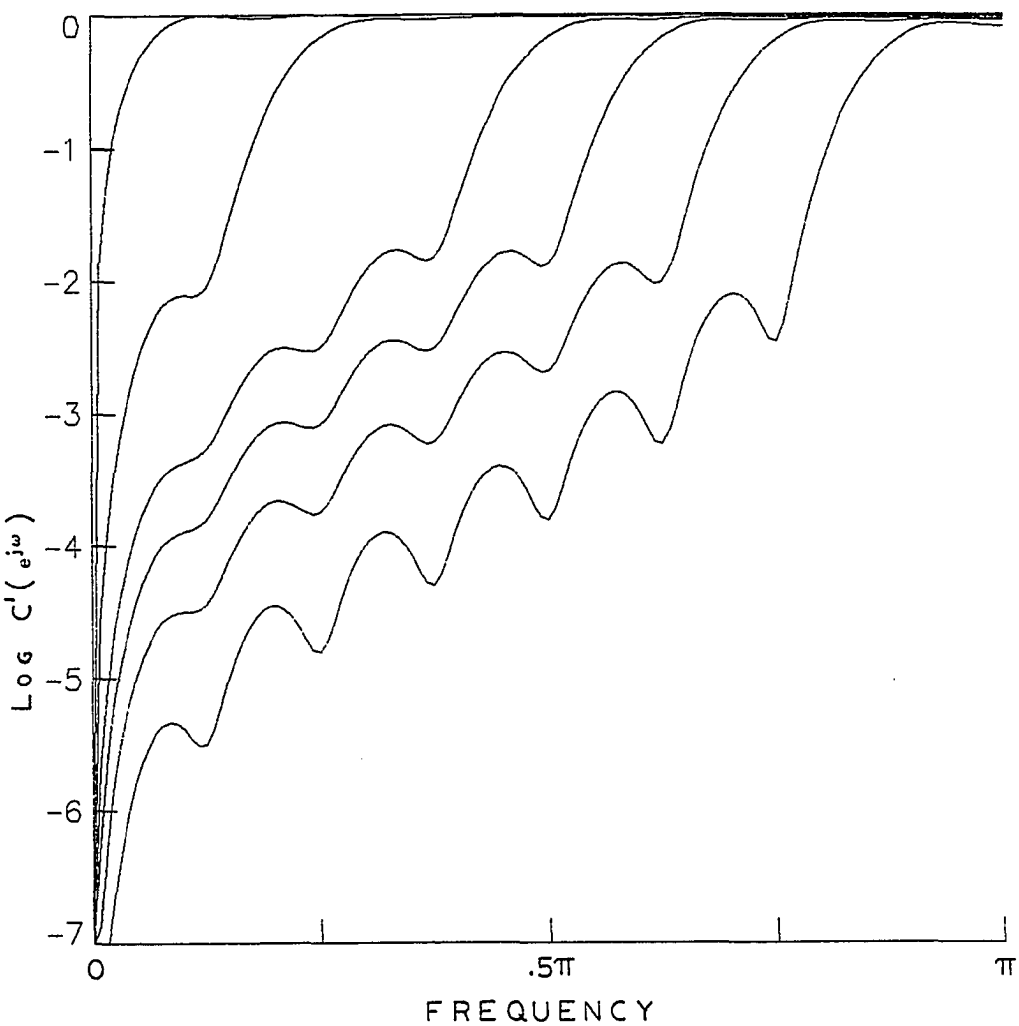

Figure 3.7(b). Log Complimentary Magnitude Squared Function, N = 16, M = 1, 4, 8, 10, 12, 14, DC Basis.

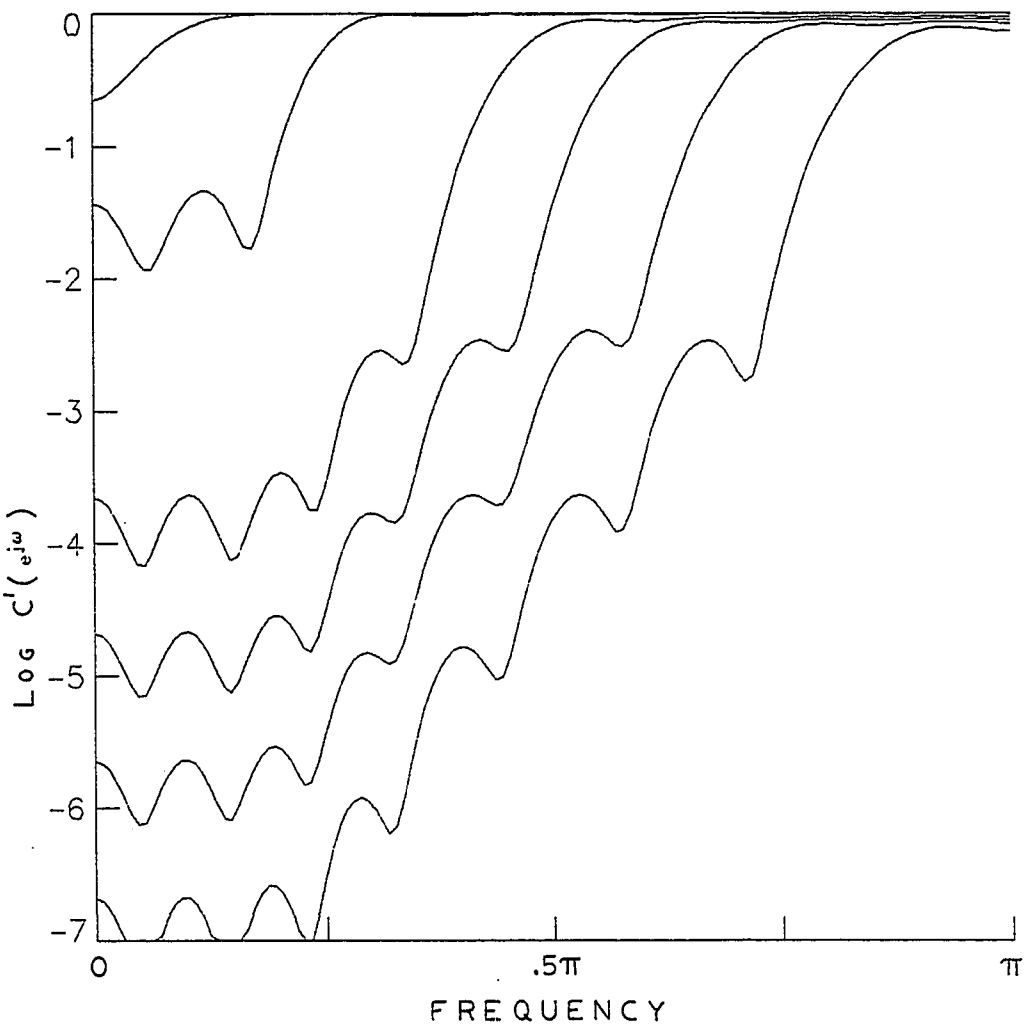

Figure 3.7(c). Log Complimentary Magnitude Squared Function, N = 16, M = 1, 4, 8, 10, 12, 14, KL_1 Basis.

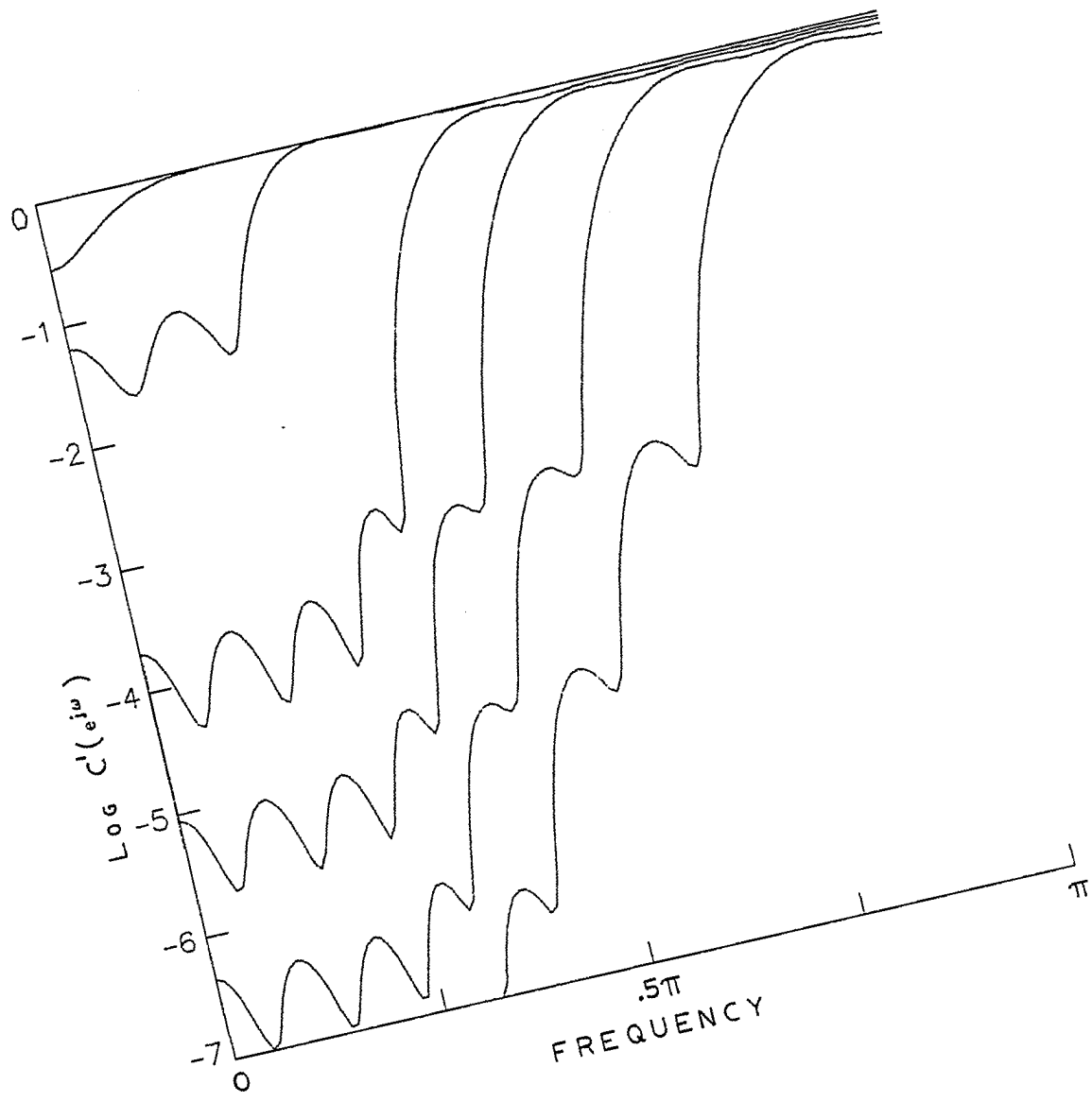

Figure 3.7(d). Log Complimentary Magnitude Squared Function, N = 16, M = 1, 4, 8, 10, 12, 14, KL_4 Basis.

3.5 Signal Plus Noise (Input Digitizer)

Consider the case of presample filtered signal $y^*(p)$ plus additive zero mean, white noise $z^*(p)$ with variance σ_z^2. Then the input to the transformation is

$$x^*(p) = y^*(p) + z^*(p) \ , \tag{3.5.1}$$

or in vector notation, the input for a segment of input is

$$\underline{x} = \underline{y} + \underline{z} \ . \tag{3.5.2}$$

As stated in Section 2.1, transformation is a linear process so the resulting coefficient vector for $\underline{x}$ is

$$\underline{\alpha}_x = \underline{\alpha}_y + \underline{\alpha}_z \tag{3.5.3}$$

where $\underline{\alpha}_y$ and $\underline{\alpha}_z$ are the coefficient vectors for $\underline{y}$ and $\underline{z}$, respectively. Now if $\underline{\alpha}_x$ is quantized, the resulting coefficient vector is

$$\hat{\underline{\alpha}}_x = \underline{\alpha}_y + \underline{\alpha}_z + \underline{\alpha}_Q \tag{3.5.4}$$

where $\underline{\alpha}_Q$ represents the quantizing error. The resulting reconstruction error is

$$\underline{y} - \hat{\underline{x}} = \underline{y} - \Phi^T \hat{\underline{\alpha}}_x = \Phi^T \underline{\alpha}_z + \Phi^T \underline{\alpha}_Q \tag{3.5.5}$$

and the error energy in the segment is

$$\|\underline{y} - \hat{\underline{x}}\|^2 = \|\underline{\alpha}_z + \underline{\alpha}_Q\|^2 \ . \tag{3.5.6}$$

Thus, additive noise at the output of the presample filter is present in the reconstruction. The same is true, of course, for PCM.

Recall that as stated in Section 2.3, white noise is expected to contribute equally to the coefficients of an orthonormal transformation. Thus, when a coefficient is discarded, the input noise energy captured by the discarded coefficient is eliminated also. This in turn reduces the expected input noise contribution to the reconstruction. This means that if additive noise is known to be present and σ_z^2 is greater than $\bar{\alpha}_m$, α_m should be discarded. This is a form of scalar Weiner filtering. The use of orthonormal transforms specifically for this purpose is fully discussed, and additional references are given in the text by Ahmed and Rao [23].

The source of additive input noise of interest here is the input digitizer (ADC) that is part of a discrete transform coding system. This generally is considered to be a white, uniform additive noise source with variance $Q^2/12$ [27], where Q represents the step size or quantization level. The input digitizer can then be expected to contribute error equally to the coefficients and be present in the reconstruction. In order to prevent the input digitizer from contributing significantly to the actual reconstruction error and invalidating the analytical analysis, the quantization level (distortion) must be made appreciably smaller than that of the coefficient quantization level.

3.6 Summary

In this chapter the three bases are compared analytically using equations from Chapter Two. First, presample filters are discussed and four filters are selected for use in the analysis. Two are taken from actual telemetry systems and the remaining two are derived from the first two based on equal attenuation at the folding frequency.

Curves of the calculated coefficient energy are presented and discussed. It is shown that the expected coefficient energy for a random process approaches the power spectral density for the DC and KL basis. This does not appear to be true for the DL. The EPE for the bases is also given for $N = 16$ and $N = 32$ which shows the comparative energy packing performance. The concept of spectral capture is discussed once more with the introduction of the composite magnitude squared function. This is shown for the basis for $N = 16$ for comparison and to provide insight into spectral energy capture. The "low pass" nature of the DL is pointed out. Finally, the coding of signal plus noise is discussed and the need to have input digitizer quantizing level less than the coefficient quantizer level is established.

As pointed out in Section 3.1 coefficients are not anticipated to be discarded from quantization distortion (bit allocation) considerations given the filter specification. Thus, subspace representation for all three bases depends on the relative energy and possibly on the spectral energy capture that is acceptable, and becomes a subjective type of consideration that is to be left up to the data user. The information and analysis given in this dissertation are included for comparison and establish spectral capture as an area of future work.

CHAPTER FOUR

EMPIRICAL RESULTS

4.0 Introduction

In this chapter the results of simulated transform coding of both simulated and real, laboratory gathered data sequences are presented. The basis length of $N = 16$ has been selected as a practical compromise between computational efficiency (speed) and bit rate reduction performance for real-time telemetry applications. As indicated by the curves in Section 3.3, the potential for bit rate reduction increases nonlinearly with N for the transforms being considered. The DL transform is seen to reach its apparent limit much sooner than either the DC or KL transforms. Thus large N would be a disadvantage for the DL. Transmission channel errors are not being addressed in this research; however, it is apparent that transmission bit errors affect the entire block (but only the block) containing the coefficient in error. So this becomes a consideration for keeping the block length small. Tasto and Wintz [10] reported on channel error effects for image transform coding.

Section 4.1 presents a description of the transformation simulation. Section 4.2 describes the generation of simulated and laboratory data sequences. Section 4.3 presents the energy distribution for simulated and laboratory generated data that are obtained by inputing white noise into two presample filters. The bit allocation (coefficient word length) for the filters used in this research are presented in Section 4.4. Also the empirical results and observations for transform

coding of data sequences obtained by sampling filtered random noise, accelerometer, and selected sinusoid signals. Section 4.5 summarizes the chapter.

4.1 Transform Coding Simulation

Transform coding is simulated on a CDC-6600, 60 bit computer using single precision floating point arithmetic. The effect of finite word length arithmetic has been left for future studies. Subroutines generate the transformation matrix Φ for each of the three bases. Once Φ is generated, transform coding is implemented as outlined in Figure 4.1. Input data $x^*(p)$ is read one point at a time to form the N-length input vectors $\underline{x}_k$. Running sums of $x^*(p)$ and $(x^*(p))^2$ are kept. Each input vector is transformed using the applicable Φ to obtain

$$\underline{\alpha}_k = \Phi \underline{x}_k \ . \tag{4.1.1}$$

Running sums of $\alpha_m(k)$ and $(\alpha_m(k))^2$ are kept. Each component of $\underline{\alpha}_k$ is then uniformly quantized by rounding to the nearest multiple of Q, where Q is the quantizing level that would be used for PCM encoding. This is done as

$$\hat{\alpha}_m = \left\lceil \frac{\alpha_m}{Q} + \frac{1}{2} \right\rceil * Q, \quad \alpha_m > 0$$

$$\hat{\alpha}_m = \left\lceil \frac{\alpha_m}{Q} - \frac{1}{2} \right\rceil * Q, \quad \alpha_m < 0 \tag{4.1.2}$$

where $\lceil * \rceil$ denotes largest integer less than *. The quantization error in α_m is obtained as

$$\alpha_{Q,m} = \alpha_m - \hat{\alpha}_m \tag{4.1.3}$$

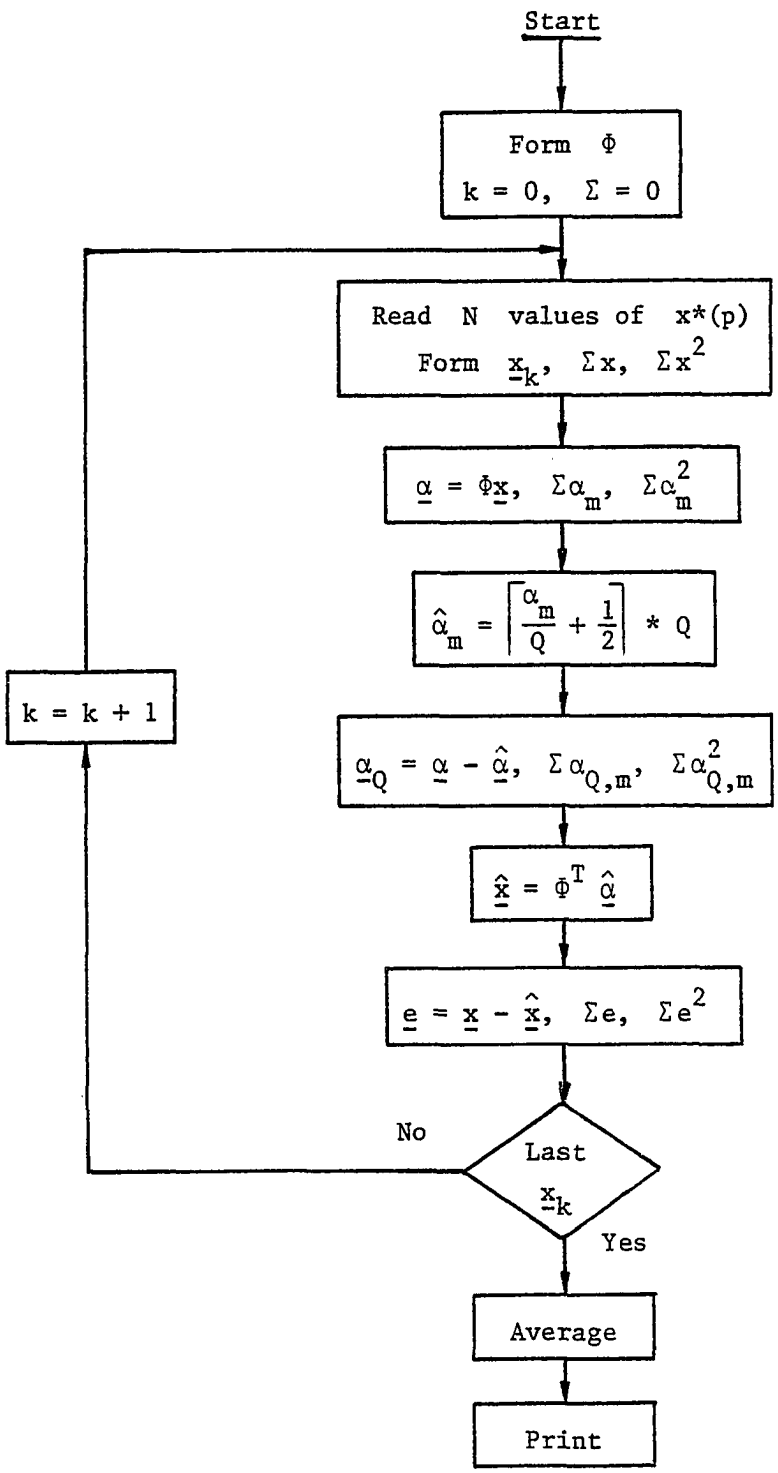

Figure 4.1. Transform Coding Simulation Flow Diagram.

and running sums of $\alpha_{Q,m}(k)$ and $(\alpha_{Q,m}(k))^2$ are kept. The reconstructed signal vector is then formed as

$$\hat{\underline{x}}_k = \Phi^T \underline{\alpha}_k \quad . \tag{4.1.4}$$

The reconstruction error is obtained as

$$\underline{e}_Q = \underline{x} - \hat{\underline{x}} \tag{4.1.5}$$

and running sums of the point by point error $e^*_Q(p)$ and error squared $(e^*_Q(p))^2$ are kept. When the last input value is processed, simple averages are found by dividing all running totals by the number of input points, P. All pertinent data are then printed.

4.2 Input Sequence Generation

4.2.1 Simulated Data Generation

Simulated data are generated on the same CDC-6600 computer. The presample filter is simulated by a digital filter implemented as a parallel combination of second order (even number of poles) sections. The digital transfer function is obtained by performing an impulse invariant design [1] derived from the analog filter specification using twice the sample rate. A normally distributed sequence is generated using a random number generator subroutine that has been thoroughly tested. The sequence is applied to the filter and the data sequence for input to the transform order are formed by taking every other filter output. This method is used because the digital filter transfer function resulting from impulse invariant design is given by

$$F(e^{j\omega}) = \frac{1}{T} \sum_{r=-\infty}^{\infty} F_A \, j \, \frac{\omega}{T} + \frac{2\pi}{T} r \quad . \tag{4.2.1}$$

With the simulation (design) based on twice the final sampling rate, the simulated filter transfer function provides close approximation to the analog filter with the resulting data sequence having the desired power spectral density.

4.2.2 Laboratory Data

In order to evaluate the transform coding strategy on real data, a system was built using presample filters and sample rates which have been used in actual telemetry data systems. Laboratory generated data are used since actual telemetry flight data have been PCM encoded and thus already contains quantizing noise with the same distortion level (variance) as the desired transform coder output. Figure 4.2 is a block diagram of the laboratory system. Signals are input to both filters simultaneously from one of three sources, either a Hewlett Packard HP-3722A noise generator, a Tektronix FG501 function generator, or a quartz accelerometer. The noise generator is based on a filtered pseudo random sequence of infinite length. The filter bandwidth is set to 1.5 kilohertz. The function generator is used to produce sinusoids. The accelerometer is mounted on a thin metal container which is excited by hand. The filters, labeled according to the transfer function designation used in this dissertation, are four pole (F1) and six pole (F4) Butterworth filter with cutoff frequencies as shown. The filter d.c. gains are equal. Data from each filtered source are gathered at a rate of 500 samples per second. A 12 bit analog to digital converter is used. The coding is to be compared to eight and ten bit PCM so a 12 bit digitizer is considered sufficient and indicative of a real application.

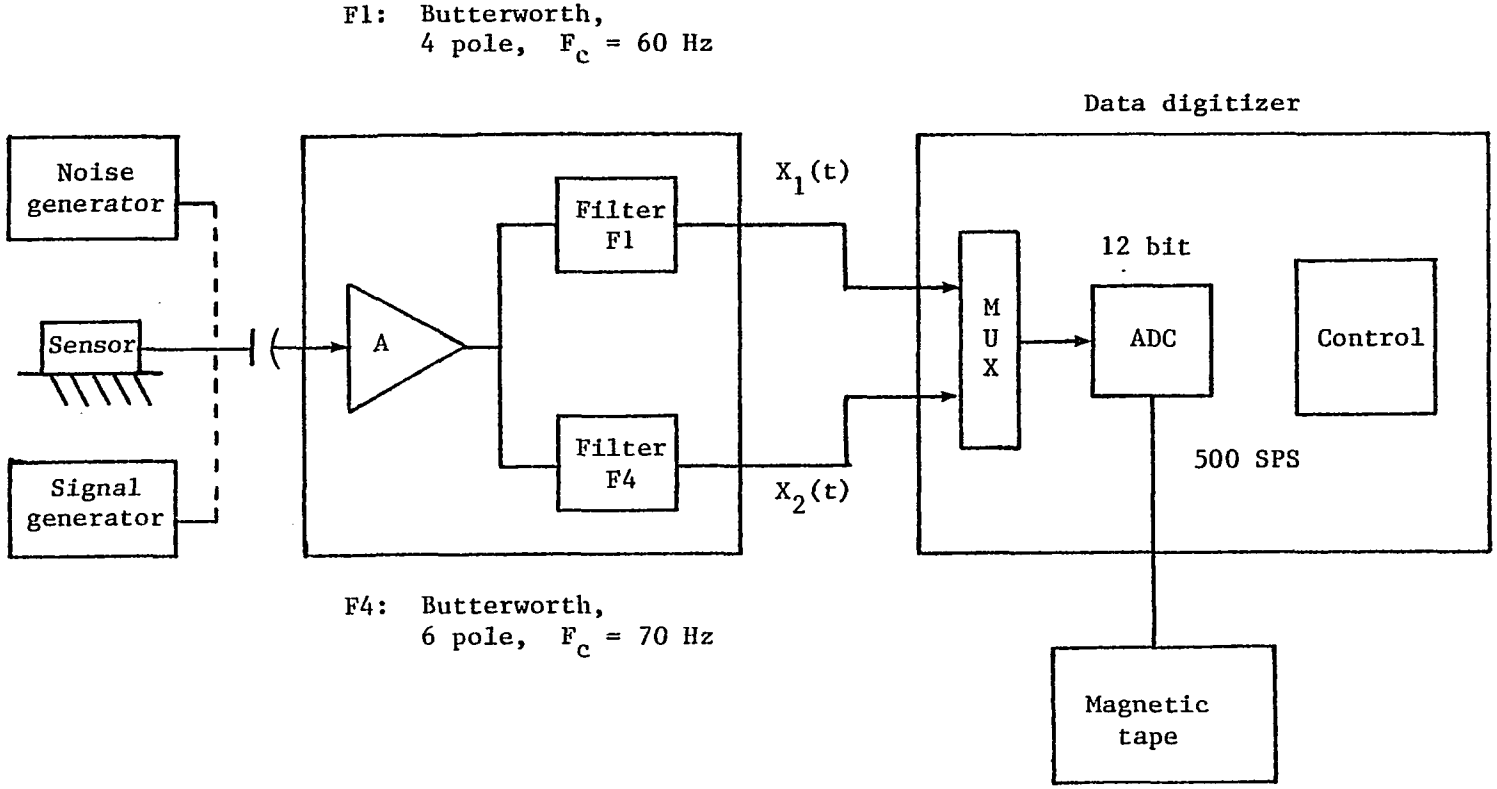

Figure 4.2. Laboratory Data Generation System.

The ADC full-scale range is ± 5 volts. The two's-complement binary ADC output is placed directly on magnetic tape. The random noise and accelerometer sequences from filter F1 that are used for the data presented in this chapter are shown in Figures 4.3 and 4.4, respectively. Table 4.1 provides a summary of the sequence mean and maximum mean square values for the signals processed.

4.3 Energy Distribution for Random Data

Table 4.2 gives the coefficient average energy normalized to the input average energy (mean square value) for the simulated and laboratory generated noise sequences. Also included are the calculated normalized energies given by $N\rho_m$. These data are for 128, length 16 transformed blocks for a total of 2048 input data points. The energy distribution indicates that energy is distributed among the transform coefficients as predicted by the analysis models and simulation. There is some distribution variation due in part to the slight d.c. offset in the data which is captured by or projects onto the $\bar{\alpha}_1^2$ term of the DL and DC bases and onto the $\bar{\alpha}_1^2$ and $\bar{\alpha}_3^2$ terms of the KL basis as expected from the $|H_m(e^{j\omega})|^2$ curves in Chapter Two. This causes a proportionate shift in the other coefficient energies. Other causes are random variation and the quality of the white noise filter input. However, the monotonically decreasing trend is consistent with the theoretical models and thus empirically supports the block transform strategy.

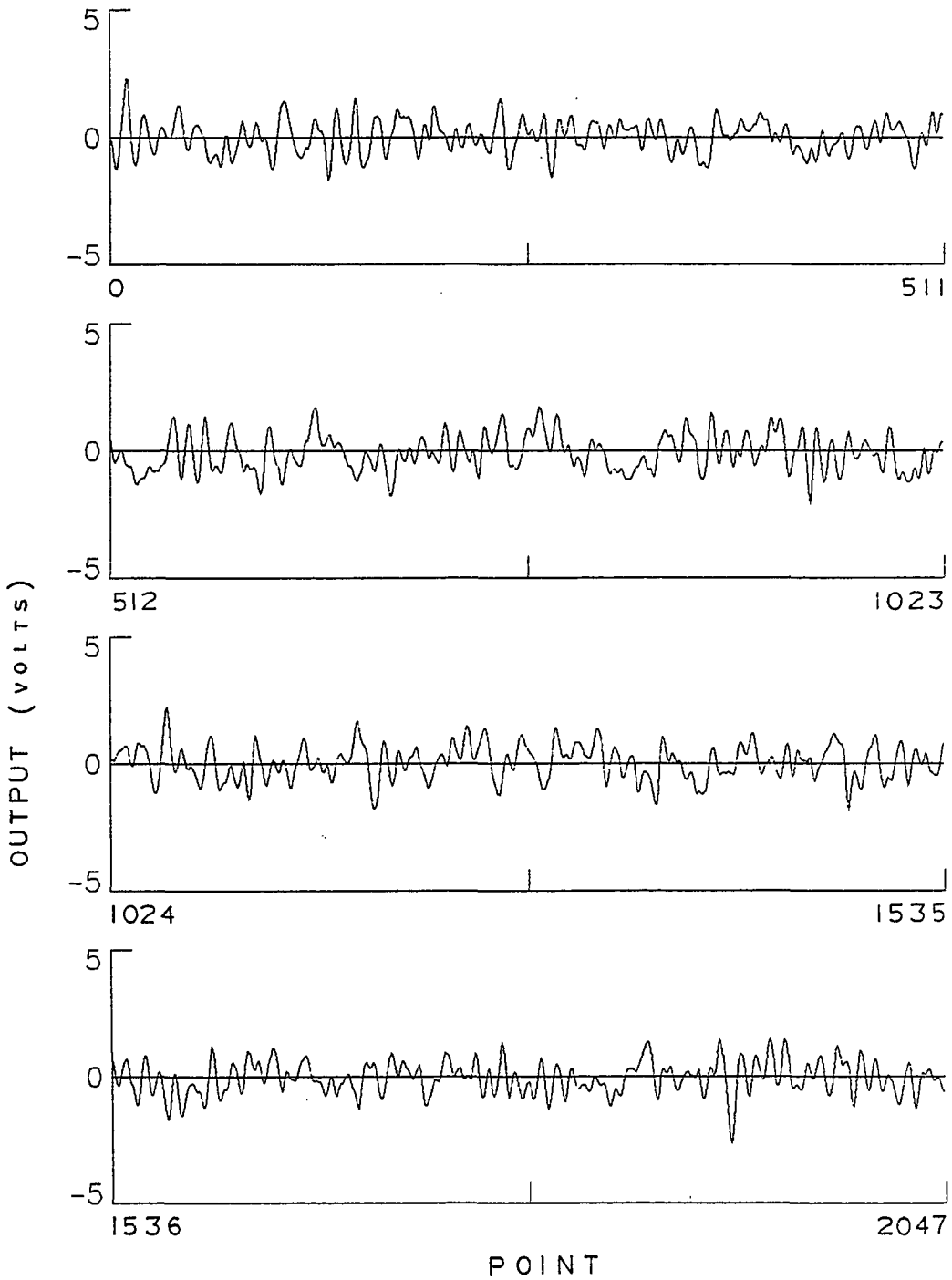

Figure 4.3. Filter F1 2048 Point Output Sequence for White Noise Input.

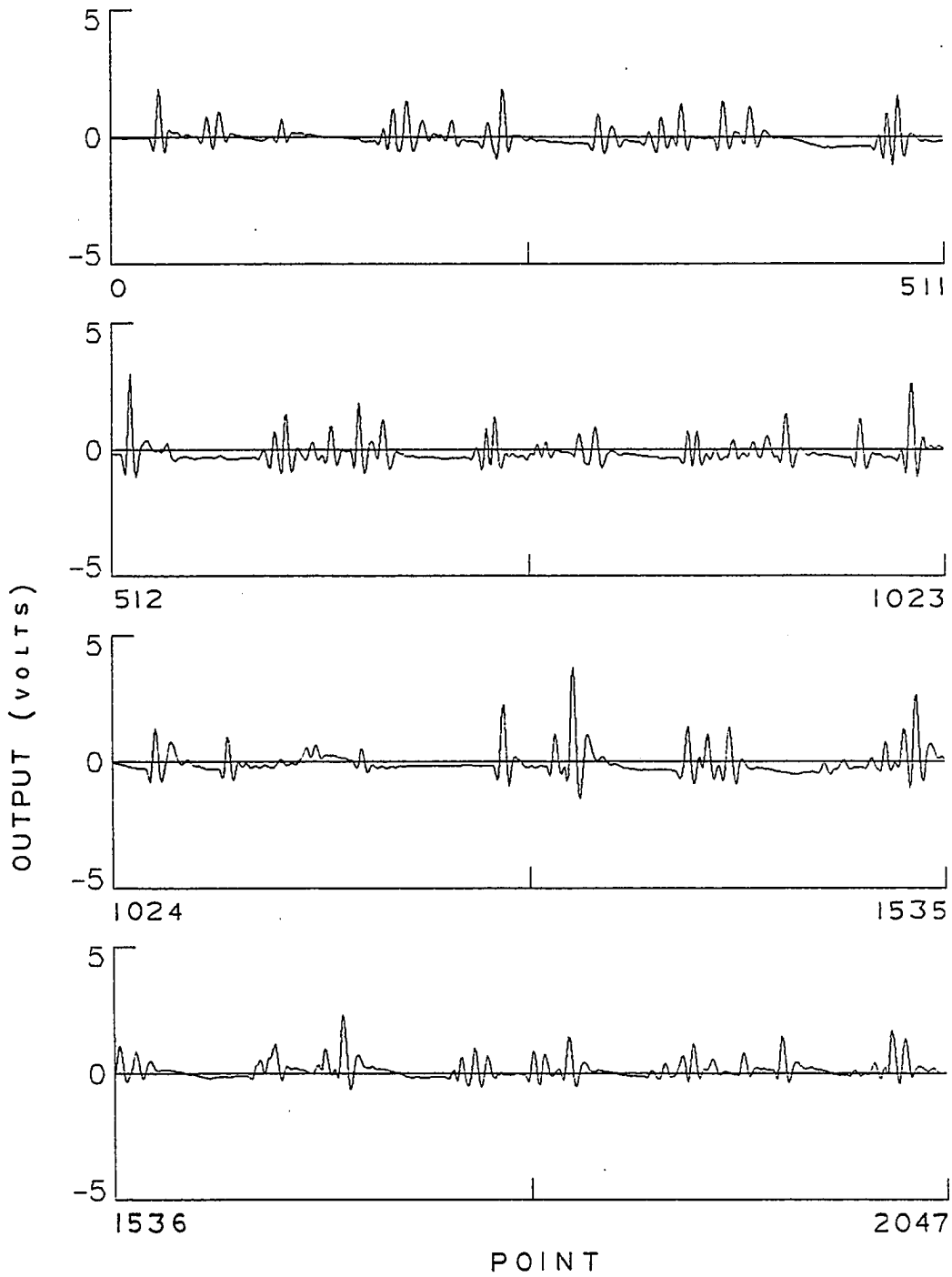

Figure 4.4. Filter F1 2048 Point Output Sequence for Accelerometer Input.

TABLE 4.1 FILTER OUTPUT SIGNAL STATISTICS

INPUT SIGNAL	FILTER F1			FILTER F4		
	MEAN	MEAN SQ	MAX	MEAN	MEAN SQ	MAX
NOISE (SIM)	-.019	1.00	-3.64	-.010	1.00	-3.77
NOISE (GEN)	-.027	.446	-2.62	-.055	.527	-2.69
ACCELEROMETER	-.023	.200	3.74	-.053	.274	4.02
SINUSOID (10Hz)	-.085	4.76	-3.18	-.114	4.86	-3.24
SINUSOID (70Hz)	-.078	1.06	-1.53	-.108	2.38	-2.28

TABLE 4.2(a) NORMALIZED COEFFICIENT ENERGY FOR WHITE INPUT TO FILTER 1

	DL			DC			KL		
m	CALC	SIM	LAB	CALC	SIM	LAB	CALC	SIM	LAB
1	3.86	4.07	4.82	3.86	4.07	4.82	4.06	4.55	4.54
2	3.42	3.61	2.99	3.61	3.78	3.22	3.98	3.83	3.87
3	2.98	3.08	2.37	3.46	3.47	2.70	3.55	3.17	3.40
4	2.43	2.03	2.68	2.76	2.24	2.96	2.49	2.32	2.39
5	1.67	1.63	1.54	1.50	1.57	1.50	1.23	1.42	1.10
6	.931	.841	.898	.536	.603	.502	.460	.486	.441
7	.432	.450	.412	.169	.165	.186	.154	.145	.164
8	.177	.176	.165	.605E-1	.529E-1	.682E-1	.520E-1	.444E-1	.618E-1
9	.680E-1	.610E-1	.770E-1	.246E-1	.288E-1	.288E-1	.187E-1	.191E-1	.185E-1
10	.261E-1	.223E-1	.318E-1	.113E-1	.913E-2	.166E-1	.724E-2	.566E-2	.113E-1
11	.103E-1	.893E-2	.132E-1	.557E-2	.661E-2	.508E-2	.302E-2	.309E-2	.285E-2
12	.429E-2	.331E-2	.624E-2	.289E-2	.299E-2	.380E-2	.135E-2	.158E-2	.162E-2
13	.186E-2	.171E-2	.193E-2	.151E-2	.172E-2	.146E-2	.651E-3	.598E-3	.623E-3
14	.839E-3	.834E-3	.102E-2	.778E-3	.767E-3	.856E-3	.341E-3	.286E-3	.248E-3
15	.389E-3	.318E-3	.395E-3	.380E-3	.377E-3	.344E-3	.200E-3	.166E-3	.193E-3
16	.185E-3	.149E-3	.184E-3	.181E-3	.147E-3	.198E-3	.138E-3	.104E-3	.120E-3

TABLE 4.2(b) NORMALIZED COEFFICIENT ENERGY FOR WHITE INPUT TO FILTER 4

	DL			DC			KL		
m	CALC	SIM	LAB	CALC	SIM	LAB	CALC	SIM	LAB
1	3.38	3.42	4.22	3.38	3.42	4.22	3.53	3.29	3.78
2	3.08	3.26	2.68	3.22	3.34	2.82	3.52	3.38	3.11
3	2.73	2.29	2.52	3.16	2.77	2.87	3.40	3.47	3.98
4	2.42	2.32	2.17	2.97	3.04	2.57	2.88	3.28	2.46
5	2.00	2.07	2.16	2.10	2.18	2.40	1.75	1.64	1.78
6	1.33	1.52	1.13	.865	.985	.832	.675	.734	.670
7	.673	.701	.722	.210	.175	.196	.186	.158	.162
8	.263	.306	.261	.591E-1	.544E-1	.516E-1	.448E-1	.433E-1	.398E-1
9	.840E-1	.814E-1	.862E-1	.207E-1	.180E-1	.204E-1	.107E-1	.990E-2	.104E-1
10	.232E-1	.247E-1	.274E-1	.966E-2	.896E-2	.909E-2	.270E-2	.255E-2	.321E-2
11	.594E-2	.512E-2	.619E-2	.452E-2	.420E-2	.467E-2	.721E-3	.669E-3	.833E-3
12	.149E-2	.153E-2	.191E-2	.251E-2	.234E-2	.226E-2	.205E-3	.244E-3	.220E-3
13	.382E-3	.365E-3	.382E-3	.121E-2	.111E-2	.127E-2	.612E-4	.586E-4	.625E-4
14	.986E-4	.101E-3	.125E-3	.626E-3	.607E-3	.579E-3	.188E-4	.168E-4	.161E-4
15	.242E-4	.265E-4	.250E-4	.234E-3	.215E-3	.258E-3	.569E-5	.568E-5	.848E-5
16	.466E-5	.519E-5	.762E-5	.595E-4	.558E-4	.550E-4	.162E-5	.254E-5	.371E-5

4.4 Bit Allocation and Coding Results

Equation (2.6.17) is used to aid in the evaluation of coefficient word length allocation. The actual integer allocation is made as

$$B_m = \left\lceil B_{PCM} + \frac{1}{2}\log_2(N\rho_m) + 0.5 \right\rceil + 1, \quad m = 1$$

and (4.4.1)

$$B_m = \left\lceil B_{PCM} + \frac{1}{2}\log_2(N\rho_m) + 0.25 \right\rceil + 1, \quad m > 1 \ .$$

This serves to provide some margin of error for coefficient excursions. The first coefficient (m = 1) has been given an extra margin to accommodate d.c. offset and low frequency drift. This conservative allocation reduces the bit rate improvement but guards against coefficient quantization saturation. The resulting assignments are given in Table 4.3. Filters F2 and F3 are included for illustration. The resulting rate reduction over PCM is shown in Table 4.4. This relative performance is consistent with the curves of theoretical improvement shown in Chapter Three. The KL affords the greatest improvement in all cases as expected. The DL provides more improvement than the DC for filters F3 and F4 which have more attenuation (greater variation in energies) than F1 and F2.

Transform coding has been performed on 2048 point sequences of the signals described in Section 4.2. The coefficients have been checked for saturation and none has been found. The resulting reconstruction average distortion (mean square error) are given in Table 4.5. Note that in all cases except one, the distortion for transform coding was better than the theoretical PCM distortion given by $Q^2/12$ [27].

TABLE 4.3 COEFFICIENT BIT ALLOCATION

	FILTER F1			FILTER F2			FILTER F3			FILTER F4		
m	DL	DC	KL	DL	DC	KL	DL	DC	KL	DL	DC	KL
1	10	10	10	10	10	10	12	12	12	12	12	12
2	10	10	10	9	9	9	12	12	12	12	12	12
3	10	10	10	9	9	9	12	12	12	11	12	12
4	9	9	9	9	9	9	11	11	11	11	12	12
5	9	9	9	9	9	9	10	10	10	11	11	11
6	9	8	8	9	9	9	9	9	8	11	11	10
7	8	7	7	9	9	9	8	8	7	10	10	10
8	7	7	7	9	8	8	7	8	6	10	9	8
9	7	6	6	8	7	7	6	7	6	9	8	7
10	6	6	5	8	7	7	6	6	5	8	7	6
11	5	5	5	7	6	6	5	6	4	7	7	6
12	5	5	4	6	5	5	4	5	4	6	6	5
13	4	4	3	6	5	4	4	5	3	5	6	4
14	4	4	3	5	4	3	3	5	3	4	5	3
15	3	3	3	4	3	2	3	4	2	3	5	2
16	3	3	2	2	2	1	2	3	2	2	4	1

TABLE 4.4 BIT RATE IMPROVEMENT
BITS PER SAMPLE(BPS) AND PERCENT

	FILTER F1		FILTER F2	
	BPS	%	BPS	%
DL	1.19	15	.56	7
DC	1.38	17	1.06	13
KL	1.75	22	1.31	16

(a) EIGHT BIT PCM

	FILTER F3		FILTER F4	
	BPS	%	BPS	%
DL	2.88	29	1.75	17
DC	2.31	23	1.44	14
KL	3.31	33	2.44	24

(b) TEN BIT PCM

TABLE 4.5 RECONSTRUCTION MEAN SQUARE ERROR

INPUT SIGNAL	FILTER F1			FILTER F4		
	DL	DC	KL	DL	DC	KL
NOISE (SIM)	.125E-3	.125E-3	.121E-3	.764E-5	.777E-5	.721E-5
NOISE (GEN)	.119E-3	.121E-3	.119E-3	.768E-5	.792E-5	.714E-5
ACCELEROMETER	.964E-4	.101E-3	.927E-4	.655E-5	.733E-5	.680E-5
SINUSOID (10Hz)	.456E-4	.116E-3	.897E-4	.420E-5	.712E-5	.688E-5
SINUSOID (70Hz)	.108E-3	.130E-3	.103E-3	.668E-5	.780E-5	.719E-5
	PCM: $Q^2/12$ = .127E-3			PCM: $Q^2/12$ = .795E-5		

This is a result of self-imposed dimension reduction due to the capture of most of the energy in the low-order coefficients. As a result, the high-order coefficients often have zero values assigned by the quantization. For the purpose of reconstruction, this is equivalent to block by block discarding the coefficient. Thus, as expressed by equation (2.6.17) the reconstruction error contribution of these coefficients tends to be more like the coefficient energy than the expected quantizing distortion. This is particularly evident in the 10 Hz sinusoid. Note that the DL basis results in less average distortion than either the DC or KL bases for the reduced bandwidth (10 Hz) signal. This is a manifestation of the composite spectral capture property discussed in Section 3.4. The effect is illustrated in detail in Table 4.6 which gives the average coefficient energies and associated quantization distortion for the DL transform of the 10 Hz sinusoid compared to the random noise signal for filter F1. Note that for the 10 Hz sinusoid the quantization distortion is equal to the coefficient energy for $m \geq 5$. These coefficients all were assigned the value zero by the quantizer.

For the signals examined here a priori subspace reduction by discarding the last two coefficients would not have been a severe penalty even from a total energy loss standpoint. This is illustrated by Table 4.7 which gives the resulting distortion for eliminating the last two coefficients prior to reconstruction. From the bit allocation given in Table 4.3 the additional bit savings can be obtained. Note that for filter F4, the DL and KL both result in less distortion than the DC.

TABLE 4.6 DL AVERAGE COEFFICIENT ENERGY AND QUANTIZING ERROR ENERGY FILTER F1

m	GENERATED NOISE		10Hz SINUSOID	
	ENERGY	ERROR	ENERGY	ERROR
1	4.07	.114E-3	52.0	.150E-3
2	3.62	.139E-3	22.3	.121E-3
3	3.08	.133E-3	1.74	.117E-3
4	2.03	.126E-3	.543E-1	.123E-3
5	1.63	.110E-3	.909E-3	.139E-3
6	.841	.121E-3	.548E-4	.548E-4
7	.450	.118E-3	.126E-4	.126E-4
8	.176	.110E-3	.441E-5	.441E-5
9	.610E-1	.126E-3	.192E-5	.192E-5
10	.223E-1	.143E-3	.116E-5	.116E-5
11	.893E-2	.127E-3	.104E-5	.104E-5
12	.330E-2	.139E-3	.882E-6	.882E-6
13	.171E-2	.102E-3	.784E-6	.784E-6
14	.834E-3	.131E-3	.727E-6	.727E-6
15	.318E-3	.143E-3	.662E-6	.662E-6
16	.149E-3	.111E-3	.850E-6	.850E-6

PCM: $Q^2/12$ = .127E-3

TABLE 4.7 RECONSTRUCTION MEAN SQUARE ERROR
(14 or 16 COEFFICIENTS)

INPUT SIGNAL	FILTER F1			FILTER F4		
	DL	DC	KL	DL	DC	KL
NOISE (SIM)	.138E-3	.142E-3	.130E-3	.884E-5	.237E-4	.726E-5
NOISE (GEN)	.124E-3	.124E-3	.115E-3	.809E-5	.173E-4	.715E-5
ACCELEROMETER	.100E-3	.110E-3	.102E-3	.692E-5	.185E-4	.681E-5
SINUSOID (10Hz)	.456E-4	.116E-3	.986E-4	.420E-5	.119E-4	.688E-5
SINUSOID (70Hz)	.108E-3	.169E-3	.103E-3	.666E-5	.135E-3	.719E-5
	PCM: $Q^2/12$ = .127E-3			PCM: $Q^2/12$ = .795E-5		

This is consistent with the coefficient energy distribution curves of Chapter Three and again a manifestation of spectral capture. For the last three signals listed, the DL and KL continue to result in less distortion than expected from PCM. Again this is because the energy in the discarded coefficients is less than the quantizing error $Q^2/12$. This is consistent with the composite spectral capture expected for the basis for reduced bandwidth signals.

Since Φ is orthogonal, so is Φ^T. Then $\underline{e}_Q$, the error vector in the reconstruction (see Chapter Two), is an orthonormal transformation of $\underline{\alpha}_Q$, the coefficient quantizing error vector. The vector $\underline{\alpha}_Q$ can be thought of as a segment from a zero mean, while uniform source with variance $\bar{D}_{TC} = \bar{D}_{PCM} = Q^2/12$ the mean square quantizing distortion. Then error $e_{Q,n}$ at a point of the reconstructed vector $\hat{\underline{x}}$ is given by

$$e_{Q,n} = \langle \underline{\psi}_n, \underline{\alpha}_Q \rangle \tag{4.4.2}$$

where $\underline{\psi}_n$ is an orthonormal vector equal to the nth row of Φ^T. Following the analysis at the end of Section 2.3 the expected error (variance) of $e_{Q,n}$ is $Q^2/12$. This agrees with the results of Section 2.6. Since the error is formed by a weighted sum (inner product) the distribution is going to become more normal by virtue of the central limit theorem [32].

To illustrate the form of the reconstruction error, Figures 4.5 and 4.6 are included. Figure 4.5(a) shows the PCM (identity transform) reconstruction error for the first 32 blocks (512 points) of filter F1 output for white noise input (Fig. 4.3). Figure 4.5(b) shows the DL transform coding reconstruction error for the same sequence.

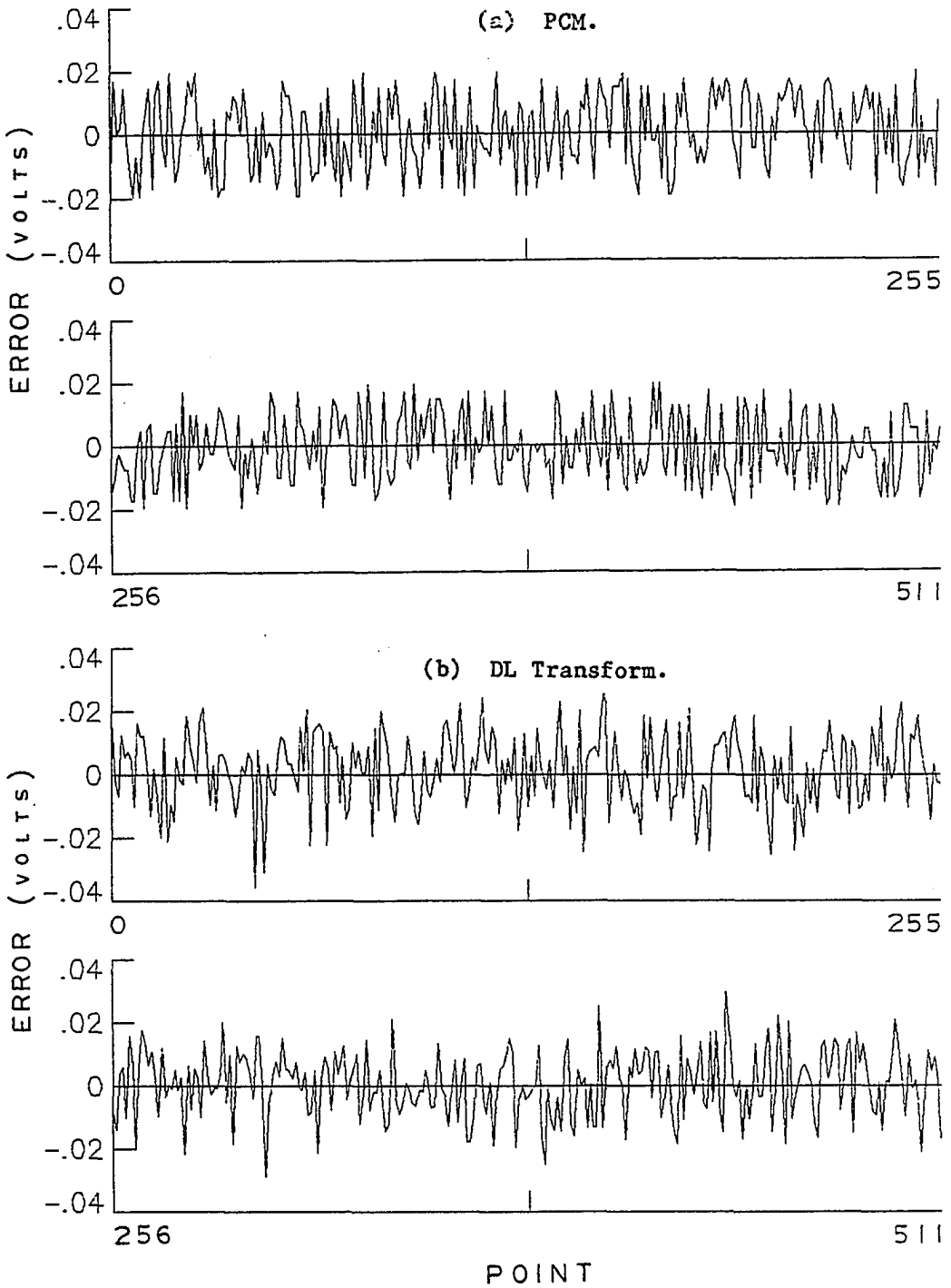

Figure 4.5. Reconstruction Error for First 512 Points of F1 Noise Sequence.

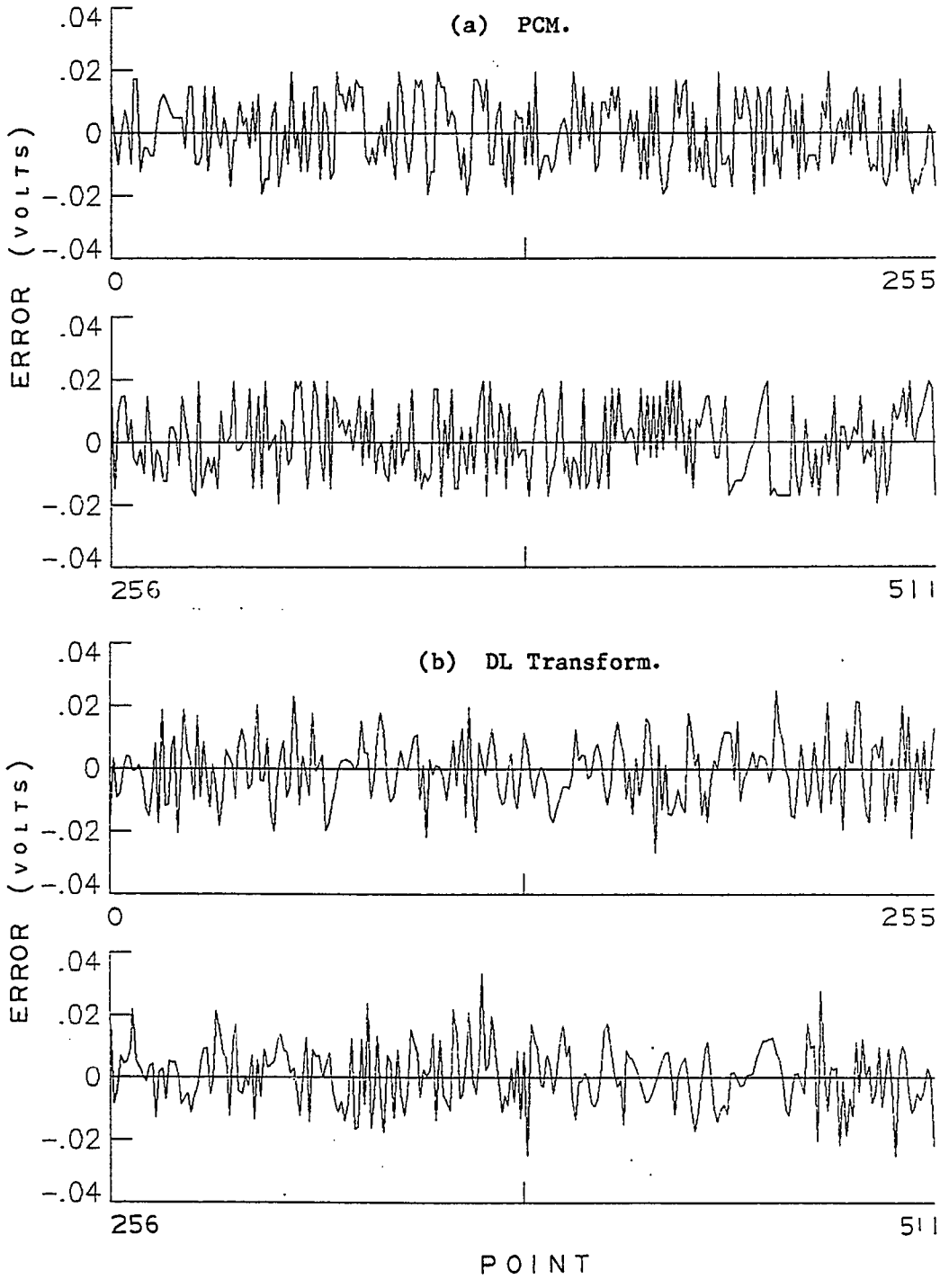

Figure 4.6. Reconstruction Error For First 512 Points of F1 Accelerometer Sequence.

Note that the PCM error appears to be uniform and bounded by Q/2 (0.02) as expected. The error from DL transform coding exceeds 0.02 and appears to be more normal as anticipated. This is representative of all three transforms. Figures 4.6(a) and 4.6(b) show the PCM and DL transform coding errors for the first 32 blocks of the filter F1 output for the accelerometer input (Fig. 4.4). Note the effect of subspace capture due to self-induced coefficient elimination (i.e., reduced distortion) for intervals of low-spectral content, particularly the interval between points 385 and 480.

4.5 Summary

In this chapter the results of transform coding simulated on a CDC-6600 computer are reported. The coding has been applied to simulated and laboratory generated data sequences. The actual integer coefficient bit allocation equations are given with the resulting assignments for the four filters being considered. The results of applying the transform coding strategy to 2048 point data sequences are presented. Tabulated results show that input energy is distributed among the coefficients as expected and that the reconstruction error for the transform coding is equal to or less than that expected for PCM. The effect of self-imposed subspace restriction as a result of spectral energy capture is discussed and illustrated. Example sequences illustrating the form of the reconstruction error are given. All the results are consistent with the analysis of Chapter Three.

CHAPTER FIVE

CONCLUSION

This dissertation addressed the application of nonadaptive transform coding to presample filtered telemetry data for the purpose of bit rate reduction over conventional PCM. Three bases were considered: a filter derived Karhunen-Loueve (KL) basis, a basis of discrete cosines (DC) which are also discrete Chebychev polynomials, and a basis of discrete Legendre (DL) polynomials which have received little or no attention for transform coding. The transform coding strategy resulted in bit rate reduction on the order of 25 percent for block lengths of $N = 16$. Additionally, transform coding was shown to reduce the quantization distortion in the reconstructed signal when the signal has intervals of low activity (reduced spectral content). The potential for further rate reduction by a-priori elimination of coefficients was also explored. It was found that the additional bit rate improvement is conditioned on the signal (spectral) energy capture within some acceptable limits. Thus the improvement is a subjective consideration that should be treated in future study.

A family of Butterworth filters was used in this study. Two of the filters were taken from actual telemetry systems. The two additional filters included for comparison were derived from the first two by changing the filter order and requiring the same attenuation at the folding frequency. Analytical basis comparisons were presented for all

four filters. Real data output from the first two filters was used for empirical study.

Transform coding leads to bit rate reduction because the input energy is redistributed among the coefficients of the transformation, thus enabling fewer bits to be used to code the coefficient sequences in lieu of the input sequence. In order to analytically determine the bound on energy redistribution, successive transformation was modeled as the output sampling of a bank of finite impulse response filters whose impulse response is equal to the reverse-order basis sequence. Parseval's relation could then be used to provide an expression for the coefficient sequence energy. The resulting expression involved the product of the basis filter magnitude squared transfer function (MSF) and the presample filter output sequence magnitude squared transfer function or power spectral density. In this way the concept of spectral energy capture of a coefficient was introduced. This provides insight into the mechanism for energy redistribution.

It is known that the KL basis is optimum in the sense of energy packing (redistribution) and, hence, bit rate reduction for stationary sources. It was assumed that the presample filter magnitude squared transfer function provides the spectral envelope or power spectral density of the worst case (most robust) filter output. The KL basis derived from the filter function was then assumed to be optimum for this application and sufficient to demonstrate bit rate reduction.

The suboptimal deterministic DC, Figure 2.3, and DL, Figure 2.4, bases were defined. They were observed to have similar basis shapes and frequency selective coefficient filter MSF's to that of the filter dependent KL, Figure 2.2. The use of a deterministic (not a function of

the filter) basis has practical significance for process storage reduction. For instance, several filters can be managed using a single processor.

Analytical comparison of energy distribution, Figures 3.2 and 3.3, and energy packing, Tables 3.1 and 3.2, for $N = 16$ and $N = 32$ were made between the three bases. The KL was observed to have the most efficient packing as expected. The energy distribution was seen to approximate the shape of the filter magnitude squared function for all three bases. Thus all three bases were observed to have a large percentage of the energy packed into the low-order coefficients. The DL, however, appeared to be diverging slightly from the KL with increasing N. The KL and DL are known to approach the power spectral density as $N \to \infty$. This is a manifestation of the spectral selectivity properties of the basis and suggests that spectral selectivity is a necessary property for transform coding.

Coefficient quantizing and bit allocation, with the requirement to have the same distortion as PCM, were examined using procedures similar to those of Zelinski and Noll [17]. This led to the result that each coefficient should be quantized using the same quantization level that would have been used for PCM. Bit allocation then becomes an adjustment in dynamic range in each coefficient. This led to a theoretical bound for full space bit rate reduction in terms of the geometric mean of coefficient energies. Comparative plots of the bound for $N = 8$ through 32 were given in Figure 3.5. The KL was again observed to be the best of the three bases. The DL and DC were seen to approximate the KL. The fact that the KL and DC approach the PSD as $N \to \infty$ leads to an expression for the asymptote for full space transform

coding. The KL and DC were observed to approach this limit at a non-linear rate that quickly led to diminishing returns for increasing N. This indicates that the increased computational load for large N may not be justified for the filter functions considered. This is encouraging for real time telemetry applications. The DL was observed to approach a lesser asymptote and apparently reach its limit much sooner than either the KL or DC basis. This is consistent with the observation that the energy distribution does not approach the PSD as $N \to \infty$ for the DL basis. However, for the two filters with greater attenuation (variation in dynamic range) the curves indicate the DL to be superior to the DC for low values of N. Thus, for applications using filters corresponding to low distortion, say 10 to 12 bits, the DL is suggested.

Further comparison based on the concept of spectral capture was addressed by the introduction of a composite magnitude squared function. This represents the combined spectral capture for a subset of coefficients (the spectral equivalent to energy packing). It was noted that the low-frequency capture properties of the DL basis exceeded both the KL and DC bases. It is suggested that subspace representation is an area that may be viewed from spectral capture for future research and that the DL basis may have desirable properties.

Transform coding of filter output plus noise was addressed for the purpose of assessing input digitizer effects. It was shown that white input noise distributes equally among the coefficients and shows up as an additive error in the reconstruction distortion. Thus the input digitizer (quantization) level should be kept smaller than the coefficient quantization level. Future analysis is to address the tradeoffs. The diagnostic properties of the DL and other transforms for the

detection of input noise is also an area for future consideration. It was also shown that the discarding of coefficients potentially reduces the input noise contribution to reconstruction error. This is a form of scalar Weiner filtering as discussed in Ahmed and Rao [23]. This is another area where the DL properties may prove beneficial.

Transform coding for block length $N = 16$ with conservative integer bit allocation as given in Table 4.3 was applied to simulated and laboratory generated data sequences. For all inputs processed the coefficients were checked for saturation and none was found. The KL provided 22 percent rate reduction for the 8 bit PCM filter F1 and 24 percent rate reduction for the 10 bit PCM filter F4. The DC and DL were slightly less for both filters (see Table 4.4). For filter F4 the DL afforded more reduction (17 percent compared to 14 percent) than the DC as the analytical curves suggested. The results for both simulated and generated white noise input as given in Table 4.2 supported the analysis in terms of predicted energy distribution.

The use of transform coding was shown to effect the form of the reconstruction error in two ways. First, the error distribution function tends to a normal distribution instead of uniform as in the PCM case. This is illustrated in Figure 4.5. Secondly, for signals with intervals of low activity (low spectral energy content) the reconstruction error can be less than that for PCM. This can be seen for the accelerometer data reconstruction error in Figure 4.6 and from the mean square distortion given in Table 4.5 for the accelerometer and sinusoid signals. This latter property is by virtue of self-imposed subspace restriction resulting from the assignment of the value zero to high order coefficients which are less than one-half the quantization level.

The experimental evidence in Table 4.5 supports the suggestion that the DL basis has superior performance from this respect.

The filters considered here were specified with maximum bandwidth relative to the filter order, quantizing distortion, and sample frequency. This is typical for telemetry applications. For other types of filters, possibly very over-sampled applications, transform coding and particularly the use of the DL basis may provide even more savings.

Other areas of research directly related to the application of telemetry are the effect of finite arithmetic on the transformation and the development of a "fast" DL transform, although large values of N are not seen to be demanded for the filters here.

It was observed for transform coding of real data that a lot of leading zero bits are transmitted. Thus the investigation into adaptive coding for applications which are not limited to fixed transmission bit rate is suggested.

Another area of application for future research is the consideration of "pass band" spectral capture and "perceptual" coding, that is, the allocation of more bits (less distortion) to the coefficients that capture energy in the spectral band of interest. This is an application where the DL basis properties appear to have promise.

LIST OF REFERENCES

1. A. V. Oppenheim and R. W. Schafer, "Digital Signal Processing," Prentice-Hall, Inc., Englewood Cliffs, New Jersey, 1975.

2. A. N. Netravali and J. O. Limb, "Picture Coding: A Review," Proc. IEEE, vol. 68, no. 3, pp. 366-406, March 1980.

3. J. J. Y. Huang and P. M. Schultheiss, "Block Quantization of Correlated Gaussian Random Variables," IEEE Trans. on Commun. Syst., vol. CS-11, pp. 289-296, Sept. 1963.

4. J. Pearl, "Basis-Restricted Transformation and Performance Measures for Spectral Representations," IEEE Trans. Inform. Theory, vol. IT-17, pp. 751-752, Nov. 1971.

5. L. D. Davisson, "Rate-Distortion Theory and Application," Prod. IEEE, vol. 60, no. 7, pp. 800-808, July 1972.

6. A. Segall, "Bit Allocation and Encoding for Vector Sources," IEEE Trans. on Inform. Thy., vol. IT-22, no. 2, pp. 162-169, March 1976.

7. P. Yip and K. R. Rao, "Energy Packing Efficiency for the Generalized Discrete Transforms," IEEE Trans. on Comm., vol. COM-26, no. 8, pp. 1257-1262, Aug. 1978.

8. S. J. Campanella and G. S. Robinson, "A Comparison of Orthogonal Transformations for Digital Speech Processing," IEEE Trans. on Commun. Tech., vol. COM-19, no. 6, pp. 1045-1049, Dec. 1971.

9. G. S. Guner and R. L. Granger, "Fast Fourier Transform Speech Compression," Proceeding of International Conference on Communications, San Francisco, Calif., pp. 33-38, June 8-10, 1970.

10. M. Tasto and P. A. Wintz, "Image Coding by Adaptive Block Quantization," IEEE Trans. on Commun. Tech., vol. COM-19, no. 6, pp. 957-972, Dec. 1971.

11. A. Habibi and P. A. Wintz, "Image Coding by Linear Transformation and Block Quantization," IEEE Trans. on Commun. Tech., vol. COM-19, no. 1, pp. 50-61, Feb. 1971.

12. H. B. Kekre and J. K. Solanki, "Comparative Performance of Various Trigonometric Unitary Transforms for Transform Image Coding," Int. J. Electronics, vol. 44, no. 3, pp. 305-315, March 1978.

13. C. Ekambaram and S. C. Kwatra, "A New Architecture for Adaptive Transform Compression of NTSC Composite Video Signal," Proceedings National Telecommunications Conference, New Orleans, Louisiana, pp. C9.6.1-C9.6.4, Dec. 3, 1981.

14. T. Ohira, M. Hayakawa, and K. Matsumoto, "Orthogonal Transform Coding System for NTSC Color Television Signals," IEEE Trans. on Comm., vol. COM-26, no. 10, pp. 1454-1463, Oct. 1978.

15. D. A. Huffman, "A Method for the Construction of Minimum-Redundancy Codes," Proc. IRE, vol. 40, pp. 1098-1101, Sept. 1952.

16. R. M. Haralick and K. Shanmugam, "Comparative Study of a Discrete Linear Basis for Image Data Compression," IEEE Trans. on Sys. Man, and Cyber, vol. SMC-4, no. 1, pp. 16-27, Jan. 1974.

17. R. Zelinski and P. Noll, "Adaptive Transform Coding of Speech Signals," IEEE Trans. Acoust., Speech, and Signal Processing, vol. ASSP-25, no. 4, pp. 299-309, Aug. 1977.

18. H. Hotelling, "Analysis of a Complex of Statistical Variables into Principal Components," J. Educ. Psychol., vol. 24, pp. 417-441, 498-520, 1933.

19. N. Ahmed, T. Natarajan, and K. R. Rao, "Discrete Cosine Transform," IEEE Trans. on Computers, vol. C-23, pp. 90-93, 1974.

20. M. D. Flicker and N. Ahmed, "A Derivation for the Discrete Cosine Transform," Proc. IEEE, vol. 70, no. 9, pp. 1132-1134, Sept. 1982.

21. F. Y. Y. Shum, A. R. Elliott, and W. O. Brown, "Speech Processing With Walsh-Hadamard Transforms," IEEE Trans. on Audio and Electroacous., vol. AU-21, no. 3, pp. 174-179, June 1973.

22. H. Kitajima, "Energy Packing Efficiency of the Hadamard Transform," IEEE Trans. on Comm., vol. COM-24, pp. 1256-1258, 1976.

23. N. Ahmed and K. R. Rao, "Orthogonal Transforms for Digital Signal Processing," Springer-Verlag, New York, Heidelberg, Berlin, 1975.

24. N. Ahmed, K. R. Rao, and R. B. Schultz, "A Generalized Discrete Transform," Proc. IEEE, vol. 59, pp. 1360-1362, 1971.

25. D. M. Peterson, "Methods in Data Reduction: I. Another Look at Least Squares," Pub. of the Astronomical Society of the Pacific, 91:546-552, pp. 546-552, Aug. 1979.

26. L. E. Franks, "Signal Theory," Prentice-Hall, Inc., Englewood Cliffs, New Jersey, 1969.

27. S. A. Tretter, "Introduction to Discrete-Time Signal Processing," John Wiley & Sons, New York, 1976.

28. A. V. Oppenheim and D. H. Johnson, "Discrete Representation of Signals," Proc. IEEE, vol. 60, no. 6, pp. 681-691, June 1972.

29. W. H. Chen and C. H. Smith, "Adaptive Coding of Monochrome and Color Images," IEEE Trans. Commun., vol. COM-25, pp. 1285-1292, Nov. 1977.

30. A. Papoulis, "Signal Analysis," McGraw-Hill Book Company, New York, St. Louis, San Francisco, 1977.

31. L. R. Rabiner and B. Gold, "Theory and Application of Digital Signal Processing," Prentice-Hall, Inc., Englewood Cliffs, New Jersey, 1975.

32. J. B. Thomas, "Statistical Communication Theory," John Wiley & Sons, Inc., New York, 1969.

APPENDIX

A.1 Evaluation of Integrals

Some of the equations presented in Chapter Two and Chapter Three require the evaluation of integrals of the form

$$\frac{1}{2\pi} \int_{-\pi}^{\pi} \left|G(e^{j\omega})\right|^2 d\omega \qquad \text{(A.1.1)}$$

where the integrand involves either $F(e^{j\omega})$ or $H_m(e^{j\omega})$. These integrals are evaluated by the common technique of approximating the continuous finite integral by a finite sum of the form

$$\frac{1}{L} \sum_{k=0}^{L-1} \left|G\left(e^{j\frac{2\pi k}{L}}\right)\right|^2 , \quad L = 256. \qquad \text{(A.1.2)}$$

It is found that increasing L makes no appreciable difference for the smooth functions in this work.

The α-filter impulse responses $h_m(n)$ defined in Chapter Two are finite length sequences. Thus the terms $H_m\left(e^{j\frac{2\pi}{L}k}\right)$ are obtained by performing a 256 point FFT on $h_m(n)$ with trailing zeroes added. This is the same method used to generate the $\left|H_m(e^{j\omega})\right|^2$ curves shown in Chapter Two for $N = 16$.

The terms $F\left(e^{j\frac{2\pi}{L}k}\right)$ are obtained by first obtaining a digital filter transfer function, F(z), based on the analog filter specification, using the impulse invariant design technique [1]. Then the resulting transfer function is evaluated at $z = e^{j\frac{2\pi}{L}k}$. The resulting response is given by

$$F(e^{j\omega}) = \sum_{m=\infty}^{\infty} F_A\left(\frac{\omega}{T} j + \frac{2\pi}{T} m\, j\right) . \qquad (A.1.3)$$

This is the same as the Fourier transform of a sequence derived by uniform sampling of an analog waveform with Fourier transform $F_A(\Omega)$. This method is selected since the coding is performed on the sequence of filter output samples.

With this approximation, the normalized maximum coefficient energy is given by

$$N\rho_m = \frac{\sum_{k=0}^{L-1} \left|F\left(e^{j\frac{2\pi}{L}k}\right)\right|^2 \left|H_m\left(e^{j\frac{2\pi}{L}k}\right)\right|^2}{\sum_{k=0}^{L-1} \left|F\left(e^{j\frac{2\pi}{L}k}\right)\right|^2} . \qquad (A.1.4)$$

Other integrals are evaluated in an equivalent fashion.

AUTOBIOGRAPHICAL STATEMENT

The author was born in Harrisonburg, Virginia on February 11, 1948. He received the BSEE degree from Virginia Polytechnic Institute in 1970 and the MSEE degree from Virginia Polytechnic Institute and State University in 1972. The author has been employed by the National Aeronautics and Space Administration since 1970.